To the Graduate Council:

I am submitting herewith a thesis written by Yuen Cheng entitled "Characterization and Control of Chaotic Bubble Behavior." I have examined the final copy of this thesis for form and content and recommend that it be accepted in partial fulfillment of the requirements for the degree of Master of Science, with a major in Chemical Engineering.

Duane D. Bruns, Major Professor

We have read this thesis and recommend its acceptance:

Accepted for the Council:

Associate Vice Chancellor and
Dean of the Graduate School

CHARACTERIZATION AND CONTROL OF CHAOTIC BUBBLE BEHAVIOR

A Thesis Presented for the Master of Science Degree

The University of Tennessee, Knoxville

Yuen Cheng

December 1996

Copyright © Yuen Cheng, 1996

All rights reserved

ABSTRACT

A knowledge of the properties and behavior of gas bubbles in liquid is a prerequisite to the detailed understanding of several chemical or other processes in which the essential action of the operation is centered about moving bubbles in liquid. The present investigation aims to add to this knowledge from the viewpoint of deterministic chaos. Special attention is given to bubble formation at a single submerged orifice as well as the movement of the bubbles in the system.

The experimental investigation identified several dynamic features of the system such as low dimensionilty, periodic cycles, entrainment using sound or gas pulsing, and evaluation of spatio-temporal character. The period-doubling bifurcation route to chaos was experimentally verified as well.

The system independent variable of gas flow was identified as the optimal feedback control variable. Taming of chaos was experimentally quantified by using periodic sound wave perturbation. Entrainment of chaotic bubble behavior to its periodic states was also obtainable by using a discrete gas pulsing method.

The engineering need related to the control of the dynamics of chaotic bubble behavior was evaluated based on the OGY and Bruns nonlinear relay feedback control schemes. The advantage of these methods is that they do not require the model equations to describe the dynamics of the system. The sensitivity of a chaotic system to small perturbation provides a clue to implement these control models. Empirical difficulties in the sensitivity of the manipulated variable calculation to the experimental data used are effectively overcome. Results from this investigation provide useful and conclusive

information for future work aimed at understanding bubble dynamics especially the control of chaotic bubble behavior.

ACKNOWLEDGMENTS

I would like to express my sincere appreciation to the many individuals whose efforts have played a major part in the successful culmination of this thesis: Dr. Duane D. Bruns for his tutelage during my stay here as graduate student; Dr. Stuart Daw, and Dr. Ke Nguyen for their invaluable guidance, support and patience throughout the course of this study; Dr. Donald C. Bogue for his valuable time to serve on my graduate committee and his instruction and individual attention during my study at UT; my fellow graduate students, Nick van Goor, Charles E.A. Finney, Dean Edward, for their support, sharing knowledge, and providing computer programs, during the course of my graduate study. I would like to thank Miss Amy Massingill and Miss Danielle Moorman for their careful editing and correction for this thesis. I would also like to thank my younger sister, Lui Cheng, for her support and contribution to make my two years at UT one of the finest.

Finally, I wish to thank my parents and the department of chemical engineering at University of Tennessee, Knoxville, for financial support of my graduate study.

TABLE OF CONTENTS

1. INTRODUCTION 1

2. LITERATURE REVIEW 6

2.1 STUDIES OF DRIPPING FAUCET DYNAMICS 6

2.2 STUDIES OF BUBBLE DYNAMICS 10

2.2.1 Experimental Studies of Chaotic Bubble Behavior 10

2.2.2 Modeling Deterministic Chaos in Gas-fluidized Beds 12

2.3 CHAOS SUPPRESSION WITH OPEN-LOOP PERTURBATION 16

2.4 CHAOS CONTROL WITH FEEDBACK PERTURBATIONS 17

2.4.1 The OGY Control Method 17

2.4.1.1 Criteria for the OGY Control Theory 18

2.4.1.2 The OGY Formula for Control 20

2.4.1.3 Idea of Control 21

2.4.1.4 Implementation of Control 23

2.4.2 Occasional Proportional Feedback Control 24

2.4.3 Nonlinear Relay Feedback Control 25

2.4.4 Comparison Between OGY AND OPF Chaotic Control Models 26

3. EXPERIMENTAL APPARATUS AND PROCEDURE 28

3.1 DESCRIPTION OF THE EXPERIMENTAL APPARATUS 28

3.1.1 Gas Flow and Metering System 30

3.1.2 Liquid Selection 31

3.1.3 Pressure Transducer and Laser Beams 32

3.1.4 Data Acquisition System 34

3.1.5 Summary of Experimental Procedures 35

3.2 PERIODIC SOUND WAVE PERTURBATION 37

3.3 ENTRAINMENT OF CHAOS TO PERIODIC CYCLES 41

3.3.1 Experimental Apparatus 42

3.3.2 Perturbation System 44

3.3.3 Experimental Procedures 44

4. DATA ANALYSIS TECHNIQUES 46

4.1 POWER SPECTRA 46

4.2 BIFURCATION AND ROUTE TO CHAOS 47

4.3 MUTUAL INFORMATION 48

4.4 PHASE SPACE RECONSTRUCTION 49

4.5 TIME RETURN MAP 51

4.6 CORRELATION DIMENSION 52

4.7 KOLMOGOROV ENTROPY 54

5. EXPERIMENTAL RESULTS AND DISCUSSIONS 56

5.1 CHARACTERIZATION OF CHAOTIC BUBBLE BEHAVIOR 56

5.1.1 Visual Observation 57

5.1.2 Time Series Pressure Measurements 61

5.1.3 Time Series Laser Measurements 65

5.1.4 Power Spectra 68

5.1.5 Bifurcation and Route to Chaos 71

5.1.6 Time Return Map 73

5.1.7 Correlation Dimension and Kolmogorov Entropy 77

5.1.8 Spatio-temporal 81

5.1.9 Comparison Between Experimental Data and The Bubble Model 92

5.1.10 Comparison With Other Bubbling System Investigation 93

5.2 EFFECTS OF OPEN-LOOP PERTURBATION 95

5.2.1 Sensitivity to System Parameters 95

5.2.2 Effects of Periodic Sound Wave Perturbation on Bubble Behavior 101

5.2.2.1 Perturbation Signals 102

5.2.2.2 Suppression and Shift near Bifurcation Points 103

5.2.3 Entrainment of Chaos to Periodic Cycles 119

5.3 EVALUATION OF THE FEEDBACK CONTROL METHODS 129

5.3.1 The OGY Quantities Calculation 129

5.3.2 Experimental Concerns for the Bubbling System 138

6. CONCLUSIONS AND RECOMMENDATIONS 140

REFERENCES 143

APPENDICES 147

Appendix A 148

Appendix B 156

VITA 170

LIST OF TABLES

Table		Page
1.	Operating conditions for entrainment of chaos to periodic states	45
2.	Operating conditions for variation of pressure at the bottom of the column	96
3.	The OGY quantities calculations	137
A1.	Calibration for rotameter (FB-1/8-077-G-10, Stainless)	146
A2.	Calibration for rotameter (R-2-15-D, Stainless)	147

LIST OF FIGURES

Figures		Page
1.	Time return maps from Shaws' dripping faucet experiment	8
2.	Time return maps from Shaws' analog model	9
3.	The geometry around an unstable fixed point on a chaotic attractor	19
4.	An outline of the OGY control method	22
5.	Phase plane illustration of CSTR dynamics	26
6.	Schematic of the experimental arrangement for bubble behavior characterization	29
7.	Schematic of the experimental apparatus for sound wave perturbation	39
8.	Experimental schematic for entrainment of chaotic periodic cycles and the OGY control method	43
9.	Illustration for time interval calculation in chaotic regime	52
10.	Bubble formation and pairing sequence as air flow rate increases	58
11.	Variation of period-1 bubble frequencies and diameters as air flow rate increases	59
12.	Interpretation for time series pressure measurement	61
13.	Time series for pressure measurements at flows [cc/min] (a) 137.9 (b) 315.4, (c) 390.1, (d) 553.9, (e) 1044.7, (f) 835.4	63
14.	Time series for lower laser measurements at flows [cc/min] (a) 137.9 (b) 315.4, (c) 390.1, (d) 553.9, (e) 1044.7, (f) 835.4	66

15. Time series for upper laser measurements at flows [cc/min]
(a) 137.9 (b) 315.4, (c) 390.1, (d) 553.9, (e) 1044.7, (f) 835.4 67

16. Power spectra of pressure measurement for different bubbling motions at flows [cc/min] (a) 137.9 (b) 315.4, (c) 390.1,
(d) 553.9, (e) 1044.7, (f) 835.4 70

17. Bifurcation diagrams for pressure measurements as air flow increases 72

18. Bifurcation diagrams for lower laser measurements as air flow increases 72

19. Time return plots for pressure measurements of different bubbling periodicity at flows [cc/min] (a) 137.9 (b) 315.4, (c) 390.1,
(d) 553.9, (e) 1044.7, (f) 835.4 75

20. Time return plots for lower laser measurement of different bubbling periodicity at flows [cc/min] (a) 137.9 (b) 315.4, (c) 390.1, (d) 1044.7 76

21. Correlation dimension and entropy for pressure signals 79

22. Correlation dimension and entropy for lower signals 80

23. Phase diagram for bubble behavior at different measurement locations 83

24. Confirmation of aperiodic bubble behavior at high measurement location with flow at 352.6 cc/min 83

25. Bubble behavior of spatial measurements at flow of 506 cc/min 85

26. Chaotic bubble behavior of spatial measurements at flow of 569 cc/min 86

27. Time series of spatial measurements at flow of 918 cc/min: (a) pressure, and (b) - (h) lasers at 1, 3, 5, 7, 9, 1, 13 cms above the nozzle tip, respectively 88

28. Entropy estimations for spatial measurements at flow of 918 cc/min (the measurement location of 0 corresponds to the pressure measurement) 89

29. Mutual information for laser signals at (a) 3 cm above nozzle tip and (b) 7 cm above nozzle tip, with respect to pressure signals at flow of 918 cc/min 90

30. Predictable time delays for spatial measurements at flow of 918 cc/min 91

31. Maximum lag valves for spatial measurements at flow of 918 cc/min 91

32. Bifurcation diagram obtained from Daw-Halow model 94

33. Bubble behavior with variation of chamber size: (a,c,e) without chamber and (b,d,f) with chamber at flows of 190.8, 390.1, 585.8 cc/min, respectively 97

34. Bifurcation diagram for liquid filled to height of (a) 10 cm and (b) 20 cm 99

35. Bubble behavior near the bifurcation points at flows of 190 and 585 cc/min for liquid-filled at 10 cm (a,-b), 15 cm (c-d), 20 cm (e-f) 100

36. Bubble behavior with different perturbation frequencies at flow of 290 cc/min 107

37. Time return plots for different perturbation frequencies at flow of 290 cc/min 109

38. Power spectra for different perturbation frequencies at flow of 290 cc/min 110

39. Bubble behavior with different perturbation frequencies at flow of 464 cc/min 111

40. Time return plots for different perturbation frequencies at flow of 464 cc/min 111

41. Time return plots for different perturbation frequencies at flow of 601 cc/min 113

42. Power spectrum for describing bubble behavior at 12.5 Hz perturbation 114

43. Time return plots for different perturbation frequencies at flow of 605 cc/min 116

44. Illustration for the system states motion 117

45. Time return plots for period-2 perturbing system at flow of 327 cc/min 118

46. Time return plots for period-4 perturbing system at flow of 506 cc/min 119

47. Overview of bubble behavior at flow of 585 cc/min 122

48. Bubble behavior due to entrainment at flow of 585 cc/min 122

49. Transient bubble behavior after entrainment at flow rate of 585 cc/min 125

50. Bubble behavior with continuous entrainment at flow rate of 585 cc/min 126

51. Bubble behavior due to entrainment at flow of 617 cc/min 128

52. System states motion around an unstable fixed point on a chaotic attractor at flow of 585.8 cc/min 130

53. Illustration for stable and unstable manifolds at flow of 569.8 cc/min 134

54. Illustration for stable and unstable manifolds at flow of 585.8 cc/min 135

55. Illustration for stable and unstable manifolds at flow of 601.1 cc/min 135

Appendix A

A1. Rotameter (FB-1/8-077-G-10, stainless) calibration at inlet pressures of 4 and 5 psig 151

A2. Rotameter (FB-1/8-077-G-10, stainless) calibration at inlet pressures of 10 and 12 psig 152

A3. Rotameter (R-2-15-D, stainless) calibration at inlet pressure of 8 psig 153

A4. Rotameter (R-2-15-D, stainless) calibration at inlet pressure of 13 psig 154

A5. Time series for testing speaker 155

Appendix B

B1. Time return maps of pressure measurements for air flows between 4.2 and 44.7 cc/min 157

B2. Time return maps of pressure measurements for air flows between 52.8 and 93.4 cc/min 158

B3. Time return maps of pressure measurements for air flows between 101.5 and 142.0 cc/min 159

B4. Time return maps of pressure measurements for air flows between 150.1 and 190.6 cc/min 160

B5. Time return maps of pressure measurements for air flows between 190.8 and 253.1 cc/min 161

B6. Time return maps of pressure measurements for air flows between 265.5 and 327.8 cc/min 162

B7. Time return maps of pressure measurements for air flows between 340.3 and 402.6 cc/min 163

B8. Time return maps of pressure measurements for air flows between 415.0 and 477.3 cc/min 164

B9. Time return maps of pressure measurements for air flows between 489.7 and 541.2 cc/min 165

B10. Time return maps of pressure measurements for air flows between 553.9 and 601.7 cc/min 166

B11. Time return maps of pressure measurements for air flows between 663.1 and 1234.5 cc/min 167

B12. Mutual information for laser signals at 2 cm above nozzle tip with respect to pressure signals at flow of 918 cc/min 168

B13. Mutual information for laser signals at 8 cm above nozzle tip with respect to pressure signals at flow of 918 cc/min 168

B14. Mutual information for laser signals at 10 cm above nozzle tip with respect to pressure signals at flow of 918 cc/min 169

B15. Mutual information for laser signals at 12 cm above nozzle tip with respect to pressure signals at flow of 918 cc/min 169

LIST OF SYMBOL

e_s	stable eigenvector
e_u	unstable eigenvector
f_s^T	basis stable vector perpendicular to stable eigenvector
f_u^T	basis unstable vector perpendicular to unstable eigenvector
M	Jacobian matrix for the OGY control method
p	system dependent variable pressure
ρ	density of liquid
λ_s	stable eigenvalue
λ_u	unstable eigenvalue
ω	natural bubbling frequency
ω'	perturbing sound wave frequency
ω_b	resonant frequency due to interaction between bubbling and perturbing frequencies

CHAPTER 1

INTRODUCTION

There are a number of operations in chemical process industries in which the operating condition is centered about moving bubbles of gas in liquid. Stripping, gas absorption, distillation (in plate towers of bubble cap or sieve type), flotation, and evaporation are operations of this type. In other operations, such as boiling, slugging behavior in fluidized-bed, and even reaction kinetics bubbles appear as an incidental role.

The phenomena associated with bubbles are of extreme complexity and there is example evidence that the occurrence of chaos is spread among chemical operations with gaseous bubbles in liquid. Therefore, research is essential to understand existing complex bubble behavior and demonstrate the roots of complexity from a viewpoint of deterministic chaos. In addition, chaos can also be used to interpret the aspects of order-disorder transition arising in the bubbling system as well as the unstable behavior. Consequently, engineers would do well to become familiar with some of the ideas and terminology of chaos theory.

The deterministic chaos theory seems to do quite well on explaining ongoing complex bubble behavior [6,15,27]. In fact, this theory has also provided interpretations for a variety of phenomena once judged as too complex to admit simple mechanistic descriptions. Nevertheless, one should also recognize that many of the uses of chaos, no matter how graceful and intellectually satisfactory they seem, are just explanations after the fact. In other words, something has been observed either in the laboratory or based on a computer model simulation by using the chaos theory to explain the results for the

complex nature of the system dynamics. Such thought leads to phase I of the present study: characterizing the bubble dynamics. This portion of the study is aimed at increasing the fundamental knowledge of the dynamic bubble behavior based on the investigative apparatus. The greater part of the experimental investigation was pointed at determining the bubble behavior at a submerged orifice when a gas is blown through it. An attempt was also made, to determine the spatial and temporal evaluation in the bubbling system. The greatest emphasis throughout this characterization study is on the understanding of fundamental bubble formation and coalescence from the viewpoint of deterministic chaos.

The basic understanding of bubble behavior from phase I of this study raises the following questions. First, is there anymore characters hiding in the bubble dynamics or is the example just another curious demonstration of pure chaos? And also, knowing chaos exists in the bubble dynamics, how will the dynamics change if system variables are changed ? To answer these questions, one must rely on experimental investigation of the responses of the bubble dynamics when the selected system variables are changed or an external perturbation is applied. To be consistent, system independent variables refer to air flow, room temperature, and sound wave perturbation. System parameters include the nozzle orifice size, column pressure (liquid height), bubble column size, and chamber size in inlet air supply line. All process variables, which are the outputs from the operation such as bubble behavior and pressure fluctuation due to both bubble characteristic and perturbation, are called system dependent variables.

The experimental efforts for phase II of this study were divided into three parts. The first attempt focused on the responses of bubble dynamics to varying system

parameters such as operating column pressure and chamber size. The second part of the investigation was pointed at determining the responses of the bubble dynamics to varying pressure fluctuations in the gas holdup section. These endeavors were used during the external perturbation to suppress the chaotic bubble behavior when the system was operating near the bifurcation points. The last part of the investigation was aimed at the entrainment of chaotic bubble behavior to its periodic cycles by using a discrete gas pulsing method. If a physical system indeed exhibits chaotic behavior and periodic motion is highly desired, this type of entrainment control scheme can be used to develop the mechanism for improving the system flexibility as well as enhancing the system from the standpoint view of engineering need. Obviously, the most desirable situation would be one which completely controlled the complex bubble behavior so that the system could be operated optimally.

From phase II study, it is clear that the chaotic bubble behavior can be made more complicated or well-ordered by applying the proper perturbations. For example, the bubbling system which was perturbed with a sound wave perturbation system is much more complicated than before the perturbation because a time dependent force term is applied during the process to the already complex system. However, the results of this show a more simpler and periodic bubbling motion. Because of these observations, it becomes ambitious to speculate as to whether or not the complex bubble dynamics can be modified to achieve the desired behavior. An affirmative answer to this leads one to develop a procedure for optimizing the operation of a nonlinear bubbling system. In fact, it motivates the evaluation of a potential control scheme for the bubbling system, and these

efforts are grouped in a control evaluation of phase III of this study. The control method (normally called as the OGY control method) of using the sensitivity of chaotic system to small perturbations, was originally proposed by Ott, Gregobi and Yorke [18] and experimentally implemented by Ditto et al. [11].

The OGY method is a continuos control method in that the control variable depends continuously on the measured system error. This method considers the linear dynamics about a fixed point of a nonlinear map, and without demanding a derivation of model equations to describes the dynamics of the system. The perturbations are discretely applied to a system parameter so that all of the system states fall on the stable manifold of the controlling fixed point, and then converge to a fixed point. The greatest emphasis of this portion of the study is the subject of determining the system control variable and their manipulate values for implementation of the OGY control scheme. This portion of the report is considered to be written specifically for subsequent workers, in the hope that they may avoid some of the time-consuming inquiries already pursued by the author during the preliminary tests. A brief section in Chapter 3 devoted to discussion of the obstacles encountered during the experiments and some awareness needed for the OGY control, is also for the benefit of the future workers.

Nevertheless, from a practical viewpoint, one may ask a question such as: is there any way to benefit from chaos in the bubble system or possible uses in other chemical engineering practice? To answer this question, it is natural for one to speculate on the issue of enhancement of transport processes such as mass and heat transfer operations. Any direct treatment of mass transfer question is, of course, beyond the scope of this

work. However, if the system is chaotic and the aperiodic motion is highly undesired, the successful attempt of future control action, can stabilize the system at a specified time-period cycle in such a way in order to produce a desired output. In such a case, the ability to control chaos is of great importance.

In fact, this thesis is intended to serve as a progress report for the whole revealing aspects of the bubble dynamics and control. The work which has been done theretofore, achieve the objectives of this study, and some of future studies are outlined in chapter 6. Chapter 2 briefly reviews some of the literature relevant to this study. Experimental apparatus and procedures for this study are described in chapter 3. The theoretical background of the diagnostic tools and calculation procedures used during this study are briefly illustrated in chapter 4. Results obtained from this study are discussed in chapter 5.

CHAPTER 2

LITERATURE REVIEW

There has been a great number of papers relating to the subject of bubble formation under dynamical conditions. An exhaustive review of all of this literature would be lengthy and somewhat pointless. Consequently, only those works that are considered representative in the area of dynamic bubble behavior and the control of chaotic systems are included in this chapter. No significance should be attached to the order in which references appear. A brief review of literature on recent experimental studies of liquid drops in air (i.e. dripping faucets) is presented in section 2.1. Literature on previous investigations on chaotic bubble behavior and the Daw-Halow bubble model is outlined in Section 2.2. Section 2.3 reviews the research in the area of chaos suppression with open-loop perturbation. Section 2.4 overviews chaos control with feedback perturbation.

2.1 STUDIES OF DRIPPING FAUCET DYNAMICS

In this section, some works relating to the topic of liquid drops forming in air and the bubble model proposed by Daw-Halow are briefly described. There are some undeniable physical similarities between bubbles forming in liquid and liquid drops in air. In fact, the present bubble experiment is considered as the inverse of liquid drops forming in air. The details of this discussion can be found in review articles of investigation on bubble behavior [6, 15, 27].

Shaw et al. [24] performed the experimental investigation of a liquid drop (i.e. dripping faucet) exhibiting chaotic behavior. A helium-neon laser beam was used to measure the passing liquid drops. The experimental results illustrated that a period-

doubling progression from periodic to chaos, followed by a variety of complex behavior in the chaotic region as the liquid flow rate increased. The time intervals t_n between successive drops are calculated and presented in the form of return maps. Some results of the study are summarized in Figure 1.

Shaw et al. furthered their investigation of liquid drop dynamics by utilizing a simulation model adding a one-dimensional "mass-on-a-spring" type of oscillatory motion. They focused on the mass of the growing drop at a single position y below the equilibrium position. The growing drop seemed to be affected by a linear restoring force exerted by the spring (-kv) and a friction force between the fluid and the faucet (-bv). The velocity of the drop is expressed as v = dy/dt ,and the acceleration of the drop is given by Newton's law:

$$\frac{d(v)}{dt} = g - \frac{(ky + bv)}{m} \tag{1}$$

where g is the gravitational acceleration. The expression for the growing mass of liquid drop after the detachment of a previous drop is shown as:

$$m = m_o + c(t-t_o) \tag{2}$$

where m_o is the mass break time at t_o. They assumed that all drops break at the location y_o. Their simulation results exhibited a similarity to their experimental results except period-1 and period-4 were missing. Results of this are illustrated in Figure 2.

Since the work of Shaw et al., other researchers have performed similar experiments under different system conditions to support the claim of the exhibition of chaotic behavior in liquid drop dynamics. Wu et al. [29,30] performed an experimental

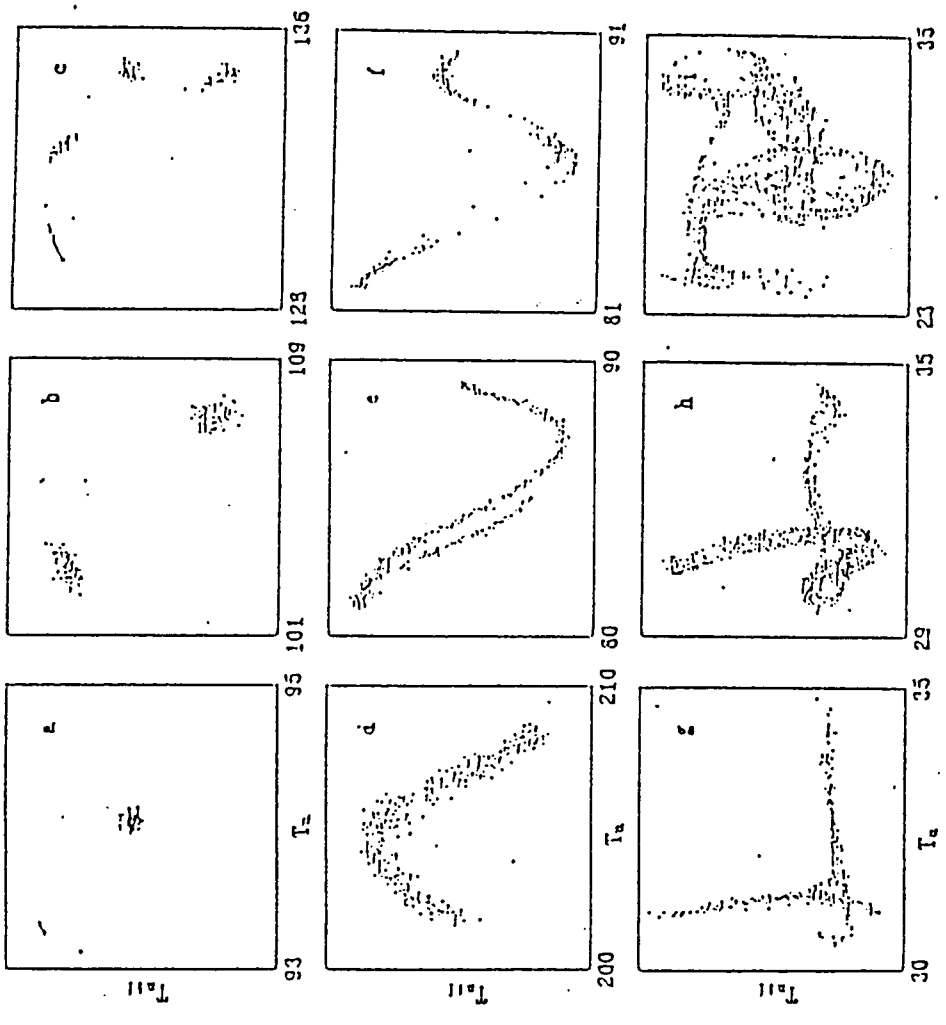


Figure 1. Time return maps from Shaw's dripping faucet experiment

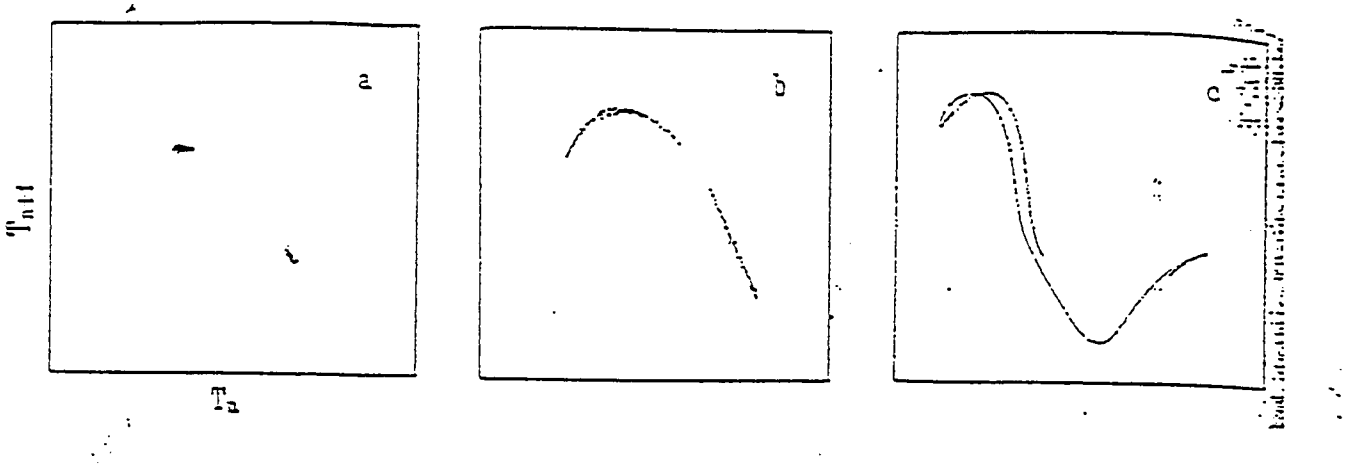


Figure 2. Time return maps from Shaw's analog model

investigation into the effects of surface tension and temperature on the dynamics of the dripping faucet by using high-resolution timing and continuous flow rate control. The concentration of the experimental liquid was varied by adding different amounts of surfactant sodium dodecyl sulfate (SDS). In this study, the return maps describing the system dynamics were more "clear and sharp" as surface tension was reduced. Once again, their experimental results exhibited water drop chaotic behavior.

Also Dreyer et al. [12] investigated the influence of variation of inner nozzle diameter on water drop dynamics based on similar experimental ideas. Experimental results from this study showed that two different routes to chaos become apparent as the nozzle diameter was varied from 0.47 mm to 1.95 mm. The periods 1 and 2 and a complicated chaotic behavior were observed for the cases of large diameter nozzles. They observed an intemittent route to chaos with period-3 and period-4 patterns for the smaller diameter nozzles.

2.2 STUDIES OF BUBBLE DYNAMICS

2.2.1 Experimental Studies of Chaotic Bubble Behavior

Chakka et al. [6] studied the chaotic behavior of bubbles in liquid columns along with the Daw-Halow simulation model. Results from this study showed that a sequence of period-doubling bifurcation progress from simple periodicity to deterministic chaos was due to the bubble-to-bubble interactions. The experimental apparatus and procedures employed are similar to those used in the present research and can be seen in section 3.1. Time-series measurements of pressure fluctuation in the gas supply line to the bubble injection nozzle and laser-beam attenuation in the column were employed in this study. They used Chaotic Time Series Analysis (CTSA) to analyze the data. The details of CTSA are presented in the data analysis chapter.

Chakka et al. studied the bubble behavior with three liquids of different densities and viscosities (i.e. glycerine, karo syrup, and water). Experimental results showed that for the three investigative liquids, glycerine relatively exhibited the most regular behavior and the clearest period-doubling progression to complex chaotic behavior. Karo syrup bubble behavior was similar to that of glycerin, except that period 4 was not observed, and a period 3 window was apparently found beyond the chaotic transition. In their study, pure water seemed to behave in a qualitatively different way compared to the other two liquids. In addition, the results on glycerin and karo syrup showed a good qualitative agreement with the Daw-Halow bubble model.

Tritton and Egdell [27] performed a short set of experiments on bubbling from a submerged orifice to investigate the possibility of chaotic bubbling. They used a water-

glycerol mixture of 24% by volume of water. Nitrogen gas was injected into a 5 liter beaker of the liquid through an upwardly pointing vertical tube with an internal diameter of 1.2 mm. A hot-film anemometer (transducer) was utilized to indicate liquid movement which is produced by formation and release of the bubbles. The anemometer was placed about 3 mm above the nozzle and 4 mm away from the axis of symmetry to ensure that the bubbles did not intersect with the probe.

Results for the bubbling system showed that a period-doubling sequence leading to chaotic behavior did occur and were presented in the form of return maps from the differential amplitude of pulses observed in the transducer signal. A further development beyond the onset of chaos illustrated that "period-3" patterns are prominent.

Mittoni et al. [15] performed a short set of experiments to further confirm the theory that bubbling systems can exhibit deterministic chaos. This investigation was performed under conditions including the variation of chamber volume, injection nozzle diameter, liquid viscosity and gas flow rate at a temperature of 20 °C. A cylindrical tank 25 cm in diameter was filled with liquid to a level of 30 cm for their experiment. Nitrogen gas was injected through the nozzle at the bottom of the tank. A pressure transducer located in the gas inlet supply line was used to monitor the bubble dynamics in the system.

Pure water and a 72% glycerol mixture was used in this study to investigate the influence of interfacial tension on the bubble dynamics. Results suggested that the general behavior and positions of period-doubling bifurcation remained approximately unchanged even though glycerol solution and water displayed different characteristics in the return map. A short set of experiments was performed in order to study the influence of varying

injection nozzle diameters of 0.8, 1.0, 1.2, 1.4 mm, respectively. Experiments with a nozzle diameter less than 0.8 mm and above 1.6 mm produced return maps with a significant amount of scatter, almost to the extent that there was no structure visible. Explanation for such indistinct return map results was due to the liquid weeping through the nozzle into the chamber during the bubbling process. Their last set of experiments was designed to study the possible impact on the dynamic bubbling system by varying the chamber volume. In conclusion, chamber volume was found to have had an appreciable effect on the bubble dynamics only at low gas flow rates and did not appear to affect the bubbling at high flow rates (i.e. fully chaotic regime). Another interesting and important observation from their chamber volume study result was that the partial period-1 regime was absent. Since the present study represents the experimental investigation on the bubble dynamics with different chamber volumes, a detail discussion of chamber impact on the bubble dynamics can be seen in section 5.2.1.

2.2.2 Modeling Deterministic Chaos in Gas-fluidized Beds

A computer model of bubble behavior in gas-fluidized beds was recently proposed by Daw and Halow [9] based on experimental observations of bubble interactions. The physical configuration of a single column of rising bubbles for the bubble model was considered similar to this experimental apparatus. Some observations obtained from the model illustrated good agreement with present experimental data. Thus, a relatively detailed review of the model is outlined in this section.

The Daw-Halow model demonstrated that deterministic chaotic bubble behavior in fluidized beds can arise readily from nonlinear bubble-to-bubble interactions. This model

showed that such interactions affect individual bubble velocity and often result in coalescence as well. The principal assumptions of the model are as follows:

- Bubbles are assumed to be rising in single-column chains along the bed axis.
- Bubbles are assumed to be spherical in shape.
- The rise velocity of leading bubbles is described as below:

$$U_s = \sqrt{\frac{gL_b}{\left(\frac{A^*}{1-A^*}\right)+2}} \tag{3}$$

where : g = acceleration due to gravity

L_b = bubble diameter

A^* = ratio of bubble cross section to bed cross section

- The vertical velocity of trailing bubbles is found by

$$U(i) = U_s\{1 + 3(D_b(i-1)/S_p^3(i-1)\} \tag{4}$$

where : i = bubble index counting from top down

$D_b(i-1)$ = diameter of bubble immediately above

$S_p(i-1)$ = center-to-center distance between bubble i and bubble i-1

- When two bubbles come into contact, they begin to coalesce by a shrinkage in size of the lower bubble and a concomitant increase in size of the upper bubble. Coalescence continues until the lower bubble is completely depleted, and the total number of bubbles in the bed is reduced by 1.
- When coalescence begins, the lower bubble velocity is equal to

$$U(i-1) = U_s(i) + U(i) \tag{5}$$

where U(i) is the lone bubble rise velocity given by Eq (3)

- During coalescence, the gas exchange rate between the lower and upper bubbles is constant and is given by:

$$Q = \frac{\pi D_b(i)^2}{4}[U(i) - U(i-1)] \tag{6}$$

where Q is the gas flow rate in volume/time.

- Two types of inlet boundary conditions (forced and autonomous) are used:
  1. bubbles of constant diameter are injected one at a time into the bottom of the bed at a fixed frequency; and
  2. the entering bubble growth and release is governed by the rising velocity of the previously released bubbles
- The exit boundary condition for the bed is that the number of bubbles in the bed is reduced by one, once the top bubble reaches the bed surface.

While incorporating the above assumptions, they used both the forced operating mode and autonomous operating mode to illustrate how the bubble model produces chaos. For forced bubble injection frequencies below a critical rate, the voidage fluctuations in the observing window are purely periodic and reflect the passage of bubbles that have remained unchanged since leaving the distributor. As bubble injection frequency is increased above the critical value, bubbles pass the observation point with two different spacings and velocities. The bubble-pairing phenomenon is seen to occur at the top of the column first, and then the pairing and coalescence zone proceeds down toward the nozzle as the bubble rate increases. The number of pairing and coalescence increases as bubble

injection frequency further increases. Periodicity disappears completely with the onset of complex behavior in which the bubble variations become limitless, and the pattern never exactly repeats. Such observation suggests the possibility of chaotic motion.

For the case of autonomous operating mode, the following additional assumptions are assumed:

- Two opposing tendencies are assumed to affect the bubble formation at the distributor; the tendency to rise in Eqs (3) and (4) and the tendency to expand in all directions as more gas is added from the bottom
- The velocity at which the bottom wall of the growing bubble near the distributor recedes from the center of bubble, which is expressed as

$$U_{bw} = \frac{dR_b}{dt} = \left(\frac{D_{bed}}{D_b}\right)^2 \left(\frac{U_c}{4}\right) \tag{7}$$

where : U_{bw} = the recession velocity

R_b = the bubble radius

D_{bed} = the bed diameter

U_c = bubble gas velocity

The bubble detaches from the distributor when the rise velocity, as determined by Eqs (3) and (4) exceeds the recession velocity from Eq (7).

The autonomous operating mode shows that it is very difficult to produce nonchaotic patterns at all. They suggested that the difficulty might be due to the fact that the nonlinear dynamics of bubble formation play a crucial role.

The most prominent result from this model is the bubble-pairing phenomenon. Also, the model predicts the onset of pairing and coalescence as bubble rate increases. Result comparisons between the present experimental study and this model can be seen in section 5.1.9 of the result and discussion chapter.

2.3 CHAOS SUPPRESSION WITH OPEN-LOOP PERTURBATION

Undoubtedly, chaos has already been determined to exist in many chemical engineering applications such as distillation columns, fluidized-beds, mixing processes, and many others. Unfortunately, the scientific knowledge of the chaotic phenomena has lagged far behind technological applications. In fact, only the mixing process has been shown to benefit from chaotic phenomenon as a vigorous mechanism for transport process. However, whether or not chaos can be beneficial in other chemical engineering applications remain in debate. Therefore, it is clearly that the ability to control chaos is of great practical importance.

One of the most interesting and important problems of study of the chaotic system is the response of a chaotic system to a given periodic perturbation. There have been several investigators who studied the effects of periodic perturbation onto the chaotic systems both at bifurcation states and fully chaotic states. Some of the previous works representative of the system's response to a forced perturbation are outlined in this section.

Braiman and Goldhirsch [1] investigated the possibility of eliminating chaos in a damped pendulum dynamic system by applying a weak periodic external force perturbation. In this investigation, a widely studied damped pendulum system was chosen

which was driven by AC and DC forces in a fully chaotic state. A periodic perturbation was driven by a second weak AC force to eliminate the chaotic behavior in the system. The results of this investigation showed that a chaotic driven pendulum can be suppressed and undergo a periodic motion by applying an external force. This external force also results in the stabilization of narrow subharmonic steps of the system.

Chacon et al. [5] used a widely studied Duffing-Holmes oscillator model to demonstrate the possibility of suppression of chaos by selective resonant parametric perturbations. A perturbative Melnikov-Holmes method was used to theoretically explain the nonlinear DH model and also to predict the selective resonance condition for the onset of chaos in the system. The results of this study showed that the application of periodic parametric perturbations could be used as an efficient route to reduce steady chaotic states in the system. These results also demonstrated that suppression of chaotic systems by periodic force perturbation depends on the right combination of perturbation parameters such as: amplitude, frequency, and initial phase.

2.4 CHAOS CONTROL WITH FEEDBACK PERTURBATIONS

2.4.1 The OGY Control Method

Recently, Edward Ott, Celso Gregobi, and James A. Yorke [18] proposed a chaos controlling model to the world of dynamics. This method (normally called the OGY method) seems to bridge the gap between the science of chaos and technological engineering. This bridge provides, or at least helps engineers to understand the nature of chaotic behavior and then possibly implement the control action onto a chaotic system. In

fact, several researchers have claimed to have successfully controlled the chaotic systems based on the implementation of the OGY control algorithm.

2.4.1.1 Criteria for the OGY Control Theory

The OGY theory of control is based on the chaotic system's characteristic of sensitivity to small changes in its initial conditions of the time history. Typically, a chaotic system has a strange attractor with an infinite number of unstable periodic orbits packing quite close together. Therefore, the idea of the OGY control technique is to give a very small perturbation that can push the system from one unstable periodic motion to the other. This method normally starts with the phase space reconstruction of the system because it contains all of the necessary information to predict the future dynamics of the system.

Since the chaotic system is extremely complicated, one would like to reduce the information of the system into a simpler formation. A useful technique called the Poincare map or return map can reduce the phase plane information without losing the generality of the system dynamics. Both of these maps describe the periodicity of the system by simply transferring the system states onto a two dimension map. In the present study, only a time return map was used throughout the course of investigation. Therefore, a familiar return map will also be used to discuss the control model. The mapping technique has been widely used for the purpose of control action, especially for the low-dimensional system. Generally, a periodic system of period n will have n number of points in the return plot. A chaotic system should have an infinite number of points as shown in Figure 3. The geometric structure of the infinite points is known as the system's chaotic attractor.

Knowledge of this attractor and of its response to a small perturbation of the system is a crucial step in the control of chaos.

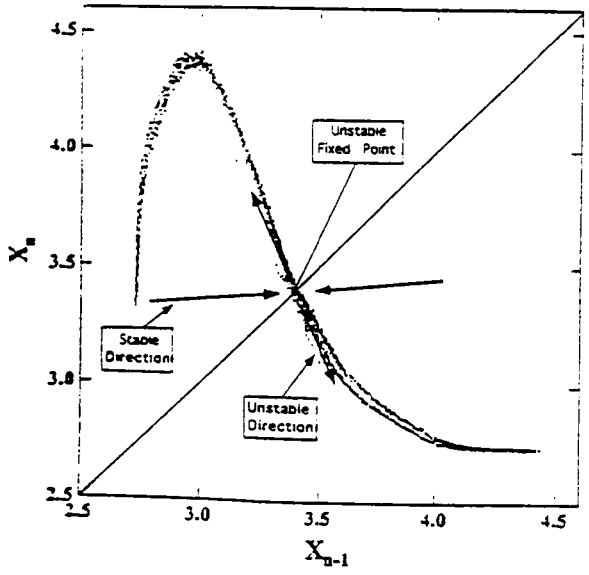


Figure 3. The geometry around an unstable fixed point on a chaotic attractor

Source: "Techniques for the control of chaos" Physica D, **86**, p201, 1995

Three criteria have to be met in order to implement the OGY control scheme:

- identification of unstable periodic motions;
- characterization of the shape of the attractor; and
- determination of the response of the attractor to an external perturbation

Since the return map summarizes the number of points which reflect the periodicity of the dynamics of the system, it should contain all the information one desires to meet the first two criteria. In fact, the first two criteria follow naturally from the return plot. The third and final criterion, which is the determination of the response of the attractor to an external stimulus, is the most difficult to determine among all criteria. One reason is that one has to identify the system parameter that has the most impact on the dynamic system

based on a thorough investigation. The second difficulty encountered during the determination of third criterion is that the selected system parameter must be capable of changing the attractor position (i.e. geometric structure of attractor must be able to shift on the return map). This second difficulty provides information about the choice of the optimum location of the unstable fixed point as well as the acceptable amount of external perturbation that is required. Some of these obstacles concerning system parameter selection for the present work will be discussed in a later section. A detailed discussion on the determination of the response of the attractor to external perturbation for this bubble column is presented in section 5.2.

2.4.1.2 The OGY Formula for Control

In starting with the OGY control scheme, one can consider a two dimensional map as shown in Figure 3. A general equation which represents the system state point on the map is dependent on perturbation, p:

$$x_{n+}1 = f(t_{n},, p) \tag{8}$$

where : x_{n+i} = system state point (i = 0, 1, 2, ...)

p = system control parameter

Consider an unstable fixed point located on the diagonal of the map and its finite region,

$$x_F(p_n) = f(x_F(p_n), p_n) \tag{9}$$

where : x_F = pre-chosen fixed point

The chosen fixed point and its finite region are used to select the qualified experimental data points. The desired controlling fixed point is calculated as presented below.

By linearizing about the pre-chosen fixed point, a linearized OGY model is expressed as:

$$(x_{n+}1 - x_F) = M(x_n - x_F) \tag{10}$$

where : M = 2x2 Jacobian matrix

x_n, ,$x_{n+}1$= nx2 matrix (n depends on the number of qualified data points)

The matrix M is characterized by its eigenvectors and eigenevalues:

$$Me_u = \lambda e_u \tag{11a}$$

$$Me_s = \lambda e_s \tag{11b}$$

where the subscripts u and s represent the unstable and stable directions. The relationship between the perpendicular basis vectors $\{f_u, f_s\}$ and old basis vectors $\{e_u, e_s\}$ is held as $f_s^T e_s = 1 = f_u^T e_u$. Therefore, one can further simplify this relation as shown below:

$$\begin{bmatrix} f_u^T \\ f_s^T \end{bmatrix} = \begin{bmatrix} e_u & e_s \end{bmatrix}^{-1} \tag{12}$$

The shift vector s due to the perturbation is calculated based on two related fixed points:

$$s = \frac{x_F(p_{n+1}) - x_F(p_n)}{p_{n+1} - p_n} \tag{13}$$

where : p_n, p_{n+1} = operating conditions

$x_F(p_n), x_F(p_{n+1})$ = the corresponding fixed points

With all the above values, one can calculate the perturbation required for control action:

$$\Delta p = \frac{\lambda_u}{\lambda_u - 1} \frac{f_u^T \delta x_n}{f_u^T s} \tag{14}$$

2.4.1.3 Idea of Control

By knowing all the linear dynamics about the fixed point on the return map, one can implement the OGY control algorithm. To briefly explain the theory of the OGY

control, a schematic of control for a fixed point is presented in Figure 4.

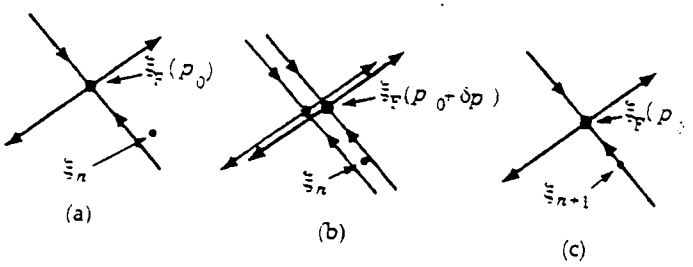


Figure 4. An outline of the OGY control method

Source: "Techniques for the control of chaos" Physica D, **86**, p204, 1995

When a system state point of n^{th} iterate falls near the fixed point (Figure 4-a), the control action force change the p value from its nominal value p_o by some δp. In such a case, the location of the fixed point is changed as well as its stable manifold (Figure 4-b). Such shifting in the fixed point force the next system state point of $n+1^{th}$ iterate falls onto the stable manifold of the unperturbed system (i.e. $p = p_o$ as shown in Figure 4-c). If the calculated Jacobian matrix that represents the dynamics is correct and no experimental noise is present, no further control would be necessary (i.e. all of the following system state points are expected to fall onto the fixed point even with the control turned off). Because of experimental noise and small errors in the least square calculation of the matrix, the OGY method suggests to repeat the control every period of the map (i.e. a period n control needs perturbation to be applied every n periods). However, applying perturbation once every n period has not had a great deal of success in a tight control

sense. Therefore, it is strongly suggested to apply a control perturbation every nth time for a period n control.

Finally, it is necessary to bear in mind that the OGY method is a continuous control with a sense of discrete perturbation. This means that the control parameter of the OGY method depends continuously on the measured system error while perturbations are discretely applied to a system parameter. Perturbations are applied such that the system states describing the dynamics land on the stable manifold, and the iterations converge to the unstable fixed point.

2.4.1.4 Implementation of Control

Ditto et al [11] were the first researchers to implement the OGY control method in an experimental system. In their magnetelastic ribbon experiment, the ribbon was driven by magnetic field, H, of the form $H = H_{DC} + H_{AC}\cos(2(f\pi t))$. Magnetic field of H_{DC} is applied to start the ribbon in the soft regime, and H_{AC} is used to take the ribbon from soft to stiff and back again at some frequency, f, so the ribbon will oscillate about its equilibrium point. The chaotic phenomenon occurs when the values of H_{AC} and f surpass some critical values. The ribbon position was measured once each period by an optical sensor. In their study, H_{DC} was used as the control parameter to control the ribbon's chaotic behavior. The experimental results showed that the system could be stabilized at different periodic orbits of the system by applying the OGY method.

The OGY chaos control techniques have recently extended to the field of biology. Garfindel et al. [14] implemented a modified OGY method to consistently stabilize a chaotic rabbit heart beat into a period 3 beat. Due to the difficulty of the determination of

a system parameter that was fast enough to respond to the external stimuli, the author managed time-dependent external perturbations in the form of electrical stimuli to the heart muscles. Garfindel et al. used the same local linearization around the unstable fixed point as used by the OGY method. In their study, the system state points were successfully placed directly onto the stable direction of the attractor. Also, the succeeding beats had a tendency to move toward rather than away from the desired unstable fixed point. For a detailed review of the OGY chaos control theory and applications, one can see the review article by Ditto et al. [11].

2.4.2 Occasional Proportional Feedback Control

Carr and Schwartz [4] proposed a control method for stabilizing steady states using only discrete pulses of an available system parameter. This implemented control technique is called occasional proportional feedback (OPF) control and it showed a certain degree of success in controlling chaotic systems. Their control parameter (discrete pulse) consisted of the three manipulate variables of pulse duration, pulse amplitude, and system delay (i.e. time between system measurement and pulsing). The control scheme was applied to a multimode laser model whose steady state becomes unstable due to a Hopf bifurcation and exhibits periodic oscillation and chaos. The details and its derivation of their control formulas can be seen in the review article by Carr et al [4].

Carr et al. demonstrated that their method is applicable to a chaotic system without modification of parameter regimes. They stated that OPF is a discontinuous control method which may be advantageous in systems where continuous feedback is difficult due to extremely fast system dynamics. However, the implementation of OPF requires

carefully tuning of the system. Also, they suggested that additional parameters besides feedback gain play an important part in their OPF control method.

While Carr et al. implemented the OPF control method to stabilize the steady state of multimode laser model, Nguyen, Daw, Bruns, and Vasu implemented a similar, but modified feedback control method to stabilize the slugging fluidized-bed at the University of Tennessee, Knoxville. The slugging behavior of Geldart's group-D particles were studied within a 6 inch diameter static fluidized-bed reactor. Pressure transducer measurements were used to monitor the bed behavior and to take appropriate control actions. Small pulses of fluidization gas were injected through a nozzle located on the bed wall just above the bed distributor. With carefully tuned system parameters, they used the system control parameters of pulse timing, pulse duration, and pulse direction (i.e. upward or downward at specified trigger level of output signals). Their control method was considered as discrete pulsing control. Results from this experiment indicated that the idea of small perturbation to a system can exhibit stabilization or destabilization of the slugging behavior in the static fluidized bed. Details of their works are summarized in review article [28].

2.4.3 Nonlinear Relay Feedback Control

The idea of the OGY scheme seems to be an astonishing method of controlling a highly nonlinear model. In fact, however, similar control strategies were developed and implemented in the early 70's. A method of this type, proposed by Bruns and Bailey [2,3], used a feedback control model for operating a nonisothermal Continuous Stir Tank Reactor (CSTR) near an unstable steady state. In this experiment, the system operation

states were stabilized by using a relay with hysteresis as a feedback controller. With the proper system design, this control scheme produced a stable operating state with only small amounts of amplitude oscillation in the neighborhood of the desired state. The same control scheme was successfully implemented on both first and second order processes. The detailed control model can be referred to in the review article [2,3]. The geometric control strategy is illustrated in Figure 5.

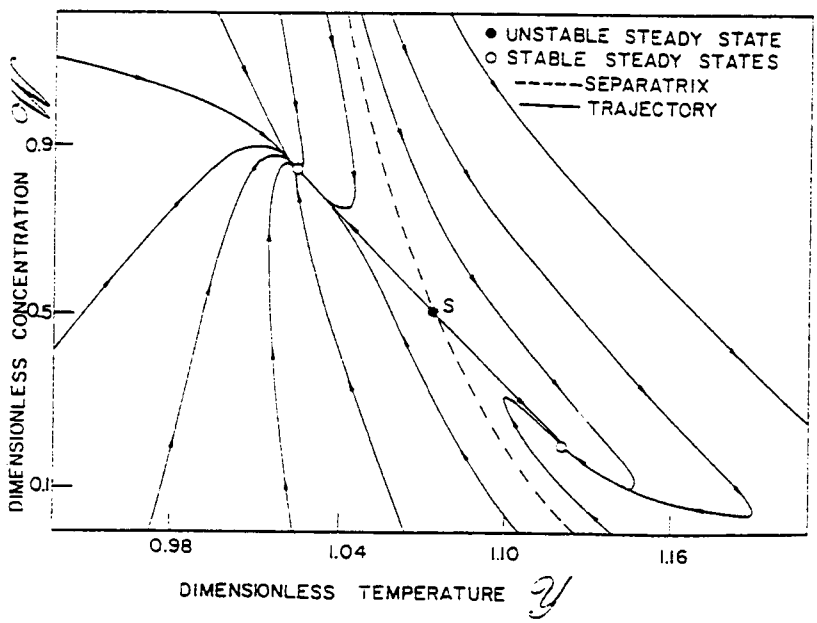


Figure 5. Phase plane illustration of CSTR dynamics

Source: Chemical Engineering Science, 1977, **32**,258

2.4.4 Comparison Between OGY and OPF Chaotic Control Models

Before leaving this chapter, some key differences between the OGY and the OPF methods need to be described. The OGY control scheme is based on an approximate linear model about a fixed point and is a continuous control method in that the control parameter depends continuously on the measured system error. The OPF method is a discontinuous

control scheme without linearizing the dynamic system. The OGY method uses only one parameter for control, while the OPF involves several system parameters. However, both control schemes seem to have some success in controlling chaotic systems in practice.

CHAPTER 3

EXPERIMENTAL APPARATUS AND PROCEDURE

This chapter describes the experimental apparatus and procedures used for the present study. Section 3.1 describes an overview of the experimental apparatus and procedures covering a set of different conditions including the characterization of bubble behavior, chamber effect, and pressure effect. A brief overview of the experimental apparatus and procedures for the response of bubble dynamics to a forced periodic perturbation is outlined in section 3.2. Section 3.3 briefly describes an overview of the experimental apparatus and procedures used for entrainment of chaos to periodic cycles.

3.1 DESCRIPTION OF THE EXPERIMENTAL APPARATUS

A square plexiglass column of 5 x 5 cm^2 in cross section and 26.25 cm in height was constructed for easy visual observation. A solution consisting of 99% pure glycerine was normally maintained at a level of 20 cm in the column. A schematic of the experimental apparatus is shown in Figure 6. This experimental apparatus was used for characterization purposes. The apparatus consisted of a gas flow and metering system, a data acquisition system, a pressure transducer for monitoring the response of upstream pressure signals to bubble formation and detachment at the nozzle, and two laser beams for monitoring the bubble behavior in the column. The experimental setup was assembled with 1/4 inch OD nylon tubing with brass and stainless 1/8 inch NPT internal fittings. A brief description of individual components FOLLOWS.

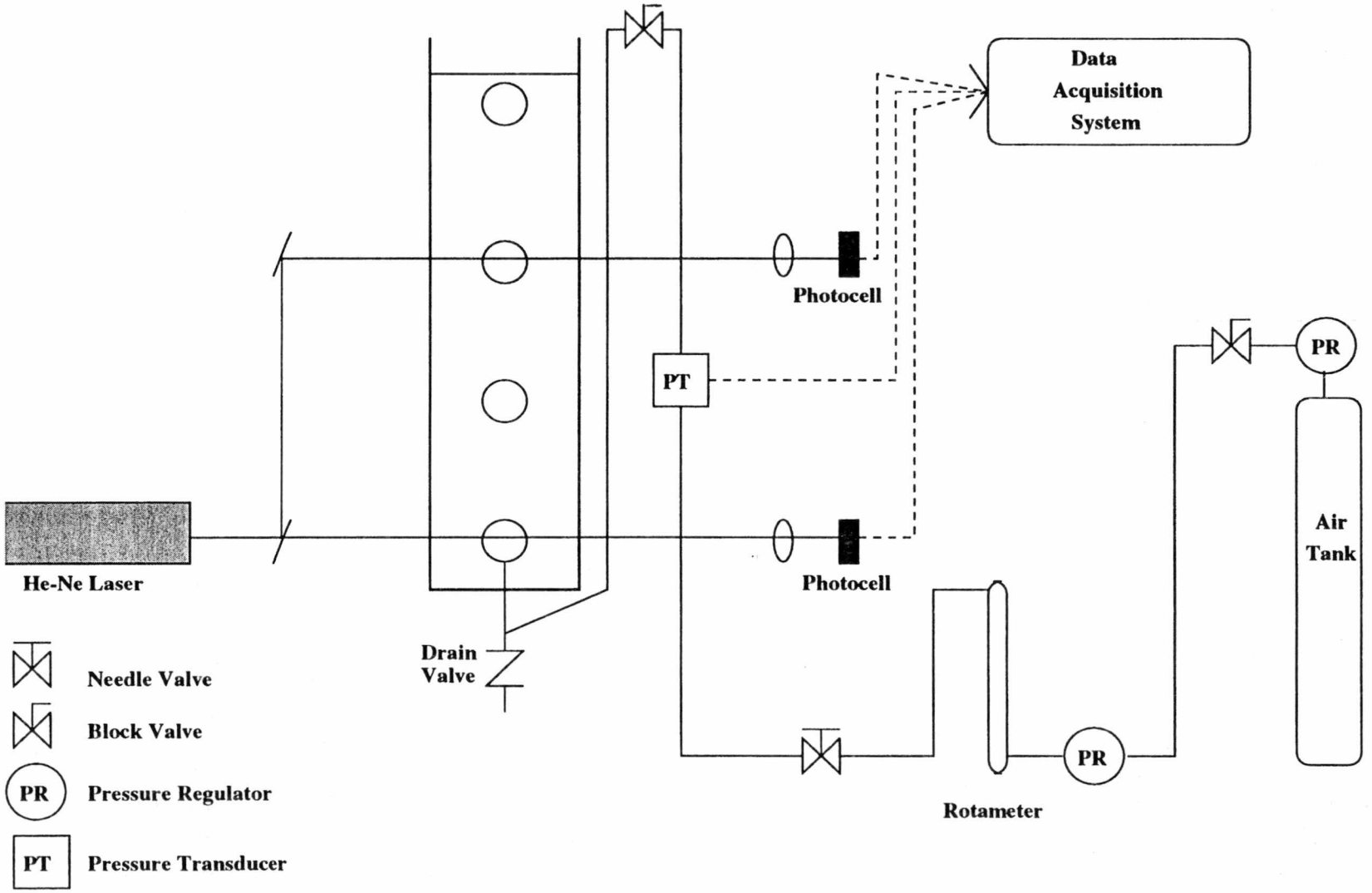


Figure 6. Schematic of the experimental arrangement for bubble behavior characterization

3.1.1 Gas Flow and Metering System

The type of gas used must not react or form solution with the liquid (glycerine). Air met the previous restrictions and was therefore satisfactory. Also, air was readily available from a standard commercial tank. The air train used in characterization experiments, consisted of a safety block valve, two pressure regulators, a rotameter, and a flow control needle valve, which were all connected in series. Because the measurements in this experimental study required a wide flow range, two rotameters that could cover the investigated air flow range were used. A Fisher model 10A1460NB22E of tube number FB-1/8-077-G-10 rotameter (10 inch) with stainless steel floats, was used for relatively low flow rate (i.e. gas flows less than 600 cc/min). A Brooks' model SHOR-RATE II of tube number R-2-15-D rotameter (6 inch) with stainless steel floats was used for high flow rate.

Since throttling at the control valve tends to minimize fluctuations in the air rate, a fine NUPPO type needle valve located downstream of the rotameter was used to improve gas flow control. The key reason for using this needle valve was to keep the stability of the gas flow constant over the range of investigated flow rates. Without this valve, variation of air flow was found at the rotameter due to the bubble formation and also the detachment at the nozzle or the damping effect of the gas holdup section (chamber). The effect of pressure fluctuation (i.e. air flow variation at the rotameter) to the bubble behavior will be discussed in the later section. With careful use of the rotameter scale and the pressure regulator scale, both rotameters were calibrated, and the results indicated an agreement in the linear relationship between float readings and gas flow rates. Calibration

at atmospheric conditions was obtained by comparing timed readings from a bubble meter. The calibrations for these two rotameters at different inlet pressures are presented in Appendix A. The calibration and the leak tightness of this bubbling system were checked periodically over the course of the experimental program.

The 7.0 mm glass injection tube was tapered to an internal diameter of 1.0 mm at the tip. The injection tube inlet was kept inclined to provide a downwardly sloped path for the air to penetrate the bottom of the column. A drain valve was provided at the bottom tip of the nozzle to allow removal of any residual liquid from the walls of the air supply tubing. This draining procedure seemed to be essential in experimental startup procedure due to the disruptive effect of residual liquid remaining in the injection tubing after startup, and therefore caused inconsistent experimental results. Failure to remove these residual liquids resulted in erratic "burping" of the gas as the bubbles formed at the tip of nozzle.

3.1.2 Liquid Selection

Some researchers have shown that the bubbling system can exhibit chaotic behavior by using low concentrations of glycerine (i.e. water-glycerine mixture of large volume of water) and liquids other than glycerine. Chakka et al. [6] investigated the influence of liquid density and viscosity on the dynamics of bubble behavior. The results from this experiment suggested that glycerine exhibited the most regular behavior and the clearest apparent bifurcation sequence among the three liquids which were studied (i.e. glycerine, karo syrup, and water). Thus, a relatively viscous liquid, glycerine (99% pure), was used in this study to reduce bubble-rise rates. Also, glycerine could provide more damping of external vibrations than low viscous solution such as water.

The variation of operating temperature and concentration might result in the formation of vertical density gradients that would disrupt the bubble patterns. Consequently, room temperature was kept at around 20 °C to minimize the effect of temperature variation and glycerine was stored in a sealed container to avoid variations in concentration while not in use. For consistence, only "fresh" glycerine from a newly opened container was used for this portion of the study. The "used" liquid was utilized for the purpose of practice.

3.1.3 Pressure Transducer and Laser Beams

In the chemical engineering industry, the analysis of upstream pressure signals has been widely used as a method of monitoring gas-liquid systems. Thus, this technique was employed to monitor the dynamics of bubble behavior for the present study. With careful analysis, pressure fluctuation traces can be associated with the bubble formation and detachment at the nozzle. In order to monitor the rapid dynamics of bubble behavior, a Setra model 228 differential pressure transducer was used and was located in the air line just prior to the injector to measure the responses of bubble behavior. This transducer had a very fast response sensor which could measure time responses of less than 30 ms. Due to the damping effect of the chamber volume (i.e. small gas supply line), all measured pressure signals were considered cleaner than laser measurements. In fact, some impressive results (i.e. period-8) were obtained by this pressure transducer but are missing in the laser signals. Also, the noise level for the pressure transducer was approximately less than 10 mV, while normal output signals obtained throughout this study were more than 500 mV.

Besides measuring upstream pressure measurement, two laser beams passing horizontally through the axis of the transparent column were also used to monitor the bubble behavior in the column. The centers of the beams were normally maintained at 1 cm and 8.5 cm above the tip of the nozzle and were continuously monitored by photocell detectors. The reason to position a low-laser beam at 1 cm above the nozzle tip was to obtain all the information about bubble formation and coalescence near the nozzle. When the system is operating at an extremely high flow rate (i.e. deep chaotic state), the bubbles "slip away" almost together as they leave the nozzle. In such cases, the lower laser beam might be unable to distinguish the differences between the bubble velocity and spacings. In fact, a short set of experiment were performed to confirm such an argument by positioning the center of the low-laser beam at the tip of the nozzle instead of positioning the center of the beam at 1 cm. From that experiment, a large range of periodic windows was observed beyond the onset of chaos. Therefore, the location of the lower laser beam was consistently positioned at the same place throughout the experimental program. Although the upper laser beam could be positioned anywhere above the low-laser beam to monitor the bubble behavior at the measurement location, it was consistently maintained at 8.5 cm above the nozzle tip. This position was chosen and held consistent because an experimental study on the spatio-temporal behavior of the bubble column verified that the dynamics of bubbling depend on measurement location.

Another experimental technique which needed to be carefully handled was that all diameters passing through the column were consistently kept at 5 mm in diameter. The laser output signals used to describe bubble behavior could be affected or sometimes

"confused" by varying the laser intensity (i.e. laser beam diameter). Thus, the positions and diameter of laser beams were consistently maintained for experimental data acquisition.

3.1.4 Data Acquisition System

Noise is always present in experiments. In this study, all unwanted measuring signals were instrumentally minimized. The data acquisition system (DAS) consisted of two hi/lo filters, a digital oscilloscope, and a PC based data acquisition system, all of which were simultaneously monitoring the system behavior. Two Wavetek model 452 dual hi/lo filters were used to remove DC bias, electrical noise from instrument devices, and random noise (e.g. any undesired signals from the surrounding). Each Wavetek model 452 hi/lo filter had separate input and output terminals, high and low pass functions, and 1-digit resolution for cutoff frequency selection. The bubbling frequencies for the investigative system were always found to be less than 20 Hz. Thus, low pass function was normally set at 20 Hz as the cut-off frequency to remove all the ground noises and high pass function was set at 0.1 Hz to remove the DC bias.

After the measured signals were filtered, the filtered-signals were transferred to a 12-bit-resolution Nicolet oscilloscope and then saved as a set of time history measurements. The oscilloscope had four channels to produce individual data records of up to 63360 points and sampling rates varying from 0.1 to 20,000 Hz. Each channel has three modes: DC, AC, and ground. The input mode for each channel must be carefully chosen in order to collect the proper data on the oscilloscope. If an input channel is set in the DC mode, the collected data would only be digitized but not filtered. The AC mode filters out some information contained in the measured signals with a cut-off frequency of

1 Hz. In fact, it was learned that the AC mode "chopped out" some important information about the dynamics of the system. Obviously, the ground mode would not perform the proper functions of data collection. For this characterization study, the oscilloscope typically collected continuous output signals at 500 samples per second with the DC input and ground output. Each acquired data set consisted of 60,000 points of time history measurements for further statistical analysis. An intel 80486-based microcomputer with a 12 bit resolution data acquisition board was also used to collect the appropriate data and convert this data into a return map which was plotted on the screen simultaneously as the experiment was performed. This PC based data acquisition system was a great convenience throughout the characterization part of the experimental performance. The key use of this data acquisition system was in the control and implementation procedures. Thus, a relatively detailed discussion of this system will be outlined in section 3.3.

3.1.5 Summary of Experimental Procedures

Glycerine from a newly opened container that was free of atmospheric moisture was used throughout the course of experimental study. Laboratory temperature was normally maintained at about 20 °C to minimize the effect of glycerine temperature variation (i.e. variation of viscosity and density) on the bubble dynamics. The entire apparatus was mounted on an optical bench that was decoupled from the floor with air cushions. While air was supplied into the column forming bubbles, the leak tightness of the system was checked on a periodic basis. For a short period after startup, liquid near the bent portion of the glass tube under the injector needed to be drained from the system in order to prevent the erratic "burping" of the gas.

Electrical devices such as a pressure transducer, lasers, filters, an oscilloscope, and PC data acquisition system need to be used appropriately as described earlier. The high and low bi-pass function of filters were normally set at 0.1 Hz and 40 Hz, respectively. Typically, the oscilloscope acquired data sets of 60,000 points at a sampling rate of 500 Hz. The data acquisition channel input was normally set at the DC mode and the output was normally set at the ground. Due to the physical phenomenon of transient bubble formation, data was collected only at "steady state" for both periodic and aperiodic states. There is no absolute time interval required for the system to reach steady state. Typically, the steady state bubble behavior can be easily determined by looking at the motion of the system state on the return plot.

One experimental concern was that small foam bubbles are produced as the rising bubbles bursting at the liquid surface, especially when the air flow rate was high. These foam bubbles are drawn down into the column due to the liquid circulation of the rising bubbles. The presence of these foam bubbles did not appear to affect the pressure measurements. This was true because the pressure transducer is used mainly to measure the pressure fluctuation traces in the gas supply line which are only associated with the bubble formation and detachment at the nozzle. In fact, the damping effect introduced by a small chamber volume between the transducer and the nozzle results in a much cleaner measurement. No significant amount of information is lost in these pressure signals. Nevertheless, these foam bubbles did appear to add noise to the laser measurements. Still, all measurements gave meaningful interpretations of the bubble dynamics for this portion of the study. This was mainly due to the fact that the diameter of the foam bubbles was

typically 20 times less than that of the rising bubbles in the liquid.

For the investigation of spatio-temporal bubble behavior in the column, all apparatus and procedures were similar to that of the previous characterization study except the laser beam locations were varied along the column. The bubble behavior in the column was monitored by varying the measurement locations from 1 cm to 13 cm above the tip of the nozzle.

3.2 PERIODIC SOUND WAVE PERTURBATION

One of the most difficult criterion of any control method is to select the system control variable which has the most impact on the dynamics of the system. Also, the control parameter (perturbation variable) has to relocate the system attractor (i.e. how much need to be manipulated to stay on the control level). In this study, system input of gas flow, system parameters of column pressure, and the dependent variable of pressure in the inlet supply tube were all considered as potential control variable for the system. The influence of different column pressures was studied in a short set of experiments where columns were filled with 10 cm, 15 cm, and 20 cm of glycerine. The experimental apparatus and procedures were similar to that used for characterization.

The effect of pressure variation in the gas holdup section was also investigated in a set of experiments. This experimental study focused on the response of bubble dynamics near the bifurcation point (instability point) since these aspects of dynamics are generally speaking expected to respond in more or less universal ways. The basic experimental apparatus used was almost the same as used previously. Only a chamber with a volume of 103.6 cm^3 was located between the pressure transducer and the needle valve. The idea of

adding a bigger chamber is to stabilize the air flow as well as to provide a larger damping effect to the bubbling action at the nozzle.

By minimizing the pressure fluctuations and thus stabilizing the air flow, the bubble behavior was shown to be somehow dependent on the pressure in the gas holdup section. Now, what about varying the pressure in this section, and what should one anticipate from such a variation? Can the pressure in the section be used as a control variable ? To answer these questions, a short set of experiments was carried out to study the effects of a periodic sound wave perturbation on bubbling pattern. An overall schematic of the experimental apparatus is shown in Figure 7. The forced periodic pressure perturbation system consisted of a FG8002 model frequency generator of Goldstar, a speaker, a plastic membrane that separated the atmospheric and tubing air flow, and a chamber directly connected to an inlet gas supply tubing system.

One of the major concerns for this perturbation system was the membrane selection. The selected membrane basically acted as a damped oscillator to apply the forced periodic motion to the bubble system without changing the net gas flow. Since a damping effect was expected to act on the bubble system, the criteria for the selected membrane was that it must be leak-free and give smooth periodic perturbation. Initially, a rubber membrane was chosen for use due to the fact that it could give smooth periodic perturbations to the system. It turned out that rubber brought a leakage problem and also seemed to provide more unwanted oscillation in the bubble system, especially when the bubble system was operating at low gas flow rate. Therefore, a membrane of plastic was substituted and used throughout the entire experimental work.

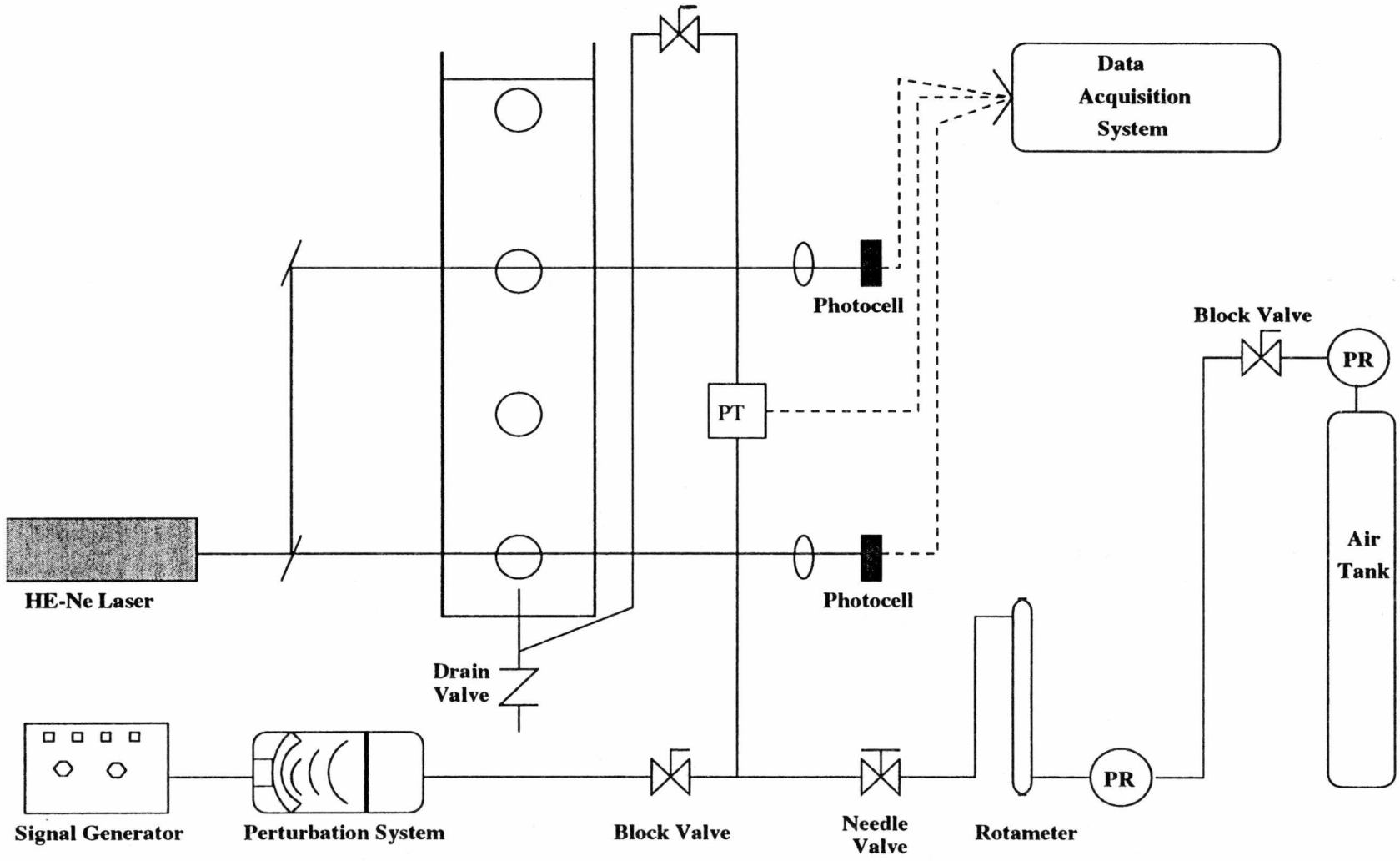


Figure 7. Schematic of the experimental apparatus for sound wave perturbation

Because a forced periodic perturbation was desired for this experiment, the response of this periodic perturbation was expected to exit in a sinusoidal wave form. To examine the output response due to the perturbation system, a short set of tests was carried out and some of those results are summarized in Appendix A. These response tests consisted of both frequency and amplitude variation. Since the power transfer of the perturbing signals involved a complicated frequency-amplitude interaction, it was considered, from the standpoint of simplicity, to give a periodic perturbation with a constant input amplitude.

By fixing the amplitude, the variations of frequency were manually adjusted on the frequency generator. The perturbation was basically initiated by the generator to send the desired frequency signal through a radio set and then drive it to the speaker. The power was transferred from the speaker through air (i.e. a small chamber between speaker and membrane) and then to the membrane (oscillator) in the form of traveling sound waves. The corresponding output frequency drove the membrane and provided the variation of pressure in the inlet gas supply line. When the driving frequency interacted with the dynamic bubble frequency (i.e. number of bubble formations at the nozzle), the harmonic phenomenon was expected. The result of this harmonic resonant changed the output of the bubbling frequencies at the nozzle as well as the bubble behavior in the column. The detailed discussion for the application of sound waves as a perturbation parameter can be seen in section 5.3.

The experimental procedures were almost the same as described in section 3.1 for the characterization study, except a periodic sound wave perturbation was introduced to

the bubble system. Typically, the perturbation would only be applied when a steady state of specified bubble operating conditions were considered to be reached. Since the pressure signals were disrupted by the membrane oscillation, "real" bubble behavior can only be monitored by using the laser measurements. The pressure measurements were only acquired to determine the interaction between the bubble dynamics and membrane oscillations. When the perturbation was applied, an external force term was added onto the time dependent variable of pressure in the supply line, so that it would initiate the interaction of natural bubbling motion and a speaker driving frequency. This interactive motion would not settle down in an unique motion until after a certain time interval had passed. These time intervals were called transient times and the motions after these intervals (steady state motion) were the same as if the forced perturbation had been acting the entire time. The transient response of the bubbling system to the forced periodic perturbation was considered one of important aspects of the perturbation study which monitored the system state motion before it reached to the steady state. To achieve such goal, data of monitoring bubble dynamics were taken at all time with and without the application of perturbation. Results of this study can be seen in detail in section 5.3.

3.3 ENTRAINMENT OF CHAOS TO PERIODIC CYCLES

Although the results obtained from the external forced sound wave perturbation study are impressive from the viewpoint of taming the chaotic bubble behavior, the perturbation does not show the capability to shift the system attractor. In other words, sound wave perturbation is unable to be used as the control variable for the implementation of the OGY scheme. Therefore, another optimum control variable needs

to be discovered. Based on the results obtained from the characterization study, the system input of gas flow leads one to believe that it could perform as the control variable. Therefore, the experimental apparatus was re-designed in order to use the input of gas flow into the system as the control variable. Based on the open-loop perturbation study, it was found that the chaotic bubble behavior can be entrained to periodic cycles by using discrete gas pulsing. In addition, this variable seems to meet all three criteria for the OGY control method. The idea of the experimental OGY control implementation will be presented in a later section. The entrainment of chaos to periodic cycles is described here.

3.3.1 Experimental Apparatus

In order to implement pulses of gas flow as the external perturbation, the gas supply lines were modified as shown in Figure 8. As shown, three gas flow supply lines were re-designed in parallel within air train. The gas flow supply lines consist of a main stream air flow line and two bypass pulsing lines. Since this experimental setup is also built for the implementation of the OGY control method, a fast responding feedback system is highly desired to produce an external force in response to the bubble dynamics. Therefore, two types of saturation pulse injectors were used to introduce the gas pulse into the system as the external perturbation. These types of injectors could be operated smoothly while the valves are either opened or closed up to 100 times per second. Based on the manufacturer's specification for the injector, the opening and closing time for the valves are 1 ms and 2 ms, respectively. Because the fast action of perturbation may cause some misfire phenomenon (the saturation type injector has a 1.2 ohm resistor which cannot short-cut the circuit if current leaks) , a diode or a resistor needs to be placed in parallel

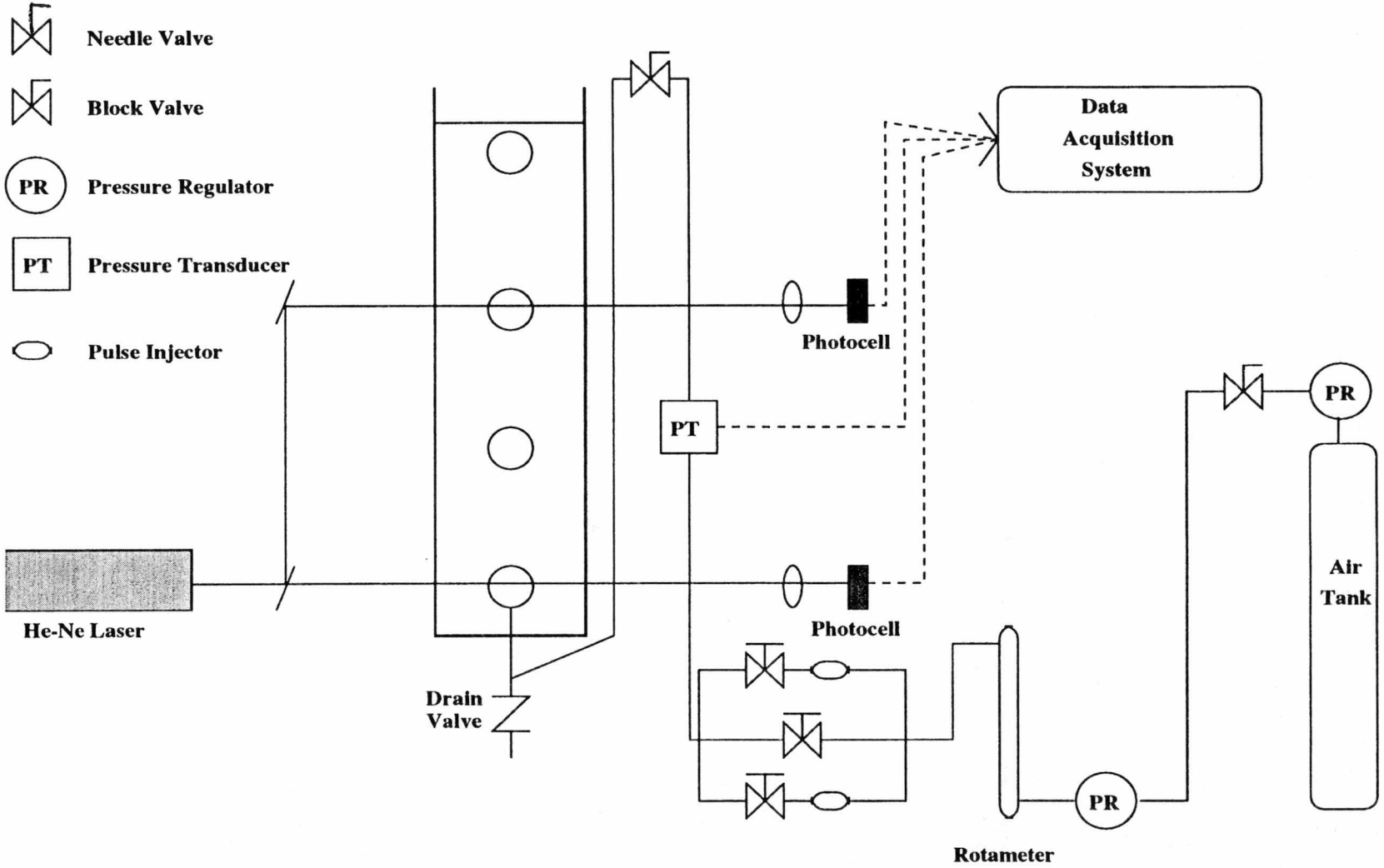


Figure 8. Experimental schematic for entrainment of chaos to periodic cycles and the OGY control method

with each injector for the purpose of the smooth pulsing action.

When the injector valve is closed, the air flow supply to the column is controlled by the needle valve located downstream of the rotameter. When the injector valve is opened, the amount of air necessary to generate bubbles is dependent on both the main air supply and the pulsing air. By opening and closing the injector valves, the variation of net gas flow to the column can be obtained by simply pulsing the system.

3.3.2 Perturbation System

The lower laser measurement was used to monitor the bubble behavior. The bandpass filtered measurements were digitized by a microcomputer with a 12-bit-resolution data acquisition board. The pulsing action was initiated and controlled by the computer to generate a 300 mA and 3 V pulsing signal to a solid state relay (DC to DC). The power supply device converted the corresponding signals to a 3 A and 14 V output which opened the injector valve for the desired perturbation action. The perturbation routine was developed in the C ++ language by Nick van Goor. Typically, the data acquisition system samples the bubble behavior measurements at 1000 points per second and graphs at 100 Hz without losing generality of the system dynamics.

3.3.3 Experimental Procedures

The experiment was performed at room temperature of 20 °C; and the air rate of 585 cc/min was chosen since it is located slightly beyond the onset of chaos. The computer acquired the measured outputs that described the bubble behavior and then mapped them onto a return plot for the purpose of monitoring the column. The pulsing amplitude, time, duration, and delay (valve open and close times) were carefully tuned for

this pulsing study. The pulsing flow of 15 cc/min was used for the external perturbation to entrain the aperiodic bubbling pattern to its periodic cycles. The detailed perturbation operating conditions are summarized in Table 1.

Table 1. Operating conditions for entrainment of chaos to periodic states

Operating Flow (cc/min)	Pulsing Flow (cc/min)	Frequency (Hz)	Duration (ms:s)	% Difference
585	15	5	377:400	2.6 %

CHAPTER 4

DATA ANALYSIS TECHNIQUES

In the present study, system signals are analyzed by the standard classical linear analysis tool and the chaotic time series analysis tools (CTSA), to observe the dynamics of bubble behavior. This chapter gives a brief description of the theoretical background for these data analysis tools and their implementation in this study. These analysis tools include Fourier power spectrum, time return map, time-delay phase-space reconstruction, mutual information, bifurcation theory, and correlation dimension and Kolmogorov entropy.

4.1 POWER SPECTRA

The classical linear method for analyzing time series measurements is to transform the information into the frequency domain using Fourier analysis. The real and imaginary parts of the transform from the Fourier series, are squared and added together to obtain the so-called power spectrum. The power spectrum analysis enables one to differentiate between periodic and chaotic signals considering both the characteristic frequencies (i.e. peaks) and the level of broadband noise. However, this distinction is often somewhat subjective. Therefore, it is important to address some cautions while one is using power spectra as analysis tool. Typically, a system exhibiting periodic motion shows a discrete spectra, and a chaotic system has more of a continuous power spectra. One caution is that power spectrum analysis indicates the features of the transition to chaos, as well as, the presence of chaotic regimes. Nonetheless, the spectrum analysis does not give detailed information on the type of chaotic motion. In other word, power spectrum analysis cannot

be used alone to detect the existence of chaotic motion.

Another important feature of power spectrum analysis that needs to be handled carefully is the appearance of multiplier peaks of the spectrum in the output, which does not imply a chaotic motion. Typically, if there is an initial dominant frequency component, ω, in the digitized measurement of the process, the harmonics or subharmonic of this frequency is also be presented in the form $m\omega/n$ ($m,n \in R$). This is particularly true due to the resonance effect if an input to the process is a harmonic motion. The discussion of the power spectrum analysis along with the possible resonance effect on bubble dynamics is presented in section 5.1.3.

In this study, the bubbling system is treated as a low dimension system based on the characterization investigation. Therefore, power spectrum can be used in determination of bubble dynamics and its influence caused by the periodic sound wave perturbation. Power spectrum analysis helps to explain the possible physical phenomenon due to the bubble-to-bubble interaction and the effect of input perturbations.

4.2 BIFURCATION AND ROUTE TO CHAOS

One sign of impending chaotic behavior in dynamical systems is a series of changes in the nature of the periodic motions as a result of a variation in some process input variable. Bifurcation theory provides model that describes transitions and instabilities created by an alternation of a system parameter. The values of those parameters where the qualitative nature of the system motion changes are called critical or bifurcation values.

A bifurcation diagram is possibly a perfect candidate to demonstrate the existence of chaos in the system as well as the overall picture of the trends of the system behavior.

This diagram is generated by plotting some measurements of system motion as a function of a system independent variable of gas flow rate for this present study. Time return map gives an useful technique to observe the periodicity of the system and its subharmonic bifurcation. It transfers all the information of the system behavior from time series signals into the number of points which exactly reflect the fundamental periodicity of the system. In this study, the time intervals between successive occurrences of the trough to trough oscillation of time series signals are calculated by defining the specific even in the signal of interest (i.e. zero, mean, or peak crossing of time series signals).

This present study shows that the bubbling system undergoes a period-doubling sequence leading to chaotic behavior. Period-doubling bifurcation means that the system behave at the simplest orbit of period-1 leads to the formation a stable orbit of period-2, period-4, period-8, and then infinity. The detail of bifurcation route to chaos is discussed in section 5.1.5 of the results chapter.

4.3 MUTUAL INFORMATION

Mutual information is used to measure the general dependence between measurements and to indicate how far into the future the process measurement is predictable, based on the measured signals. This technique can simply be considered as a nonlinear analog of the autocorrelation function.

Shannon and Weaver [23] exploit the basic concept of the mutual information function which states that the uncertainty for any measurement depends on the probabilities for the various possible outcomes. Mutual information is determined by evaluating the difference between the average unconditional uncertainties of making two

successive measurements and the average conditional or joint uncertainties. For time series measurements, the range of the measurement value is divided into N bins and the unconditional probability, p(i), and conditional probability, p(i,j), within a bin are determined. The uncertainties and the mutual information function are then determined as follows

$$\begin{aligned} H(s) &= -\sum_i p(i)\log_2 p(i) \\ H(s+k) &= -\sum_j p(j)\log_2 p(j) \\ H(s,s+k) &= -\sum_i p(i,j)\log_2 p(i,j) \\ I(k) &= H(s) + H(s+k) - H(s,s+k) \end{aligned} \tag{15}$$

where I(k) represents the average number of bits that are predicted correctly for the subsequent measurement of k time steps in the future which are based on the present measurement at time step, s. In addition to indicating the nature of chaotic behavior, mutual information calculation provides a characteristic time of predictability of the motion in the future which is useful for phase space reconstruction as embedding delay value.

4.4 PHASE SPACE RECONSTRUCTION

A classical phase space trajectory plotting of a dynamic system with N dependent variables requires N dimension with orthogonal coordinate directions in order to represent each dynamical variable. That put one in the position of knowing all the dynamical variables of the system and that is virtually impossible. One of the most celebrating data analysis technique, known as phase space method (also called the embedding space method) is exploited by Roux et al in 1983. Their claim is that for system governed by an

attractor, the dynamics in the full phase space can be reconstructed from measurements of just one time dependent variable and this time dependent variable carries sufficient information about all the others.

The method is based on time delays of Takens' embedding theorem. For a N degree-of-freedom system with time series signals x(t), the signals are plotted versus the delayed or advanced signals by a fixed time constant. The time series x(t) generates a trajectory p(t) in a N dimensional phase space.

$$p(t) = \{x(t), x(t+k), x(t+2k), \ldots\ldots, x(t+(m-1)k)\} \qquad (16)$$

where m is embedding dimension, and k is the time delay or time lag. According to Takens' theorem, the rule of thumb for selecting time delay or lag involves satisfying the following criteria

$$m > 2d + 1 \qquad d: \text{actual dimension of attractor}$$

The choice of m and k are not crucial, except to avoid a natural period of the system. A simple example of time series x(t) and its trajectory vector p(t), with the assumption of embedding in 6 dimensions and a time lag of 3, is illustrated as follows:

Time series : $\{x(1), x(2), x(3), x(4), x(5), \ldots\ldots\ldots\ldots, x(n-1), x(n)\}$

Vector p(t) : $\{x(1), x(4), x(7), x(10), x(13), x(16)\}$

$\{x(2), x(5), x(8), x(11), x(14), x(17)\}$

$\{x(3), x(6), x(9), x(12), x(15), x(18)\}$

.

$\{x(n-16), x(n-13), x(n-10), x(n-7), x(n-4), x(n-1)\}$

$\{x(n-15), x(n-12), x(n-9), x(n-6), x(n-3), x(n)\}$

For past study at the University of Tennessee, the lag is taken as the number of time steps for the mutual information function to decay to 50% of its initial value. In this present study, time lag is arbitrary chosen until the trajectories achieve the optimal unfold based on visual inspection (this program is developed by Nick van Goor). The embedded trajectories obtained is then mapped onto a new set of orthogonal axis called principal axis by using principal component analysis (PCA). In such case, the system trajectories is visualized as projections on a standard set of coordinate axes.

4.5 TIME RETURN MAP

Time series signals give all the information one needs to observe the dynamics of the system. The complicate phase space trajectory give all the information to predict the future dynamics of the system. But somehow one wants to reduce the information to a manageable level by using a Poincare map or time return map, the geometric structure can be simplified and without loss generality of the dynamics of the system. In this study, the time return map technique was primarily used to calculate the time intervals between successive occurrences of the trough to trough oscillation of time series signals by defining the specific even in the signal of interest. This technique is particular important for the OGY control method because the manipulate variables for control (i.e. eigenvalues, eigenvectors, controlling steady state and others) can be computed from the plot.

The computation process of time return map requires some assumptions in order to reflect the "real" dynamics of the system. Figure 9 illustrates a typical chaotic regime of time series measurement for chaotic bubble behavior. A zero crossing in the up direction has been consistently specified for time interval calculations. The measured time intervals

are generated as a sequence of $\{t_1, t_2, t_3, ..., t_{n-1}, t_n\}$. The calculated time interval values, which less than a 0.01 s (t_3 as shown in Figure 9), are consistently added to the previous period cycle in order to retain all the dynamical information of the system.

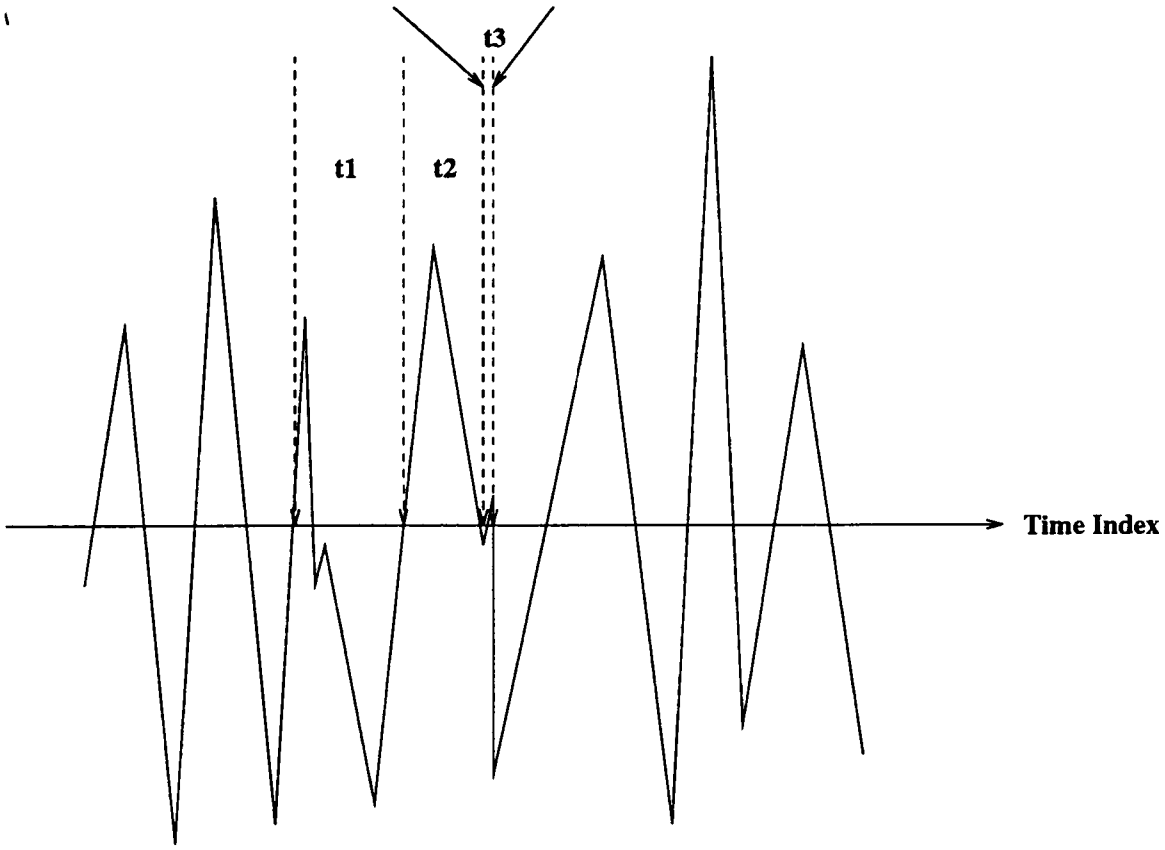


Figure 9. Illustration for time interval calculation in chaotic regime

4.6 CORRELATION DIMENSION

Correlation dimension is a term used to estimate the minimum dynamcial degree of freedom of the attractor in phase space. Various correlation dimension definitions have been proposed through different areas. In this present study, the maximum likelihood

method based on the correlation integral, proposed by Schouten et al [20-22], is used for the correlation dimension estimation. A finite sequence distances (l_1, l_2, l_3, ..., l_m) is considered between m randomly chosen pairs of the trajectory segments (x_i, x_j). A fixed maximum distance, l_o, (the cut-off length), needs to be assumed in the dimension computation. The correlation integral is defined according to power law, $C(l) = l^D$ for $l < l_o$. The normalized cumulative probability distribution of the correlation integral C(r) is defined as:

$$C(r) = r^D \tag{17}$$

with $0 < r < 1$. The maximum likelihood dimension (D_{ML}) is, therefore, obtained by making the derivative of the logarithm of function L(D) equal to zero and is expressed as:

$$D_{ML} = -(\ln(r_j))^{-1} \tag{18}$$

A detail discussion on maximum likelihood method procedures is available in review articles by Schouten et al [20-23]. The average cycle length is assumed to be the initial segment length for single period behavior. The initial segment length needs to be adjusted to the longest period for multiple period behavior. The correlated dimension estimations must be positive rational numbers. A positive integer value indicates a periodic phenomenon, and a fraction refers to chaotic system. Typically, the measured time series signals of 60,000 were divided into 30 replicates to produce 30 independent estimated dimension values (D_{ML}). The final estimate D_{ML} is the average of these 30 dimension values, and the uncertainty normally ranges from 1 to 5 percent of the estimate D_{ML}.

4.7 KOLMOGOROV ENTROPY

Kolmogorov entropy is an invariant measurement for the rate of information loss along an attractor or for the degree of predictability of points along an attractor given an initial point. A zero entropy implies a periodic or cyclic phenomenon of the system. A positive entropy indicates a deterministic chaos phenomenon. An infinite entropy refers to a random or non-deterministic phenomenon.

Once again, the entropy estimation method proposed by Schouten et al [20-22], is employed in this study. Schouten et al. assumes the separation of nearby orbits to be exponential. This exponential distribution function for a pair of initially nearby points that separate over a distance larger than a cutoff length l_o is expressed as:

$$C(b) = e^{-K'b} \tag{19}$$

with K' = Kmt, where t is the sampling time interval, m is the embedding dimension and K is Kolmogorov entropy. By using the probability of finding the samples of (b_1, b_2, b_3, ..., b_M) depending ln K, this method derives the maximum likelihood estimation of Kolmogorov entropy, K_{ML}, as

$$K_{ML} = -\frac{1}{m\tau}\ln\left(1-\frac{1}{\frac{1}{M}\sum_{i=1}^{M} b_i}\right) \tag{20}$$

where M is sample size, and K_{ML} is expressed in bits per unit of time size.

For entropy estimation in this study, the initial segment length and cutoff length are assumed to be average cycle length and average absolute deviation of time series, respectively. A replicate random sampling of 30 was normally used to produce 30 independently approximated values for the Kolmogorov entropy (K_{ML}). The final

estimated K_{ML} is the average of those 30 entropy values, and the uncertainty normally ranges from 1 to 5 percent of the estimated K_{ML}.

CHAPTER 5

EXPERIMENTAL RESULTS AND DISCUSSIONS

This present study is organized into three experimental phases: characterization of chaotic bubble behavior in the bubble column, experimental study of the response of bubble behavior due to a forced periodic perturbation, and investigation of possible feedback control schemes to control the bubble regime with emphasis on implementation of feedback control method proposed by Otto et al. [17] (normally called the OGY control method) and the discrete nonlinear relay method proposed by Bruns et al. [2,3]. The results presented in this chapter focus on those data and figures which are considered clear, concise, and typical, as well as, illustrates bubble character and helps in the understanding of chaotic phenomenon. Some of the data analysis for the investigated operating conditions are presented in Appendices B. Section 5.1 presents the results from the characterization study. Section 5.2 discusses the effects of open-loop perturbation including sensitivity to system parameters, perturbation with sound wave, and perturbation with gas pulsing. Section 5.3 illustrates the evaluation of model identification of required system characteristics for both the OGY and nonlinear relay control schemes.

5.1 CHARACTERIZATION OF CHAOTIC BUBBLE BEHAVIOR

The first phase of this research was to approach the bubble dynamics from a detailed experimental evaluation in order to understand the source of irregular but non-random dynamical behavior in the bubble column. The ability to classify the nature of its complex behavior can provide clues on methods to control the bubble dynamics. To identify the chaotic behavior of the system, the following data analysis techniques are used

on the time series measurements collected:

1. Power spectrum density
2. Bifurcation and route to chaos
3. Time return map
4. Correlation dimension and Kolmogorov entropy

As described in section 3.1, a square plexiglass column which is 5x5 cm in cross section filled with glycerine to 20 cm in height was used. Bubble dynamic behavior was monitored by using bubble injector inlet supply pressure and laser beam signals. The bubbles in the column exhibit transients when the independent variable air flow rate is changed. In this portion of the study, only non-transient behavior is investigated so care is taken to ensure that all transients have decayed.

5.1.1 Visual Observations

Air for generation of the bubbles is supplied from a commercial cylinder, where pressure drops are taken using pressure regulators. The air passes through a gas metering system, and is injected through a glass nozzle facing upward through the bottom of the column. The bubble formation at the nozzle is a surprisingly complex phenomenon. The pressure fluctuations in the gas supply line, due to the formation and detachment of bubbles at the nozzle, cause variations in the gas flow rate. In order to stabilize the pressure and thus the air flow rate in the rotameter, the control needle valve is located downstream of rotameter. With this placement of the needle valve, the pressure drop taken across the needle valve largely isolates the gas flow measurement in the rotameter from the bubbling. A typical sequence of bubble behavior as the air flow was gradually

increased from a low flow rate to a higher flow rate is illustrated in Figure 10.

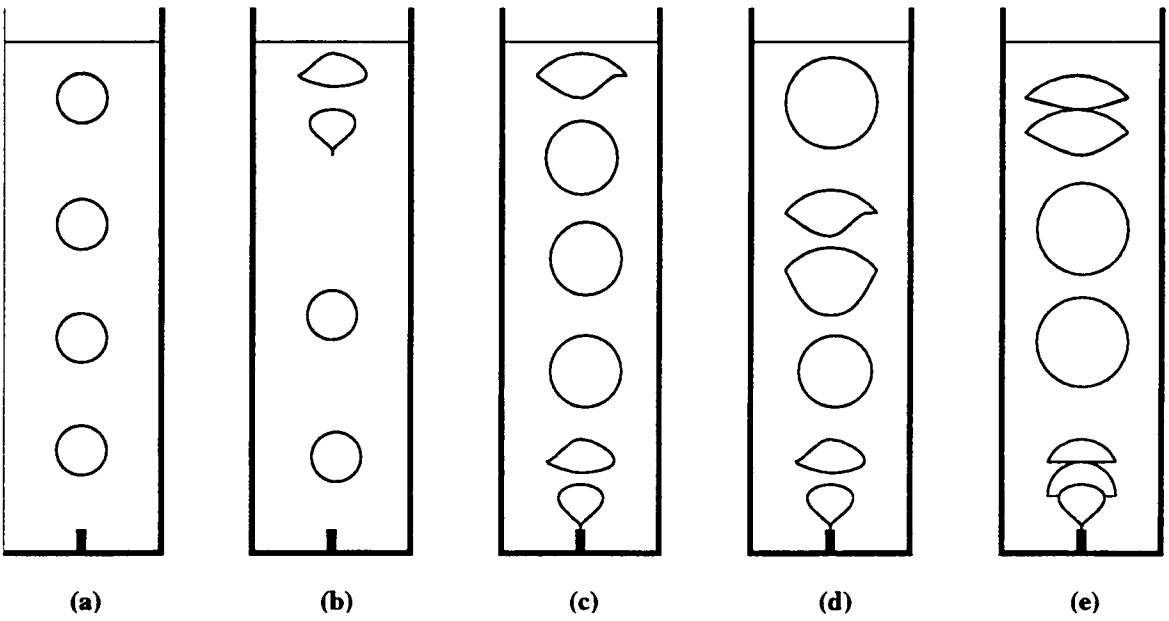


Figure 10. Bubble formation and pairing sequence as air flow rate increases

At low air flow rate, the bubbles are considered spherical and they form and rise in a smooth and periodic fashion as shown in Figure 10a. This assumption seems reasonable based on visual observation and time series measurement of both pressure and laser signals. All the time series signals illustrate same time interval and peak height which implies that all the bubbles have the same formation rate, velocity, and diameter. As the air flow is increased, both the generation frequency and bubble volume are observed to increase gradually as depicted in Figure 11. The number of bubbles in the column at any instant also gradually increases with air flow. All the air flow rates presented in this figure are before bubble pairing occurs at the nozzle orifice. The experimental flow corresponding to the first period-doubling bifurcation point (from period-1 to period-2) is at an air flow rate of 240 cc/min.

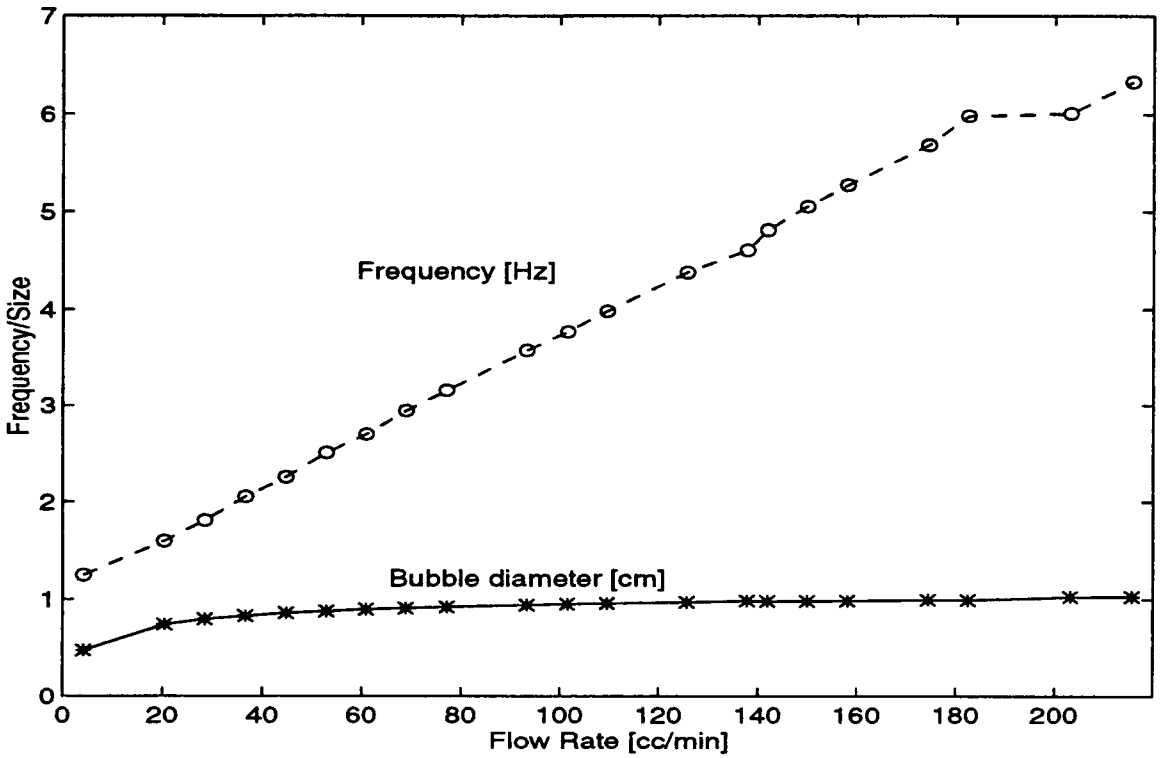


Figure 11. Variation of period-1 bubble frequencies and diameters as air flow rate increase

At sufficiently high air flow, the observed bubbles from pressure and laser measurements have two different spacings and velocities. The rising bubbles near the top of the column begin to group into pairs, and the qualitative bubble pattern is illustrated in Figure 10b. The physical bubble-pairing phenomenon occurs as a "trailing" bubble moves up relative to its "leading" bubble. Such observation is mainly due to the reduced drag on the trailing bubble by the wake of the leading bubble. This behavior begins when the bubble formation rate is sufficiently high to reduce bubble spacing so that trailing bubbles start to feel the wake effect of their leading ones and then accelerate upward. As the trailing bubble gets closer to the leading bubble, the shapes of both bubbles are observed

to distort smoothly toward coalescence. The bottom of the leading bubbles are distorted, becoming concave to accommodate the merger with the trailing bubble. Subsequently, the interfacial tension is observed to collapses, and a single larger bubble is formed which returns to a spherical shape.

The pairing and coalescence zone moves toward the nozzle as air flow is further increased. When the coalescence point is near the nozzle tip, a pair of bubbles is generated from the nozzle and their shapes are slightly different. A period-2 pattern in the pressure and laser monitoring measurements indicates the formation of two distinctive bubbles which immediately coalesce. The new spherical shaped bubble with a relatively bigger volume (due to coalescence) rises in the column. With further increase in air flow, a second coalescence, similar to the first is observed. Again it begins at the top of the column, and then migrates down with increased flow. When the second coalescence reaches the nozzle, a period-4 pattern from four different bubbles is obtained due to the combination from a first and second coalescence.

When the air flow is increased beyond that for the period-4 bubbling pattern near the nozzle, no clear pattern is visually observable. Visually, multiple coalescences appear to occur at random locations in the column, and the bubble patterns appear chaotic. A detailed description of bubble behavior is quantified using Chaotic Time Series Analysis methods (CTSA) as well as verifying the existence of the chaotic regime. CTSA methods also identify a period-8 regime from the pressure signals. This period-8 regime has not been previously observed in chaotic bubble analysis.

5.1.2 Time Series Pressure Measurements

The first indication that the experiment has chaotic behavior is the observation of the signal amplitude with time on an oscilloscope or data acquisition system display. A system with a repetitive cyclic motion is called periodic, a system with neither a visible pattern nor periodicity but is not random, is considered chaotic.

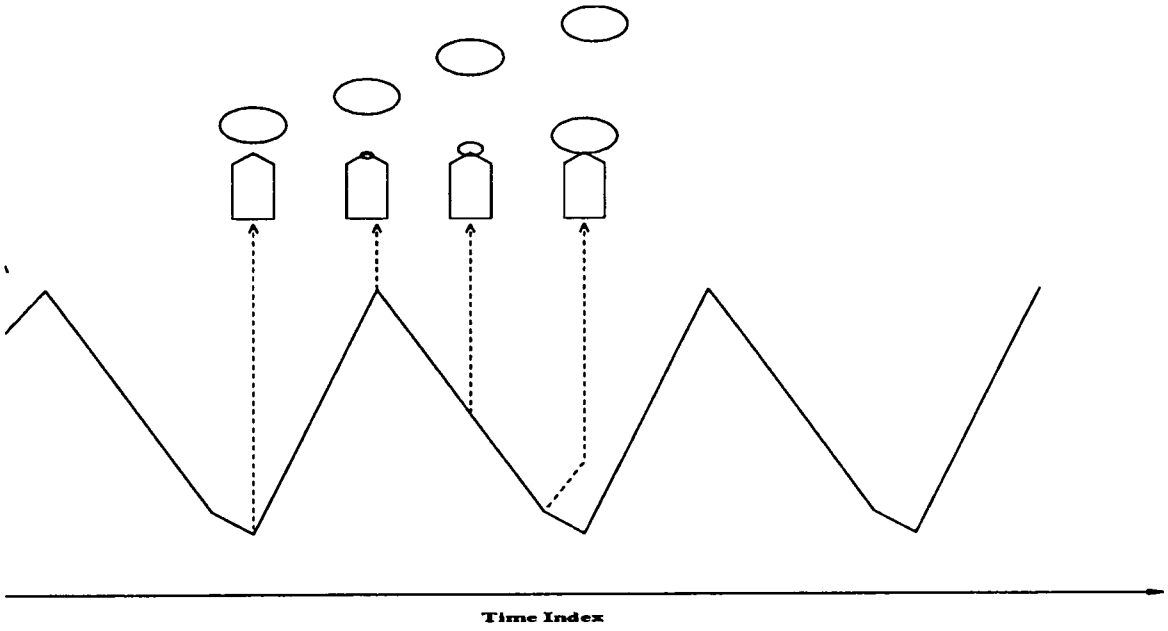


Figure 12. Interpretation for time series pressure measurement

Air flow is supplied to the air supply system for bubble generation. When the nozzle orifice is covered with liquid (there is no bubble connected to the nozzle), the pressure in the supply line, as determined by the transducer, gradually increased. Once the surface tension of the liquid across the orifice is overcome and a bubble just forms, the pressure stops increasing. Then the bubble grows at the nozzle and the air pressure drops. When the bubble is large enough that the buoyancy force and momentum from air flow

into the bubble overcomes the surface tension holding the bubble on the nozzle, the bubble pulls away and detaches from the nozzle. The cycle then repeats and another bubble is formed. This hypothesis of bubble pressure increases and decreases in the supply line is illustrated in Figure 12. Typical time series pressure signals corresponding to period-1, period-2, period-4, period-8, and aperiodic bubbling are shown in Figure 13a-f.

Visual inspection of period-1 bubbling of Figure 13a, shows that the positive and negative peak height and shape are all very repetitive. This observation suggests that each bubble produces the same pressure oscillation and is the same as the previous or the following bubbles. This period-1 bubbling behavior, obtained by the pressure signal, occurs at a flow below the first bubble pairing near the nozzle, and all the measured signals are considered "clean". As air flow is increased, the bubble pairing phenomenon starts near the top of the column and then gradually moves down toward the nozzle. This observation is mainly attributable to the wake effect of the leading bubble on the trailing bubble. The pressure transducer measuring bubble formation at the nozzle is unable to detect coalescences in the column.

When the bubble pairing phenomenon occurs very near the nozzle as air flow is increased to a critical value, the pressure fluctuations of a bubble differing from its previous and following bubbles is detected by the transducer as pressure oscillation differences. The time series plot the exhibits two distinct peaks and intervals. A higher peak and longer time interval represent the larger leading bubbles while the smaller trailing bubble leads to a lower peak and shorter time interval. This period-2 bubbling behavior involves the formation of two distinct bubble types for a complete cycle, and a period-2

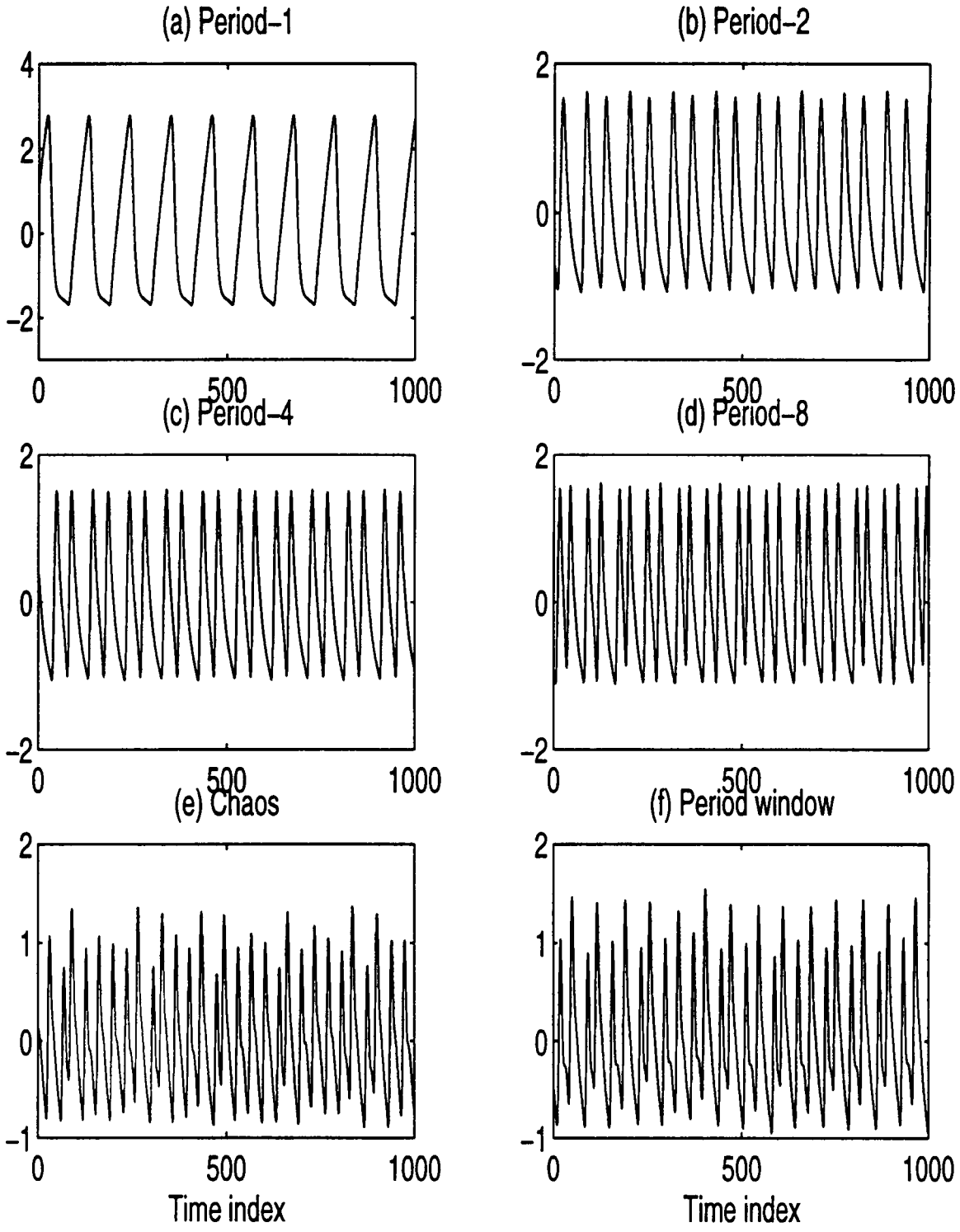


Figure 13. Time series for pressure measurements at flows [cc/min] (a) 137.9, (b) 315.4, (c) 390.1, (d) 553.9, (e) 1044.7, (f) 835.4

plot is illustrated in Figure 13b.

Figure 13c shows time series signals with four distinct pressure peaks and time intervals due to two sequential coalescences near the nozzle at an even higher flow rate. Each peak and interval represents the bubble behavior of four different types of bubbles for a complete cycle. This type of bubble formation is designated as period-4 bubbling. As air flow is further increased, a narrow period-8 region is observable and its representative time series plot is shown in Figure 13d. Theoretically, a complete cycle of four bubble coalescences are expected to occur near the nozzle with eight distinct peaks and time intervals. However, it is difficult from visual observation of the time series plot to definitely confirm the presence of this period-8 regime in the column. Therefore, additional diagnostic tests are necessary to confirm the presence of this period-8 regime. In a later section, this period-8 regime observation based on time return map calculation is revisited.

As air flow is increased above the critical value for a period-8 regime, multiple coalescences are observed to take place at seemingly random locations in the column, and the bubble formation and detachment appears chaotic as shown in Figure 13e. The peaks and time intervals presented in the plot confirm the nonrepeating nature of the bubble behavior. However, the pattern is not random and exhibits deterministic chaos as illustrated in the later analysis. Beyond the onset of chaos, a multi-period bubbling pattern is also observed in the measurement. This observation indicates the existence of periodic windows in this bubbling system, and its time series plot is depicted in Figure 13f.

5.1.3 Time Series Laser Measurements

The results of the time series measurements from the lower laser beam located 1 cm above the tip of the injection nozzle are shown in Figure 14a-f. The selected laser signals represent the typical period-1, period-2, period-4, and aperiodic bubbling pattern and seem to be consistent with pressure measurements. Figure 14a shows a period-1 bubbling motion so that each bubble passes the observation point of the laser beam with same velocity and sharpness. Figure 14b shows two distinguish peaks in the period-2 pattern. The period-4 bubbling pattern of double coalescences is illustrated in Figure 14c. At a flow rate where the pressure signal has period-8 character, the laser signal seems to have noisy period-4 or very noisy period-8. For chaotic bubbling, an aperiodic pattern in the laser beam measurements is observable in Figure 14e.

For comparison with the lower laser signal and pressure signal, measurements from the upper laser signal, located 8 cm above the nozzle tip are presented in Figure 15a-f. All of these measurements are recorded simultaneously with the measurements for pressure and lower laser signals. The time series signal from the upper laser at a flow rate giving period-1 for the pressure and lower laser signal shows two peaks and two time intervals. Since bubble coalescence first occurs near the top of the column and migrates toward the nozzle, this upper laser measurement indicates a period-2 bubble behavior while the bubbling process measured by the pressure and lower laser demonstrates a period-1 pattern. At the air flow used during pressure and lower laser measurements for period-2 bubbling patterns, the upper laser signals exhibit a single periodic bubble behavior corresponding to almost identical sharpness and speed. The noisy period-1 bubble

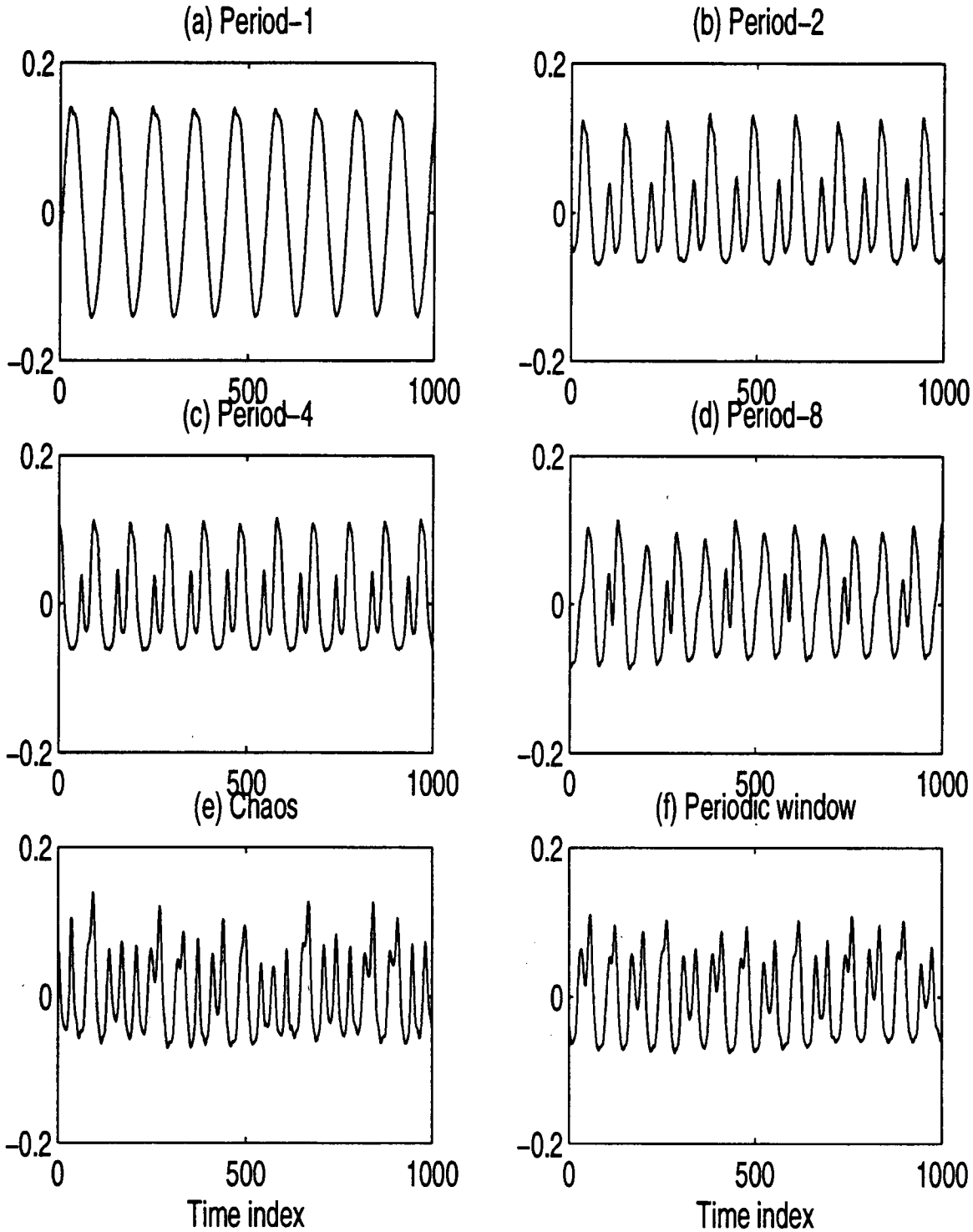


Figure 14. Time series for lower laser measurements at flows [cc/min] (a) 137.9, (b) 315.4, (c) 390.1, (d) 553.9, (e) 1044.7, (f) 835.4

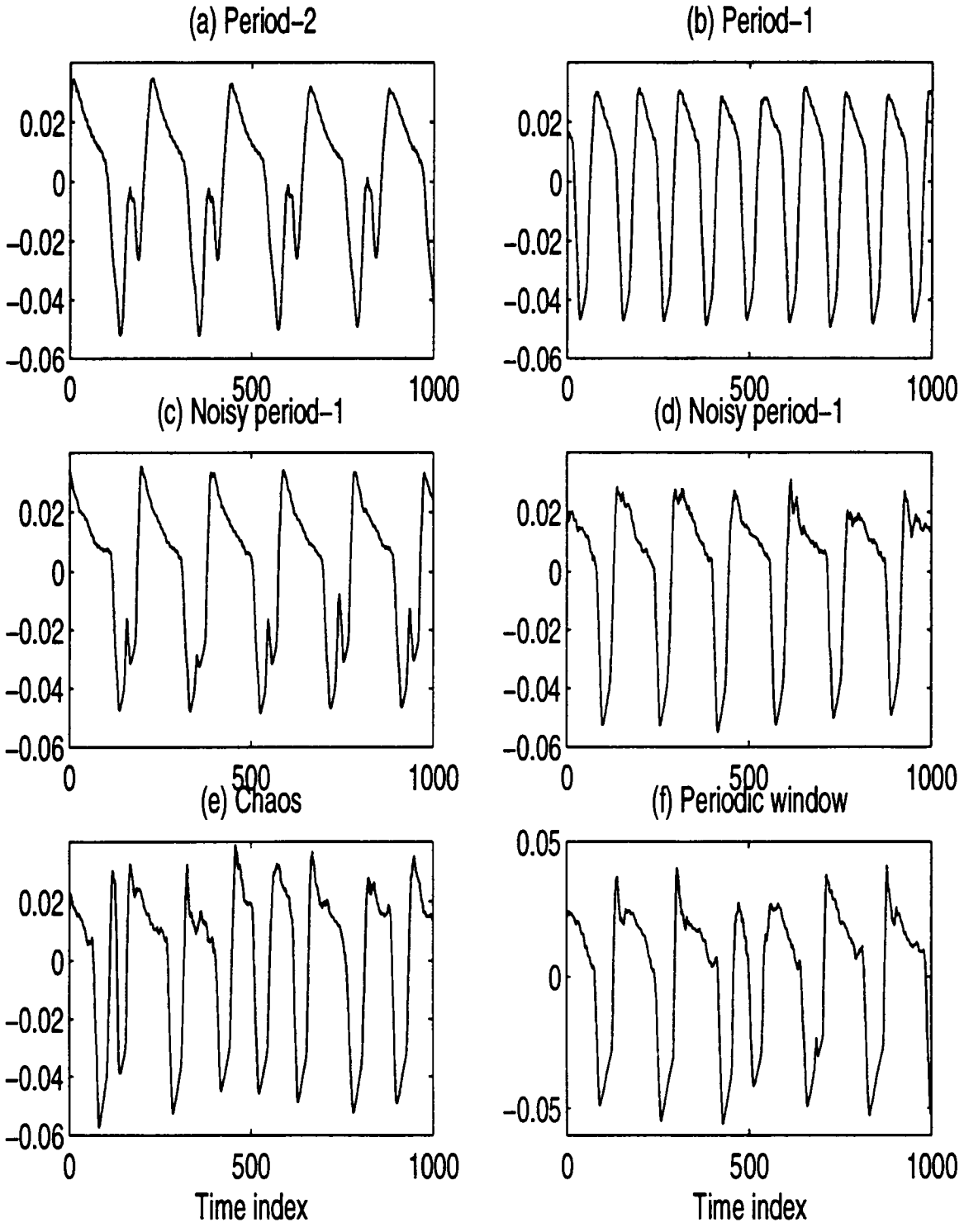


Figure 15. Time series for upper laser measurements at flows [cc/min] (a) 137.9, (b) 315.4, (c) 390.1, (d) 553.9, (e) 1044.7, (f) 835.4

behavior detected by the upper laser is attributable to the influence of liquid circulation in the column and of "burst" foam bubbles as well as continual shift in the vertical and horizontal point of bubble coalescence in the column space. The above observations lead one to speculate that the system exhibits spatial and temporal character.

To confirm the spatial and temporal character, a short set of experiments was carried out to study the bubbling pattern depending on measurement location in the column. Results of these are discussed in a later section. Based on the pressure signal of period-4 and period-8 flows, the upper laser again exhibits a fuzzy period-1 pattern as well. As the air flow is increased into the chaotic regime, the bubbling patterns at the upper laser signals appear to behave irregularly.

5.1.4 Power Spectra

One of the indications of chaotic behavior in a system is the appearance of a broad spectrum of frequencies in the output when the inputs to the system are held constant. The characteristic frequencies of power spectra often enable one to differentiate between the periodic and chaotic motions of a system. This classical linear method is considered useful for the bubble system of low dimension (i.e. low number for degree of freedom). The character of low dimension will be quantified in the correlation dimension and entropy section.

Power spectra are generated by transforming the information from time series measurements into Fourier frequency domain series. Time series data of 60,000 points are equally divided into 7 blocks, and the real and imaginary parts of the transform for each block are squared and added together to obtain the corresponding power spectrum. The

results of each block are averaged in order to produce a composite power spectra for each experimental condition. A complete presentation of power spectra results for all the experimental conditions would be lengthy and somewhat pointless. Therefore, typical power spectra of pressure signals corresponding to the same data sets as the time series measurements presented in section 5.1.2 are shown in Figure 16a-f. The results of this analysis demonstrate period-1, period-2, period-4, and aperiodic bubbling processes in the column.

An example of power spectra for bubbling at the period-1 regime is illustrated in Figure 16a. A single dominant peak at a frequency of 4.6 Hz as well as two smaller peaks in the spectrum plot represent period-1 bubbling. If the dominant frequency is ω, then the appearance of small peaks after ω are called the harmonic of the dominant frequency ω. Numerically, these two smaller peaks are just the harmonics of the dominant peak of 4.6.

Figure 16b depicts the power spectrum for a single coalescence occurring near the injector. The dominant peak gives the bubbling frequency of 8.7 Hz. The peak at 4.4 Hz is the bubbling frequency resulting from the period-2 cycle. The other 4 peaks are again harmonics. Similarly, the power spectrum for double coalescence occurring near the nozzle is shown in Figure 16c. The principle bubbling frequency is at 10.3 Hz and the frequencies of 5.1 Hz, 7.8 Hz, and 15.4 Hz indicate the complete cycle involves formation of four distinct bubble types.

An illustration of a broad spectrum of frequencies is shown in Figure 16e. The spectra show a broad-band with a power-law type decay at higher frequencies. Figure 16e indicates the possible chaotic bubbling behavior of the system. Figure 16f shows discrete

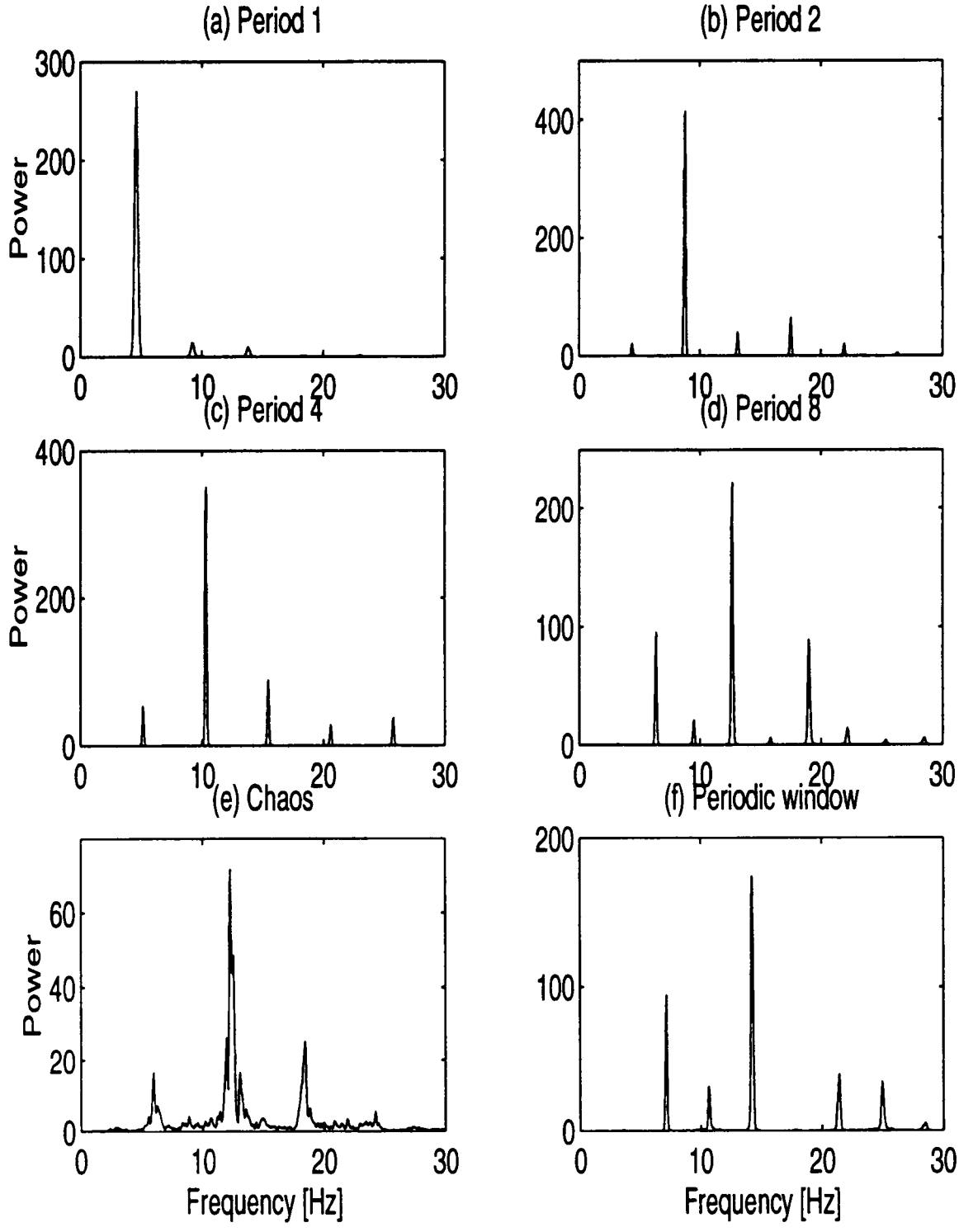


Figure 16. Power spectra of pressure measurements for different bubbling motions at flows [cc/min] (a) 137.9, (b) 315.4, (c) 390.1, (d) 553.9, (e) 1044.7, (f) 835.4

peaks which further confirms the existence of a periodic window in the chaotic regime.

The observed changes in the power spectra such as the transition from a sharp peak to a broad band suggest that the bubble system undergoes a transition from periodic to aperiodic as air flow is increased. However, these results do not give detailed information on the type of chaotic motion as well as the evolution of subsequent chaotic regimes. Therefore, further investigation needs to be carried out to confirm the system bifurcation and the route to chaos as a system variable is altered.

5.1.5 Bifurcation and Route to Chaos

The investigation into the transition from periodic to aperiodic oscillation by changing a system variable is a crucial step in identifying a deterministic chaotic system and evolving route to chaos. This procedure is designed to determine if the bubbling system has steady or periodic behavior for some range of the parameter space. In this way, one can have confidence to claim the system is in fact deterministic and such deterministic chaotic behavior is not caused by random noise. To achieve this goal, a bifurcation diagram is constructed in order to demonstrate system motion change with a variation in the system independent variable of air flow.

With a change in the input variable of air flow for this bubble system, the bifurcation diagrams are constructed to exhibit an overall pattern of change in bubble periodicity of the system. The results are illustrated in Figure 17 and Figure 18 for pressure signals and low laser beam signals, respectively. At each flow condition, bubble oscillation periods are determined by calculating the time intervals between successive crossings in the upward direction of the zero values for both measurements. All the

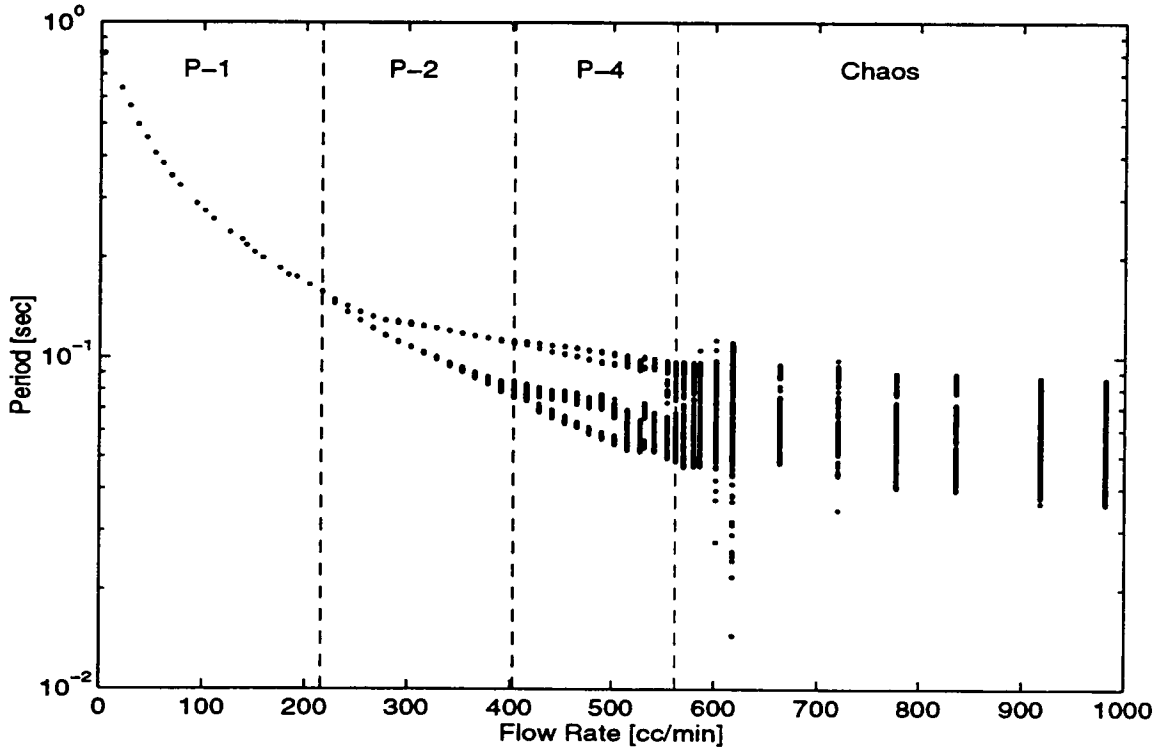


Figure 17. Bifurcation diagrams for pressure measurements as air flow increases

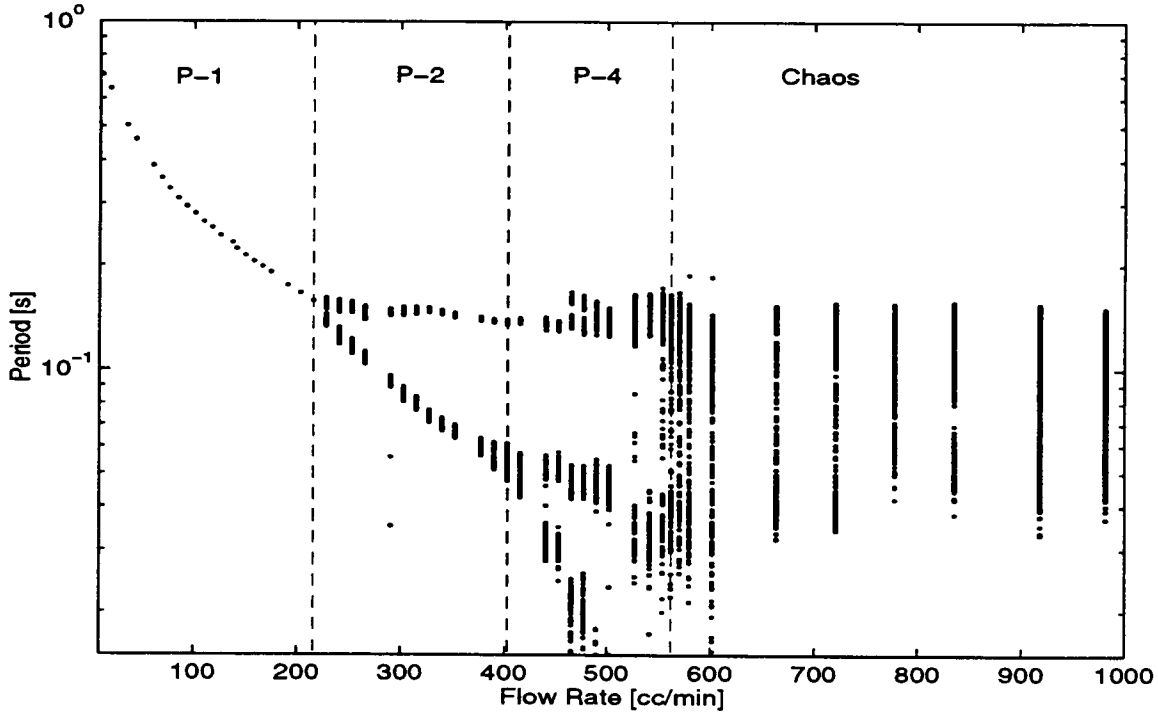


Figure 18. Bifurcation diagram for lower laser measurements as air flow increases

calculated intervals are plotted against the operating condition of air flow.

For both diagrams, the system starts with a fundamental periodic motion of period-1. As air flow is increased, the system motion undergoes a bifurcation and changes to a periodic motion with twice the period of the original oscillation. At even higher air flow, the system bifurcates to period-4 bubbling motions. Finally, a band of periodicity values is obtained as air flow is increased beyond the critical value for period-4. Based on the above observations, the investigated bubble column exhibit a period-doubling route to chaos.

5.1.6 Time Return Map

Time return map perhaps provides the simplest visual presentation to describe the dynamics of the system allowing periodic and nonperiodic motions to be distinguished. To construct the map, a sequence of time interval data needs to be extracted from time history measurements. The sequence of time interval data is generated with the notation that $t_{n+1} = f(t_n)$, based on the calculation of the time difference between successive signal crossings of a designated valve in the positive direction. The calculated interval t_{n+1} is plotted against its previous data point t_n. The points produced by plotting successive pairs of time intervals of the signals reflect the periodicity of the system motion and are used to characterize the behavior of the bubbling over time. Time return plots for pressure measurements corresponding to five distinct regions of periodicity are depicted in Figure 19a-f. In addition, Figure 20a-d illustrates the return plots for the periodicity of lower laser measurements. Upper laser measurements are not presented because they seem to be inconsistent in describing the bubbling behavior, due to the spatial and temporal character in the column.

As described in the bifurcation section, a period-doubling phenomenon is observed in the bubble column. Figure 19a-d depicts time return plots that contain 1, 2, 4, or 8 pints as air flow is increased using the calculated time intervals to describe bubble behavior from pressure measurements. Each of the points represents a system steady state or a fixed point and the plots indicate the bubbling periodicity of 1, 2, 4, or 8. Figure 20a-c shows that the return plot of the laser signal time intervals form maps of 1, 2, and 4 points, which correspond to the occurrence of no, single, and double bubble coalescences, respectively. A periodicity of 8 for lower laser signals is missing due to the presence of dynamic noise or the spatio-temporal nature of the system. A detail discussion of noise effects on bubble measurements is beyond the scope of this study. However, the dynamic noise for this experiment is conjectured to come from the surroundings in the form of mechanical vibration, air flow deviation, and small foam bubbles in the column. In fact, the period-4 and period-8 maps show the apparent "fuzziness" of the time intervals in Figure 19c-d and Figure 20c. Still, the fuzzy regions around these points are not just random but rather suggest that there is a partial filling-in of the attractor that emerges more completely at higher flow rates.

As air flow reaches beyond the onset of chaos, the bubbling becomes aperiodic resulting in a chaotic attractor on the return plots as shown in Figure 19e and Figure 20d for pressure signals and lower laser signals, respectively. The return plots show that they consist of an infinite set of return points and these successive points seem to define a curved region like a "walking stick". This structured set of points continues to exist as long as the measuring time. This kind of motion is called a strange attractor of the system.

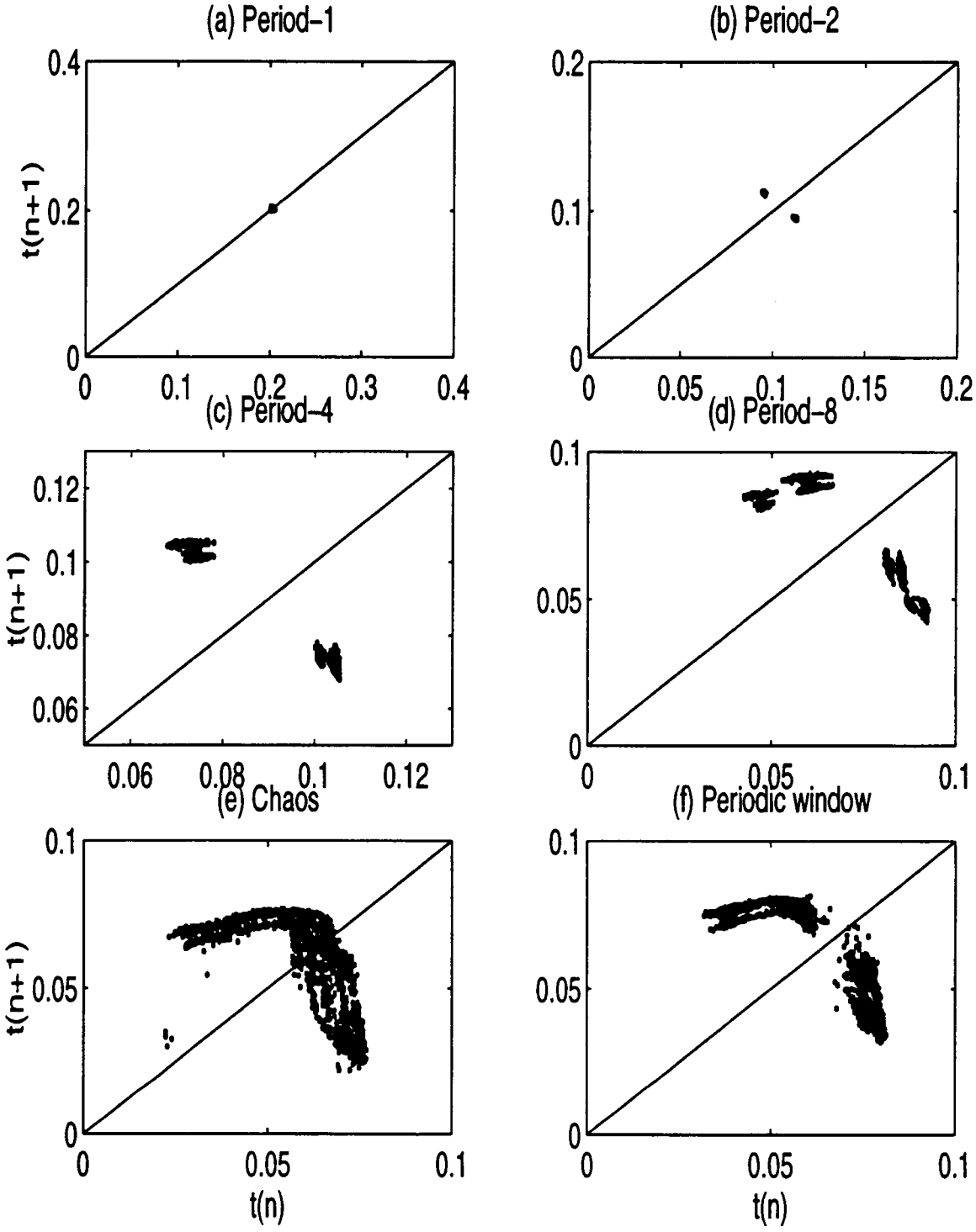


Figure 19. Time return plots for pressure measurements of different bubbling periodicity at flows [cc/min] (a) 137.9, (b) 315.4, (c) 390.1, (d) 553.9, (e) 1044.7, (f) 835.4

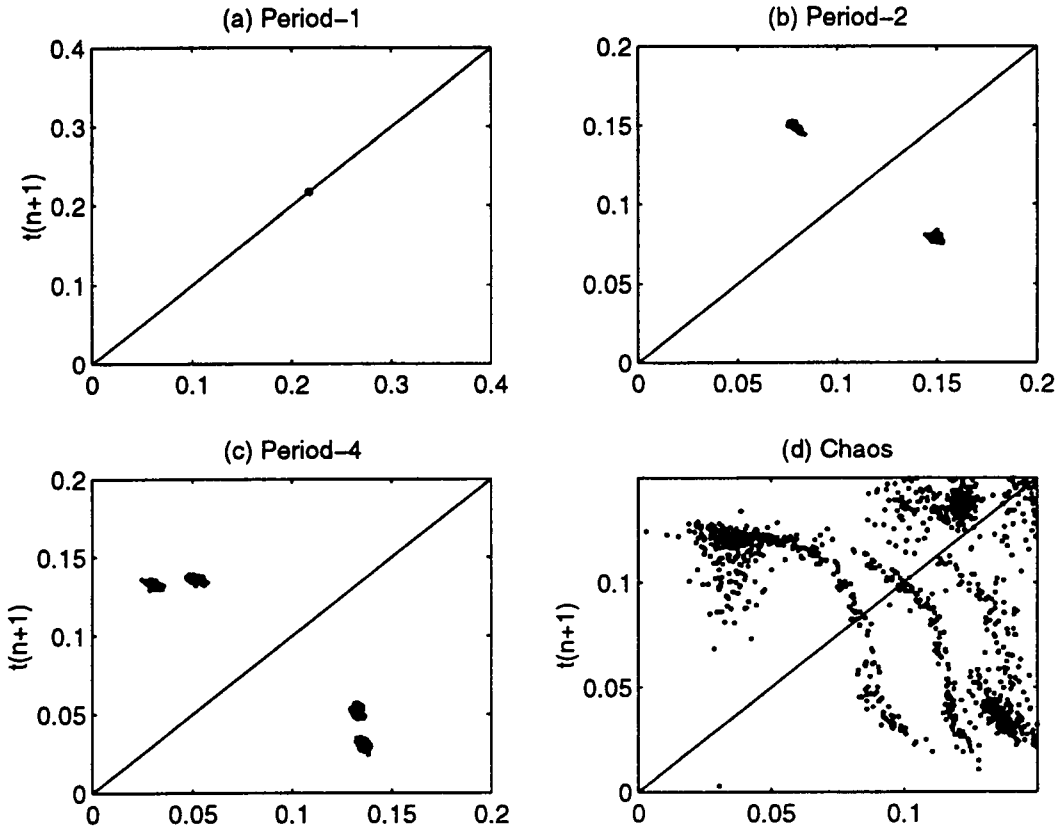


Figure 20. Time return plots for lower laser measurement of different bubbling periodicity at flows [cc/min] (a) 137.9, (b) 315.4, (c) 390.1, (d) 1044.7

A quantitative measure of the strangeness of the attractor (correlation dimension and entropy) will be discussed in the following section. Another important feature is the appearance of the noisy periodic windows. At this stage of the bubble column investigation, no definite conclusion can be drawn from this observation. However, such periodic window phenomenon is conjectured to result from the resonant effect of bubble-to-bubble interaction and the dynamic noise that participates in the bubble dynamics as opposed to measurement noise. As described earlier, a period-8 regime reflecting a

complete cycle of four bubble coalescences for pressure signals is observed based on the return map plots. This observation indeed suggests the presence of a period-8 regime as well as period-doubling routes to chaos.

5.1.7 Correlation Dimension and Kolmogorov Entropy

In previous section of this chapter, a set of qualitative diagnostic tests that describe the characteristic of both periodic and chaotic oscillation generated by the bubbling system were presented. Obviously, many other diagnostic tools can be used to verify the chaotic behavior of the bubbling system such as phase space reconstruction, mutual information, Poincare map, and others. Regardless, numerical methods for estimating the correlation dimension and Kolmogorov entropy seem to be extremely useful and convincing to quantify chaotic behavior in the bubble column. Both methods are, in principle, the same for estimating the complexity of the system behavior and provide information for readily detecting the system changes as air flow is varied.

The estimated values of dimension and entropy for each data set are calculated using the maximum-likelihood approach along with their corresponding confidence limits. As described in Chapter 4, the algorithms for determining both of these values, require the specification of appropriate embedding segment lengths of average cycle time and cut-off length scale for determining maximum-norm separation between trajectory segments for each data set. In this present study, data files with 60000 points are normally grouped into 30 bins for the average cycle time calculation. The segment method (i.e. points or factor) needs to be specified in order to apply these algorithms. For those data sets within period-1 and chaotic regimes, the average cycle time is used as the segment length and the

segment factor method is implemented by setting the cut-off length equal to one average absolute deviation of the mean for each data point. The value for the average cycle time of the flow just prior to the occurrence of the first period-doubling bifurcation (i.e. 228 cc/min with 73.8 sampling points per cycle) is used as the segment length to estimate the dimension and entropy values for all the data in period-2, period-4 and period-8 regimes (i.e. segment point method).

The correlation dimension and entropy estimates for pressure and lower laser measurements are depicted in Figure 21 and Figure 22, respectively. The entropy values are reported in bits per cycle, where a cycle is defined by successive upward crossings of the value specified at zero on the time series plot. These cycles represent the corresponding time interval between successive bubble formation in the column. For all the periodic regimes of pressure signals, the correlation dimension remains slightly above one and the entropy remained basically at zero. The lower laser measurements provide similar trends as observed by the pressure signals but the estimated values lie between one and one and a half for period-2 and period-4 regimes. This phenomenon is not surprising due to the fact that pressure measurements describe damped bubble behavior while laser signals reflect the exact bubbling pattern of the system. It might also arise due to the spatial dependence of the laser signal with height from the nozzle as discussed in the next section. Also, a slight error from the theoretical values for periodic regimes for the laser signals is mainly attributed to the effect of noise or possibly segment length obtained from the average cycle time is somewhat inaccurate. Nevertheless, all the above dimension and entropy estimations indicate periodic bubble behaviors in the column.

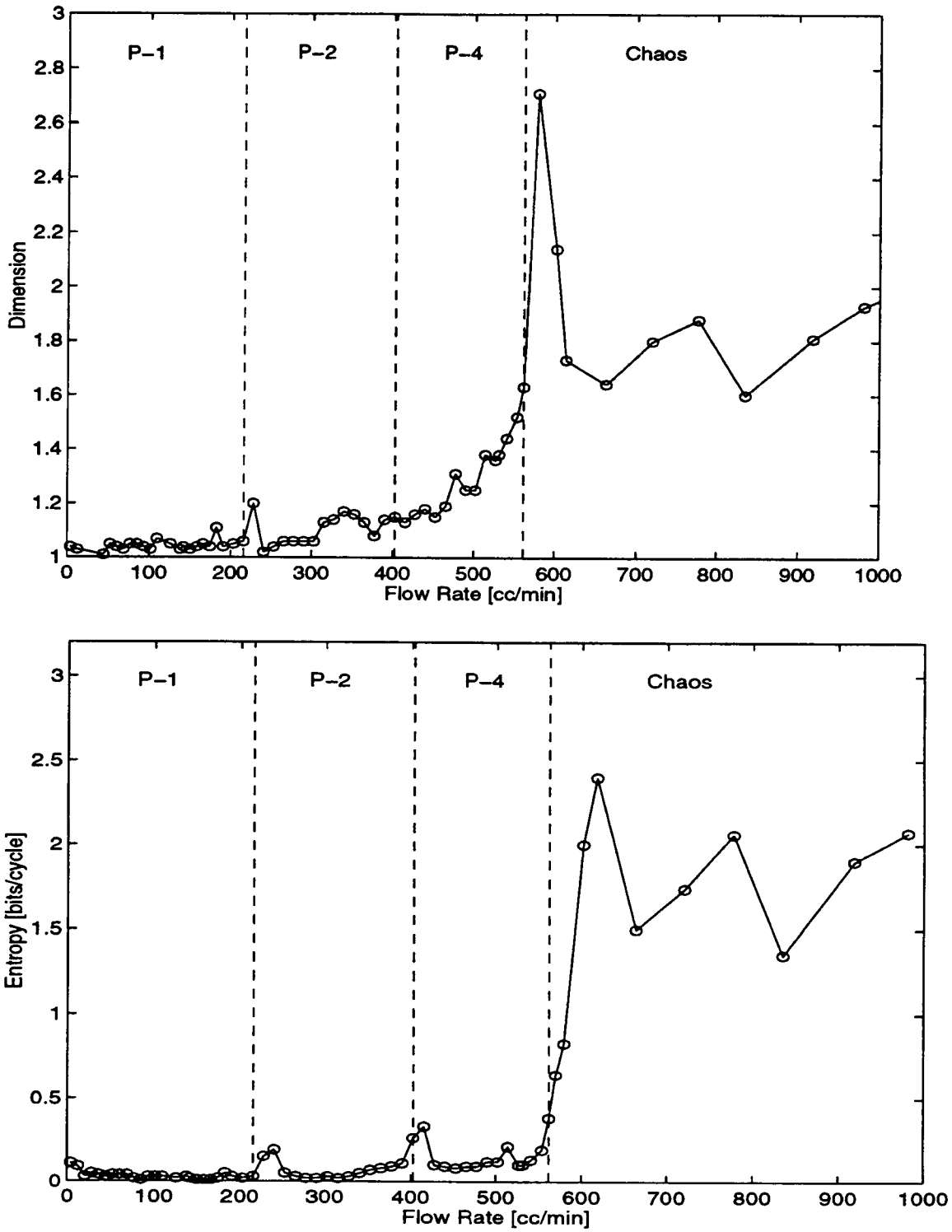


Figure 21. Correlation dimension and entropy for pressure signals

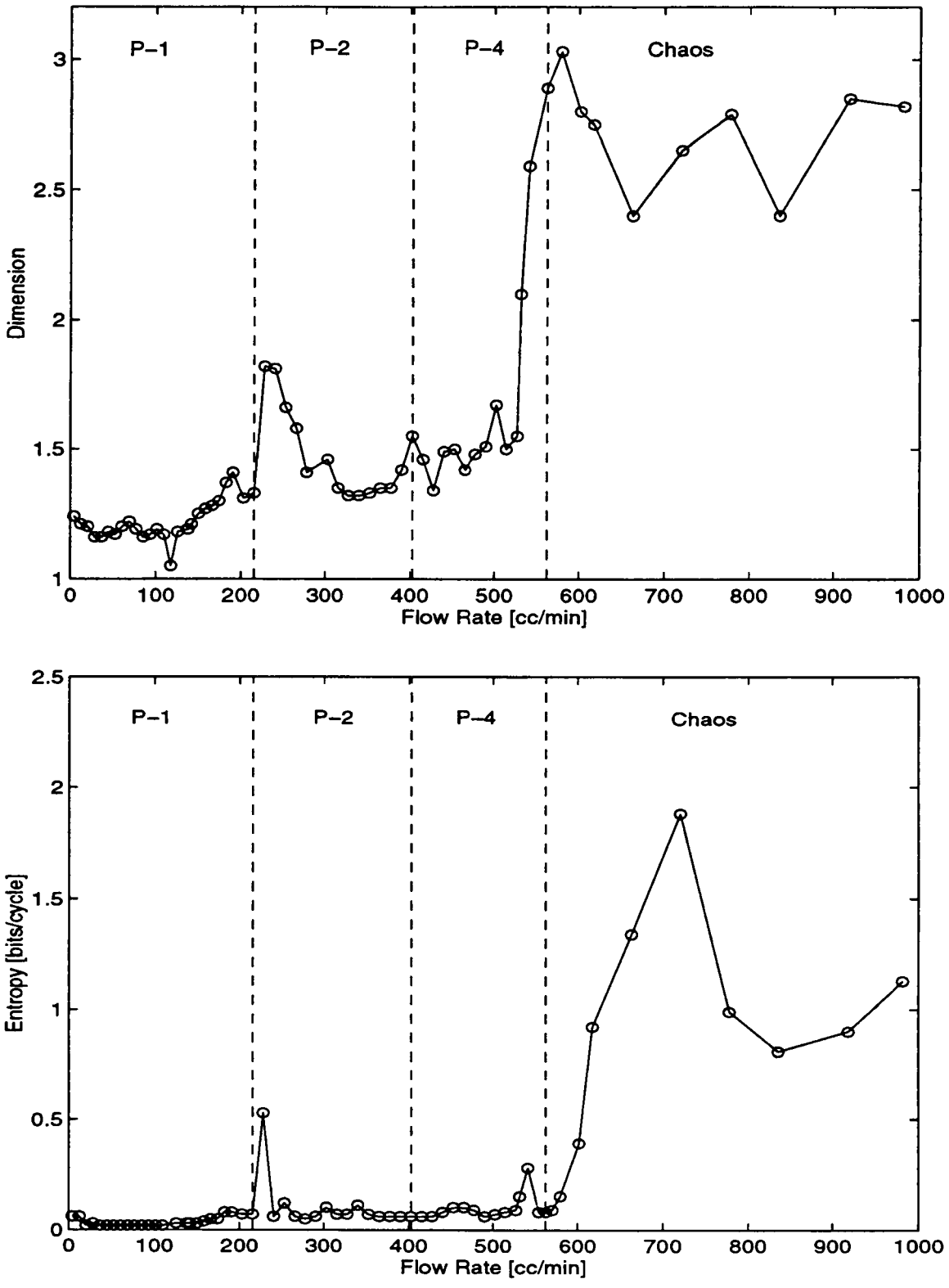


Figure 22. Correlation dimension and entropy for lower laser signals

For air flow beyond the onset of chaos, the correlation dimension increased rapidly above two and the entropy increased to a significant positive value for pressure signals. For laser signals, similar trends are observed with a higher value in dimension estimation. In chaotic regimes, the sudden drop in both dimension and entropy estimations take place at flows of 663.1 cc/min and 835.5 cc/min for pressure and laser signals, respectively. This observation indicates the existence of apparent periodic windows in the dynamics.

5.1.8 Spatio-temporal

Throughout the course of experimental study, several observations have demonstrated the dynamic features of the bubbling system depend on measurement location. Bubble coalescence that occurs near one measurement point (i.e. pressure and lower laser beam) is detected with respect to time, whereas the information of coalescence is damped to another measurement point (i.e. upper laser beam). Such information loss in both space and time suggests that the bubble column is a spatio-temporal system.

In order to investigate the spatial and temporal evolution in the bubble column, multiple laser beam locations along with pressure measurements are used to monitor the column. The centers of laser beams are positioned from 1 cm, 3 cm, 7 cm, and 9 cm above the tip of the nozzle in various experimental runs. The experimental apparatus and procedures are similar to that used in previous characterization study. The system dynamic states are determined based on the following data analysis techniques: time series measurement, time return map, power spectra, mutual information, and Kolmogorov entropy. These diagnostic tests seem to give consistent results for describing bubble behavior in the column.

All the system states are sampled after the decay of transients. A phase diagram that describes bubble coalescences in the bubble column along with its dynamics is shown in Figure 23. The system behaviors are separated by regions of different bubbling patterns (i.e. period-1 bubbling, bubble-pairings, and onset of chaos) for all the monitoring locations. Due to the wake effect and the instability of bubble-to-bubble interaction, bubble-pairing starts taking place near the top of the column.

In this discussion, the laser beams of 1 cm and 3 cm are grouped as lower laser signals while 7 cm and 9 cm are classed as higher laser signals. The phase diagram shows bubble-pairing initially occurring in the upper laser beam (9 cm) and then migrating down toward the nozzle. As the air flow is increased, the phase diagram shows the migration of the pairing zone down toward the nozzle. When the bubble coalescence occurs near the nozzle, both pressure and lower laser beams, determine a period-2 bubbling motion while the upper laser signals reflect a fuzzy period-1 pattern. However, the upper signals occasionally demonstrate aperiodic bubble behaviors.

To confirm such an argument, Figure 24 illustrates the return maps and mutual information plots for the laser beams positioned at 1 cm and 9 cm above the nozzle tip. The return plot for 1 cm consists of 2 points, and the corresponding mutual information plot shows a sequence of discrete peaks. The presence of these peaks indicates that the bubbling pattern is periodic and predictable. For the upper laser signal (9 cm) return plot, the system states fall in several regions and the bubbling pattern behaves irregularly. Based on the corresponding mutual information plots, the function for predicting the dynamics of the system decays exponentially to the extent that only very small peaks can be observed.

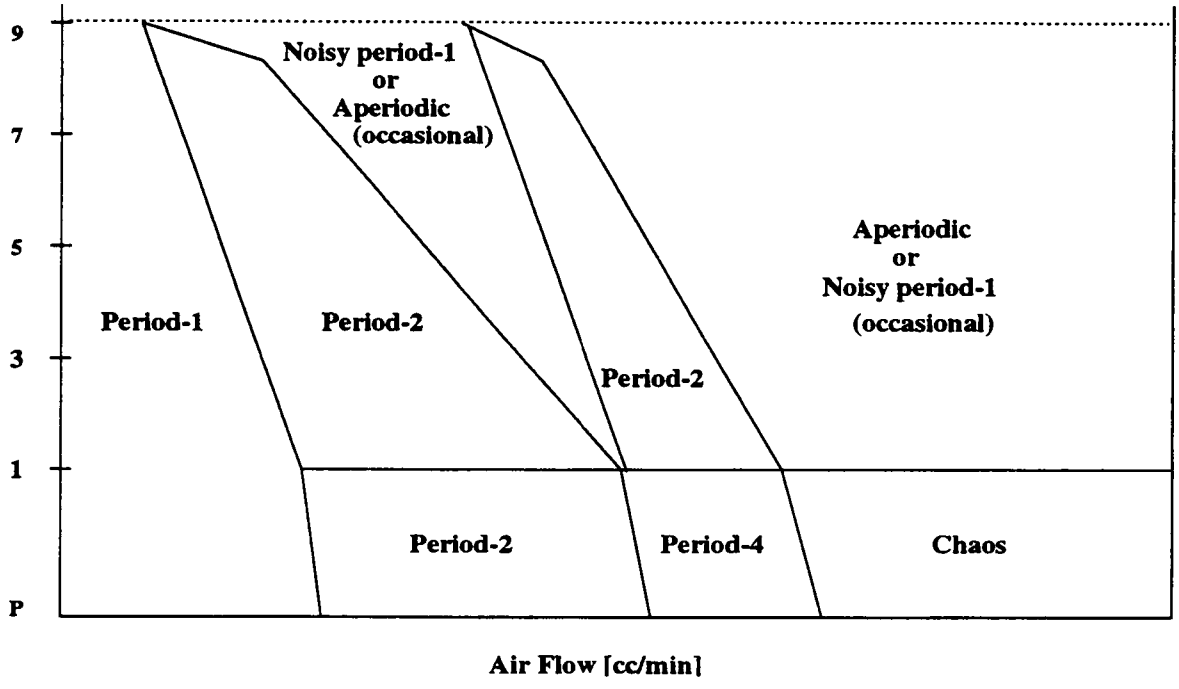


Figure 23. Phase diagram for bubble behavior at different measurement locations

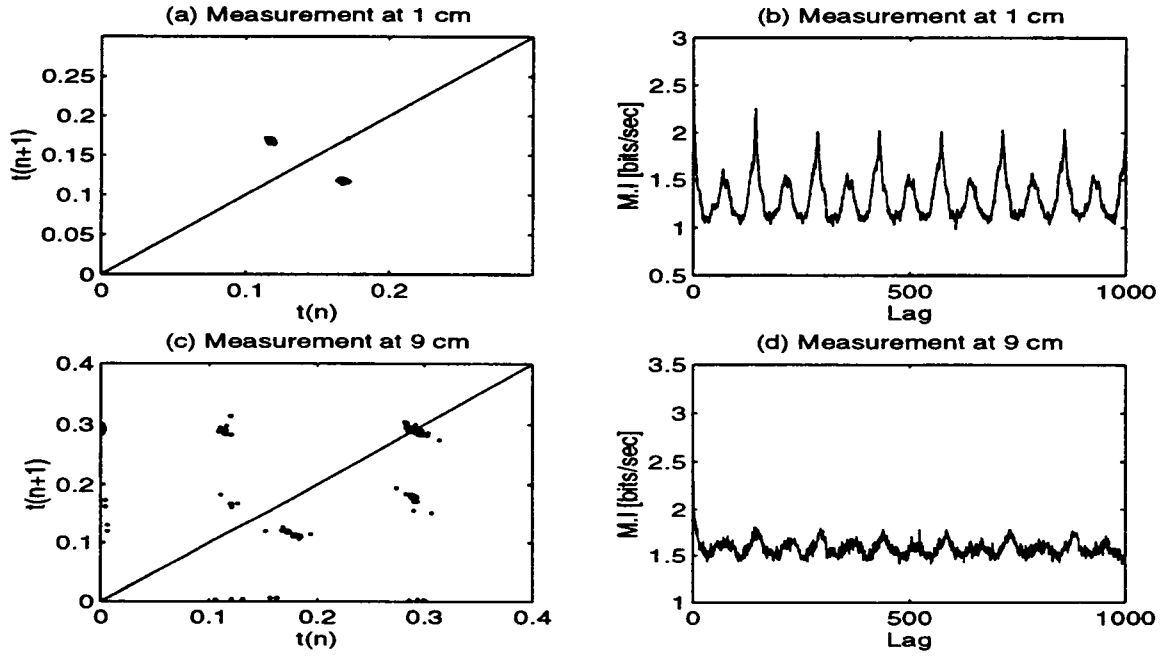


Figure 24. Confirmation of aperiodic bubble behavior at high measurement location with flow at 352.6 cc/min

This information further confirms the aperiodic bubbling pattern for the upper laser measurement location.

With the onset and migration of a second coalescence at still higher air flow, a transition pattern from unstable period-2 to noisy period-1 is observed again from the upper laser measurements. When air flow is further increased to the extent that pressure and lower laser signals exhibit a period-4 bubbling pattern, the upper laser measurements show an aperiodic bubble pattern with the exception of an occasional noisy period-1. Experimental evidence of this at different measurement locations, is summarized in Figure 25. The spatial results suggest that the system information is lost mainly due to bubble coalescence.

As the onset of chaos is reached and surpassed, the phase diagram features a chaotic and periodic region for lower lasers and upper lasers, respectively. Figure 26 summarizes the return plots to describe chaotic bubbling at different measurement locations. The lower laser signals show a layered appearance for the return plot and the upper laser signal give an aperiodic bubbling pattern. Based on the phase diagram, one can clearly see both pressure and lower laser signals undergo period-doubling routes to chaos as air flow increases. The upper laser measurements indicate the "irregular" bubble behavior depends on the location and movement of the paired bubbles in the column. Also, no clear route to chaos is observed for upper laser signals.

The phase diagram and its supporting plots illustrate some spatial and temporal information about the dynamics of the bubble column changing from periodic to chaotic as air flow increases from periodic to chaos. Next, the spatio-temporal behavior in the deep

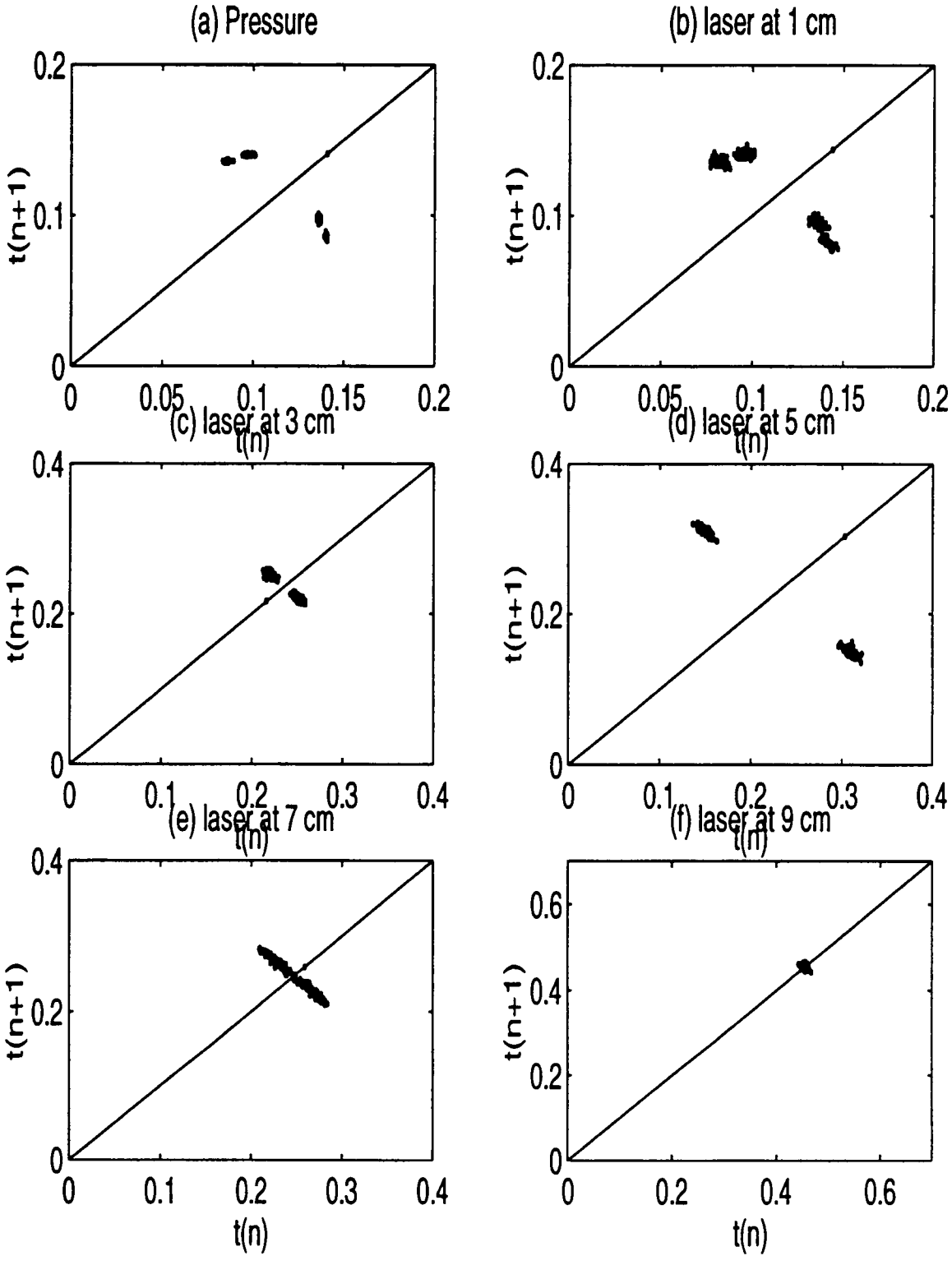


Figure 25. Bubble behavior of spatial measurements at flow of 506 cc/min

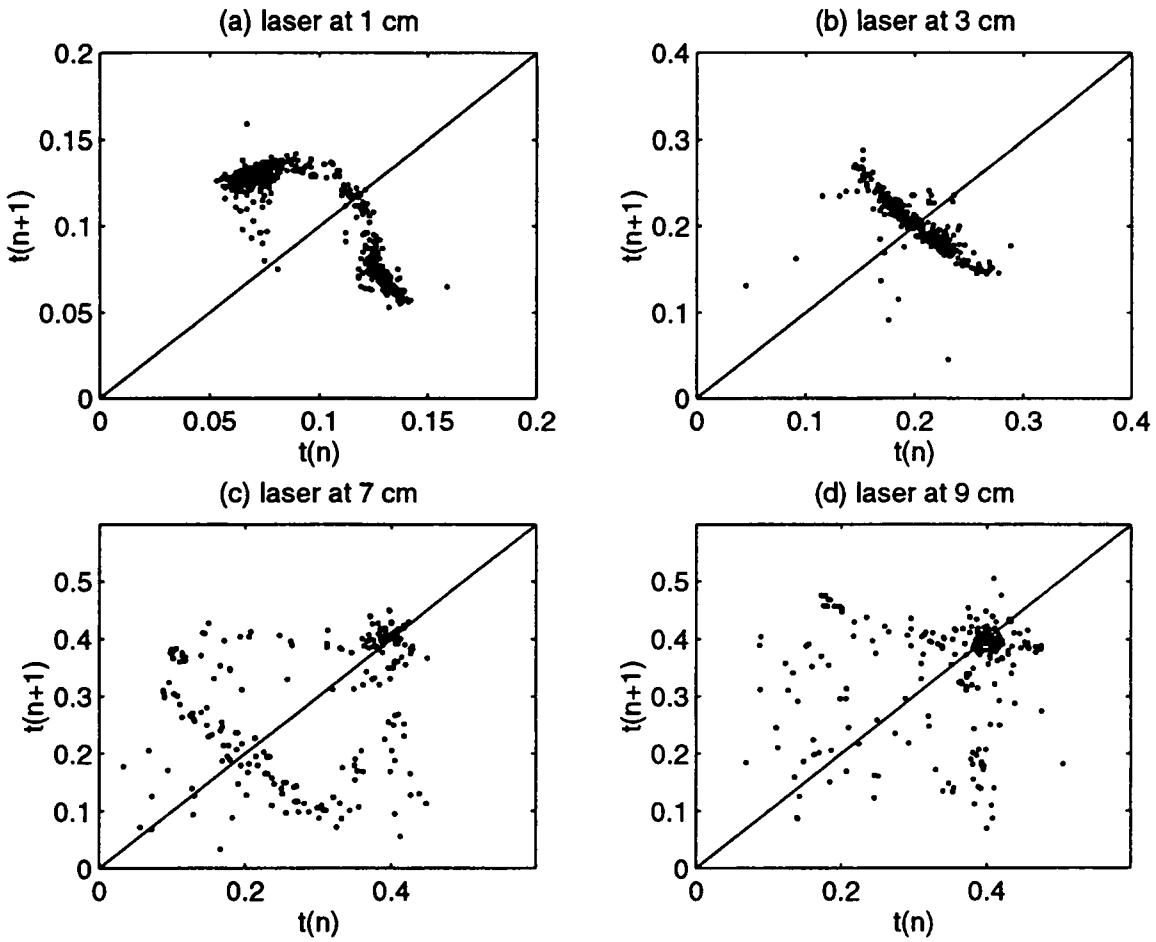


Figure 26. Chaotic bubble behavior of spatial measurements at flow of 569 cc/min

chaotic bubbling regime is quantified using Kolmogorov entropy and bivariate mutual information analysis. Entropy measures the degree of predictability between measurement locations and the bivariate mutual information function quantifies the shared information between localized measuring locations. Both of these methods are useful tools to verify the spatial and temporal behavior of the system.

The spatial character of chaotic bubbling is illustrated in Figure 27, which shows temporal measurements at 8 locations in the bubbling system. In Figure 27, the pressure

and laser measurements at 1 and 3 cm are measured simultaneously (equipment is available to only make 2 laser measurements simultaneously). As shown, chaotic bubbling is associated with bubble coalescence as well as the time and location at which the bubbling pattern is measured in the column. The corresponding Kolmorgorov entropy estimations are plotted as a function of measurement location in Figure 28. All the entropy estimations indicate finite positive values which imply the column is a chaotic system.

As described in the data analysis chapter, periodic phenomenon is characterized by zero entropy estimation; a random system yields an infinite entropy value; and a chaotic phenomenon is typically characterized by a finite entropy estimation. The plot shows the general increasing trend of the entropy estimations as the measurement location rises in the column up to 11 cm. This trend indicates an increase in complexity and a loss in information due to the spatio-temporal impact on the system. A sudden drop at a measurement of 13 cm suggests that the dynamics of the system are associated with bubble coalescence as well as their movement in the column. Also, this drop might involve the rising bubble burst at the surface of the liquid at 20 cm.

Typical bivariate mutual information plots for quantifying the relationship between the laser signals height above the nozzle of 3 cm and 7 cm with respect to pressure signals, are shown in Figure 29a-b. The maximum time delay to predict the spatial measurements with respect to pressure signals are summarized in Figure 30. The plot clearly shows that the degree of predictability in terms of delay between a location in the column and the nozzle pressure signal increases with distance as expected. The maximum peak value of the delay, which is associated with the degree of coupling between the

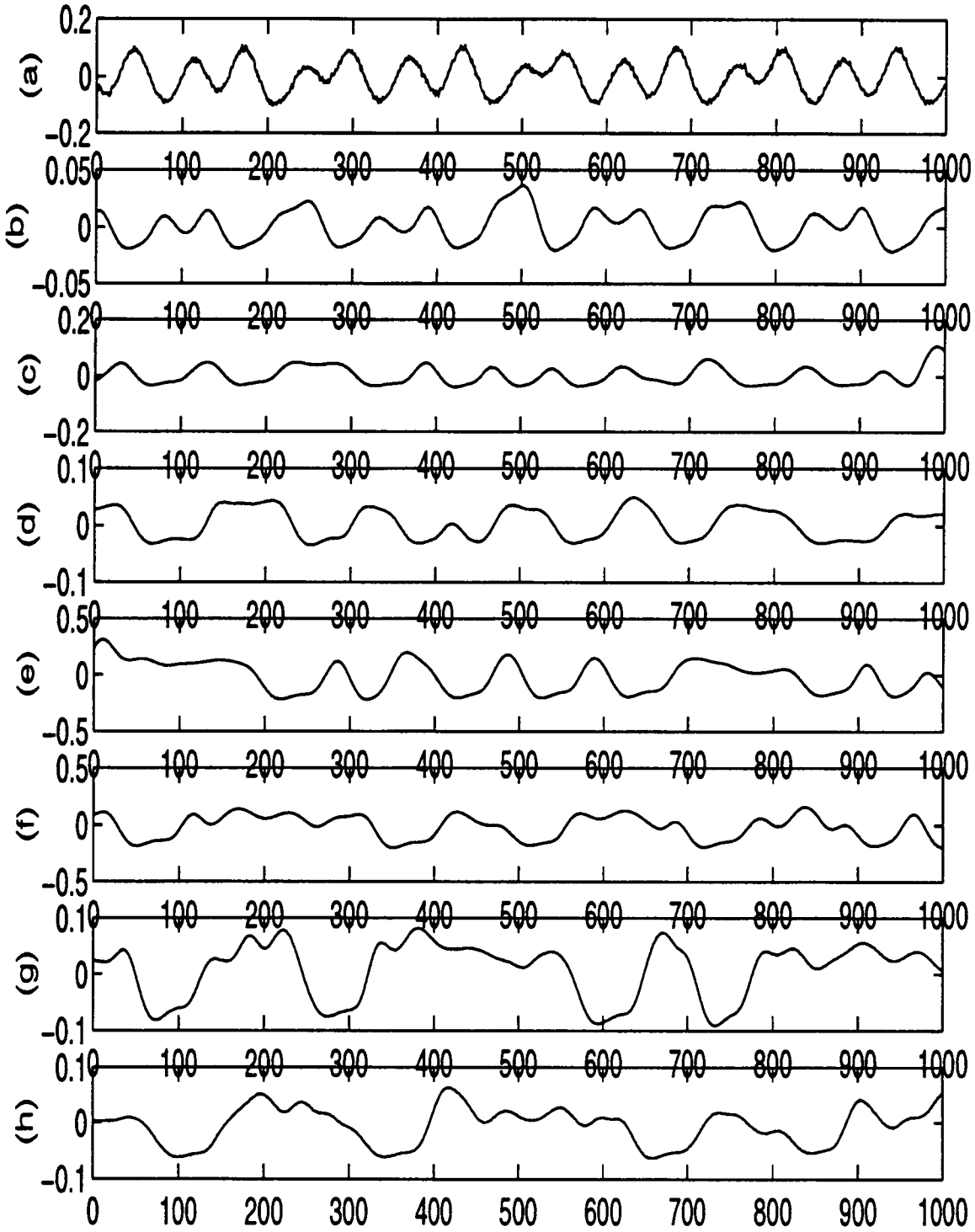


Figure 27. Time series of spatial measurements at flow of 918 cc/min: (a) pressure, and (b) - (h) lasers at 1, 3, 5, 7, 9, 11, 13 cms above the nozzle tips, respectively.

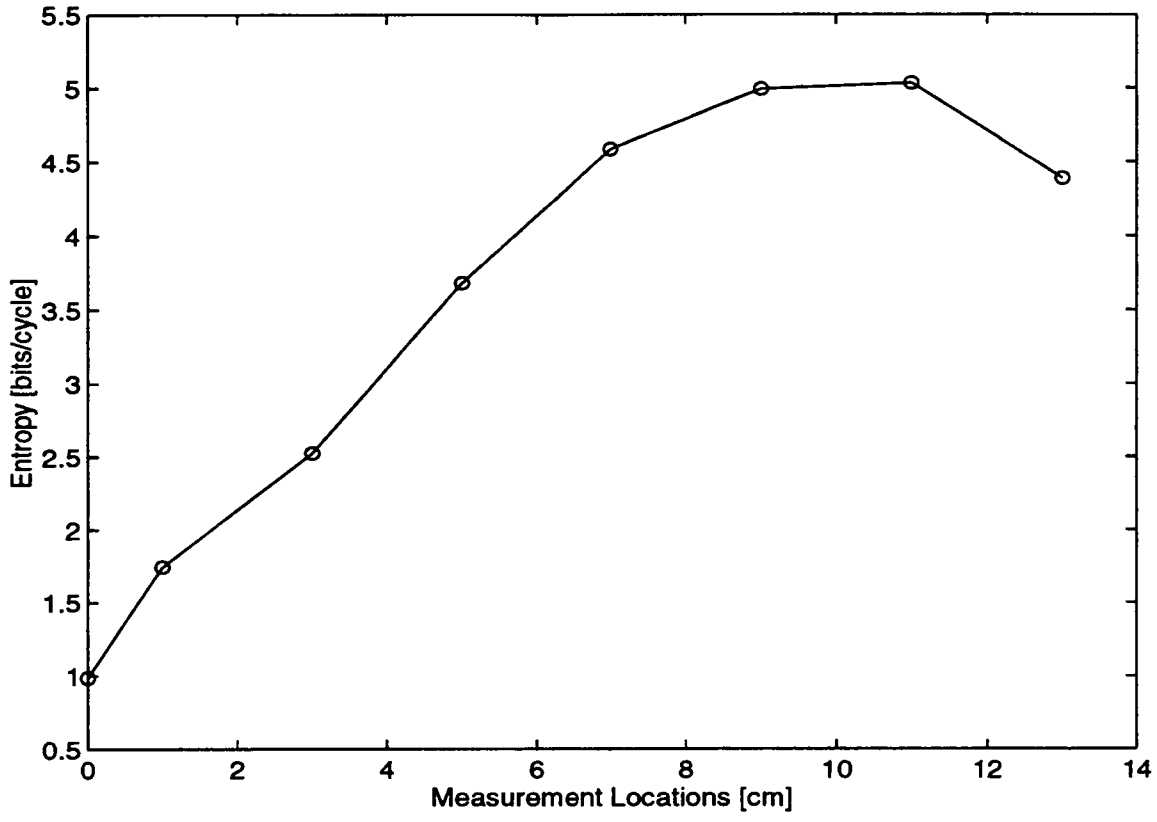


Figure 28. Entropy estimations for spatial measurements at flow of 918 cc/min (the measurement location of 0 corresponds to the pressure measurement)

measurements are plotted against measurement location and are depicted in Figure 31. Figure 31 indicates the degree of coupling between the laser and pressure signals decreases with distance. The leveling off of the peak values around 0.05 bits at a height of 5 cm, shows that there is almost no predictability of the state in the top of the column from the pressure signal. Such degradation of information indicates the character of spatial instabilities in the column and suggests that the bubble column is indeed a spatio-temporal system.

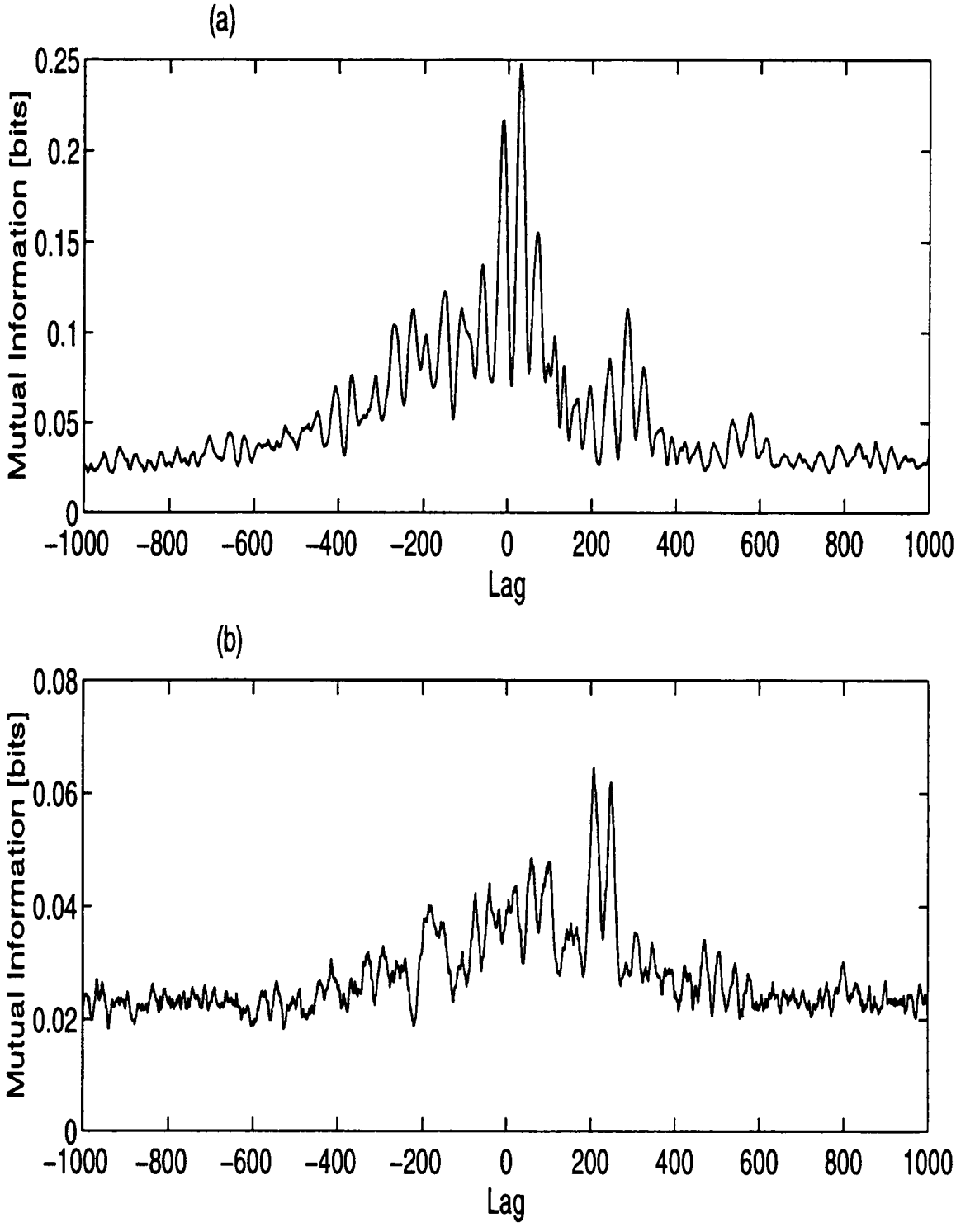


Figure 29. Mutual information for laser signals at (a) 3 cm above nozzle tip and (b) 7 cm above nozzle tip, with respect to pressure signals at flow of 918 cc/min

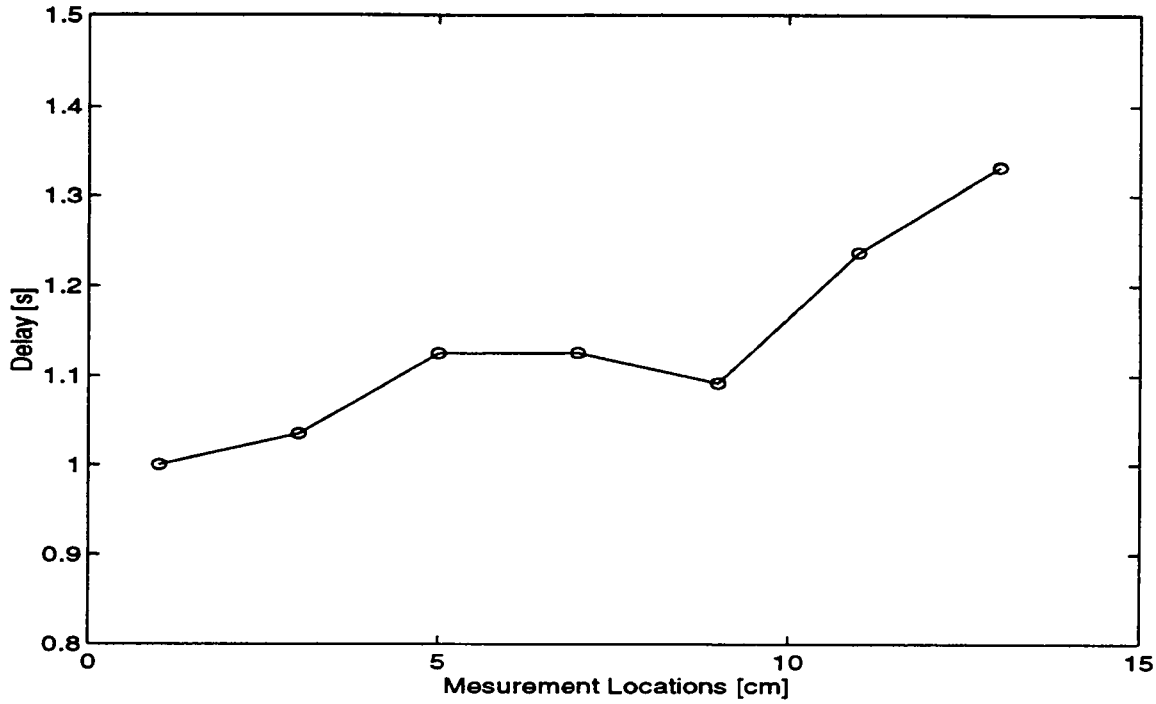


Figure 30. Predictable time delays for spatial measurements at flow of 918 cc/min

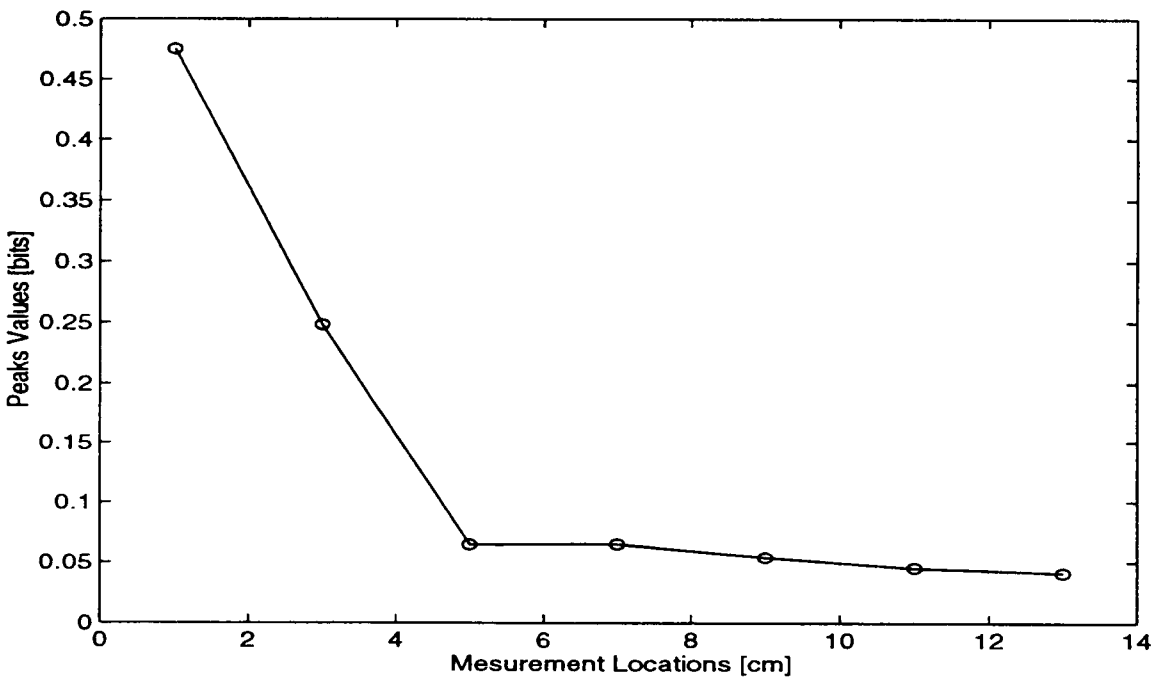


Figure 31. Maximum lag values for spatial measurements at flow of 918 cc/min

5.1.9 Comparison Between Experimental Data and the Bubble Model

Daw and Halow [9] proposed a computer model to investigate bubble behavior in the fluidized bed based on one nozzle bubbling at the bottom of the column. The physical configuration of a single column of vertical rising bubbles for the bubble model is considered similar to the experimental apparatus. Their model seems to provide useful perspectives for understanding the bubble column as well as further development in modeling gas bubbling in liquid. Based on the observations from the bubble model, there are some important similarities between the experimental data and the model.

The most prominent similarity is the bubble-pairing phenomenon due to the instability of bubble-to-bubble interaction. A bifurcation diagram from the model simulation is depicted in Figure 32, exhibits an overall pattern of change in the bubble periodic response of the system as air flow varies. Air flow in the model is represented by injection frequency of constant diameter bubbles, and the bubble period is determined by time intervals between peaks in time series measurement at the monitoring location. The monitoring measurements are acquired immediately above the injection point. As is evident in the bifurcation diagram, the model predicts the onset of pairing and coalescence as air flow increases. Also, the model shows bubble-pairing first occurring near the top of the column and the coalescence zone moving down toward the nozzle as air flow increases. On the whole, the results obtained from the model show a period-doubling progression from periodic to chaotic as air flow varies and all the observations are consistent with the experimental results prior to the onset of chaotic bubbling behavior. Beyond the critical flow for chaos, the model gives the occurrence of periodic windows

and also demonstrates some important similarities with the experimental data.

5.1.10 Comparison With Other Bubbling System Investigations

As mentioned in Chapter 2, previous investigators have used the concept of chaos theory to investigate bubble formation in their systems [6,15,27]. In comparing their results with this portion of the characterization study, the most prominent similarities are the period-doubling bifurcation and the presence of periodic windows beyond the onset of chaos. In addition, all the investigative results seem to link to the classic chaos example of liquid drops in air from a dripping faucet.

In spite of these similarities, the characterization portion of this study investigates the theory of spatio-temporal bubble dynamics for bubble formation in liquids. The results show that the bubble dynamics depends on the bubble-to-bubble interactions (coalescence) as well as the spatial measurement locations. Moreover, this investigation confirms apparent low dimensionality of the bubbling system and a period-8 regime is experimentally identified as further confirmation of period-doubling bifurcation during the progression route to chaos. Nevertheless, the procedures in this portion of the study are necessary in order to understand the nature of the bubble dynamics so that one can use the investigative information for the last portion of the study: evaluation of feedback control methods.

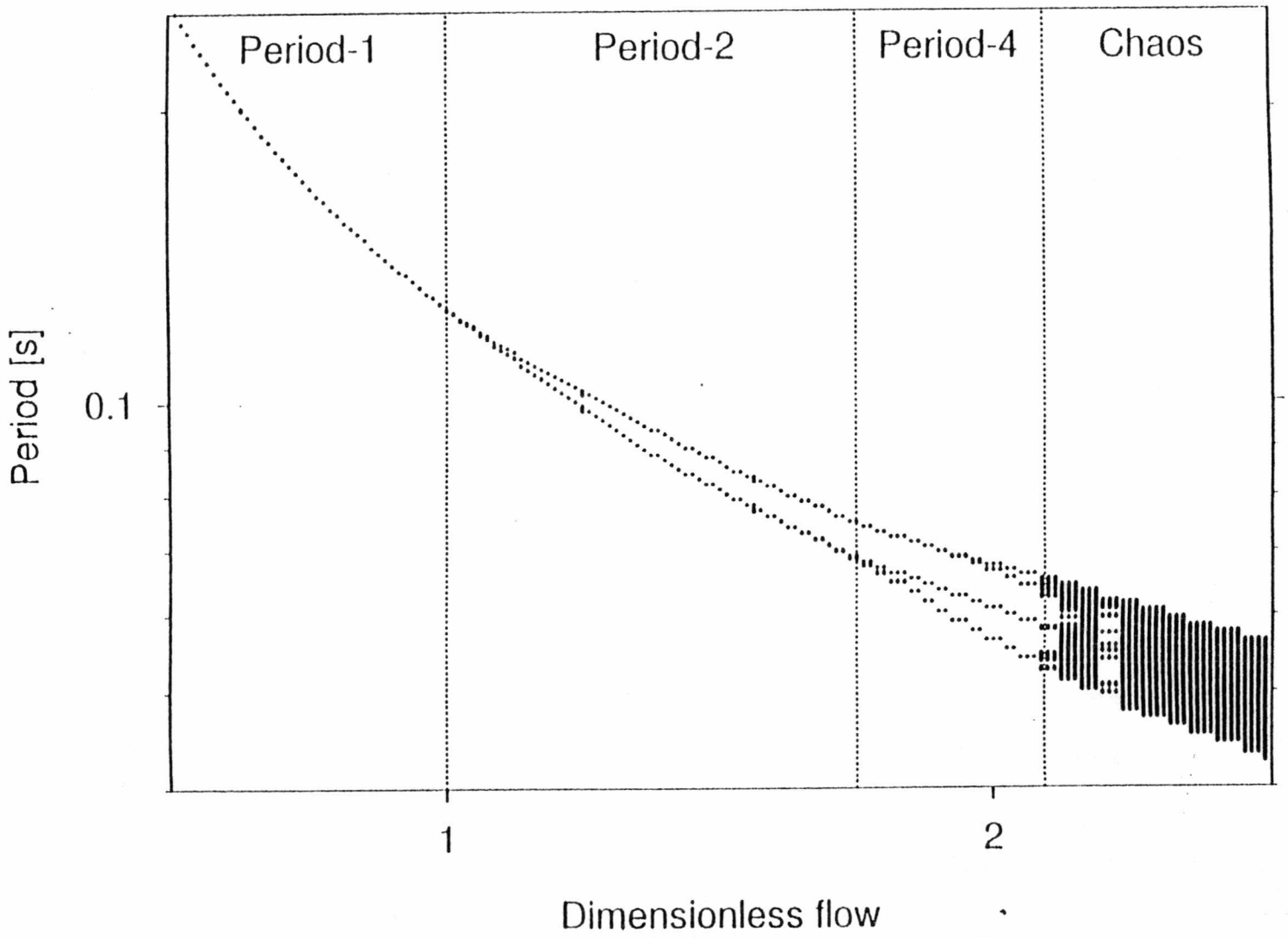


Figure 32. Bifurcation diagram obtained from Daw-Halow model

5.2 EFFECTS OF OPEN-LOOP PERTURBATION

Knowing chaos exists in the bubble dynamics, how do the dynamics change when some input independent variable is changed? Also, in order to utilize the OGY or Bruns feedback control scheme, it is necessary to determine the optimum manipulated variable based on a open-loop type perturbation study. Thus, the ability to manipulate the potential control variables needs to be assessed. Based on the information obtained from the characterization study, the dynamics of the bubbling system are affected by the system independent variable of net gas flow and its state is characterized by the dependent variable of pressure in the inlet supply line. The system operation parameters include column pressure (liquid height), column size, liquid surface tension, injection nozzle size, and chamber volume (gas holdup section between the needle valve and the nozzle).

5.2.1 Sensitivity to System Parameters

The first two attempts at perturbing the gas flow rate, focuses on the response of the dynamics due to variation of the manipulate variable. In other words, these attempts can confirm that the system is in fact deterministic and such deterministic chaotic behavior is not caused by neither special operating conditions nor random noise. The first short set of experiments investigated the bubble behavior change due to chamber size variation in the gas supply line. Increasing the chamber size basically stabilizes the gas flow prior to the nozzle and creates a larger damping effect on the system. A larger chamber has more volume to pressurize and depressurize over a bubble cycle. The experimental setup and procedures were similar to those used for characterization study except a chamber volume of 103.6 cm^3 was located in the bypass with respect to the gas supply line. The results for

this comparison are presented in the return plots shown in Figure 33. From the plots, the system dynamics clearly exhibit chaotic behavior with transition of period-doubling bifurcation route to chaos. One interesting observation is that the bifurcation points are delayed (i.e. a shift to the prior operating regimes or occur at higher flow rates) by introducing extra damping via the chamber to the system. These delays indicate the bubble dynamics are sensitive to the system parameter of gas supply system volume. The effect of the larger volume is to damp the pressure signal. In fact, this observation supports the speculation that the system dynamics can be modified by varying the pressure. The investigation of this concept is presented in section 5.2.2: effects of periodic sound wave perturbation on bubble behavior.

The second investigation to determine the system response due to change in supply pressure involved variation in column pressure by adjusting the liquid height in the column. A short set of experiments was performed with similar procedures and apparatus as previously used except that the liquid was filled to a height of 10 cm, 15 cm, and 20 cm. The calculated pressure values at the bottom of the column are summarized in Table 2 .

Table 2. Operating conditions for variation of pressure at the bottom of the column

Column Height (cm)	Density ($Kg/m^{\wedge 3}$)	Viscosity (cp @26.7°C)	Pressure (atm)	Pressure % Difference *
10	1.248	836	1.012	1.2 %
15	1.248	836	1.018	0.6 %
20	1.248	836	1.024 *	0.0 %

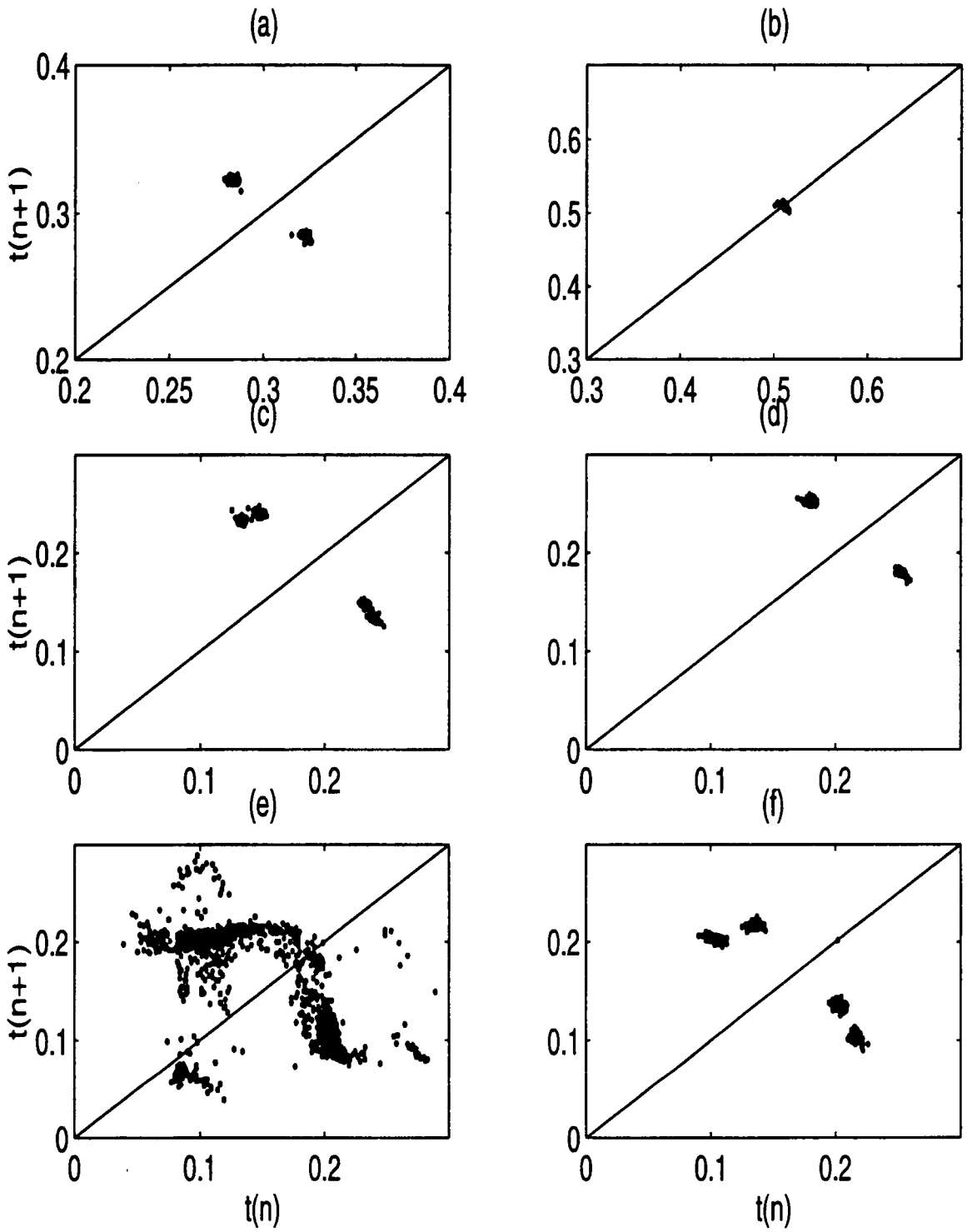


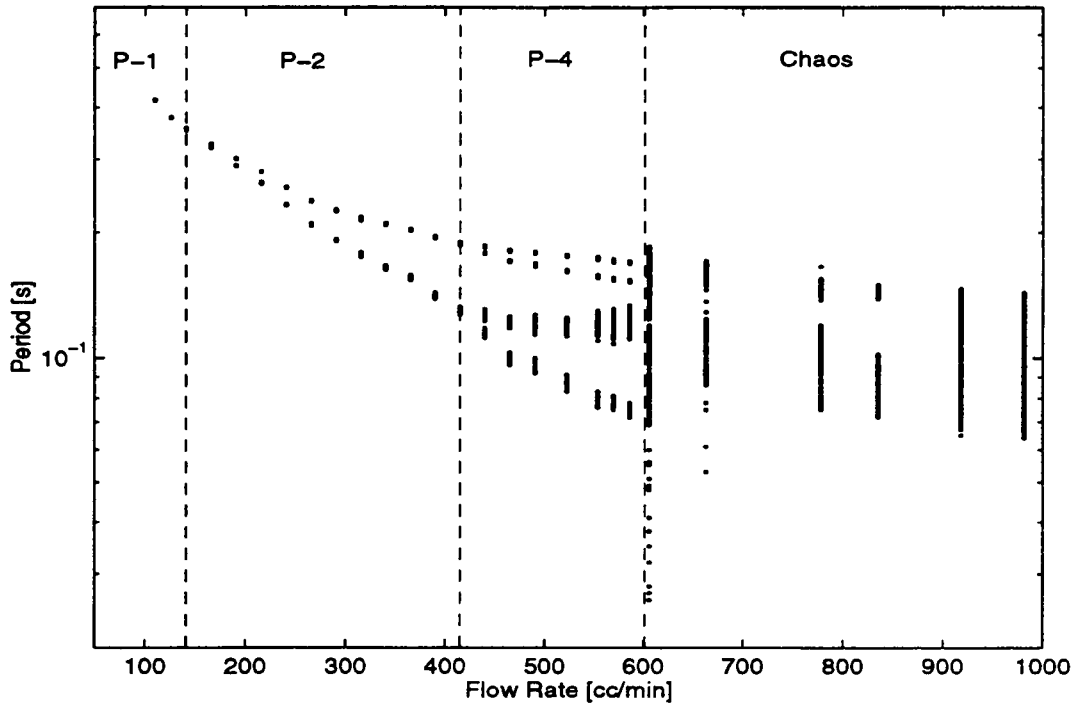
Figure 33. Bubble behavior with variation of chamber size: (a,c,e) without chamber and (b,d,f) with chamber at flows of 190.8, 390.1, and 585.8 cc/min, respectively

Figure 34 depicts bifurcation diagrams for the overall bubbling pattern for column liquid height of 10 cm and 20 cm liquid-filled as air flow changes. For comparison return plots between liquid height of 10 cm and 20 cm, are shown in Figure 35. These results demonstrate chaotic bubbling pattern changes caused by using different operating conditions of pressure. Moreover, the investigation indicates the instabilities of the system strongly depend on the operating condition of pressure. As shown, the first bifurcation point seems to be acceded and the critical valve for onset of chaos is delayed by using smaller column pressure. This observation, once again, implies the complexity of the bubble dynamics would be difficult to explain by using classic mechanistic descriptions.

Nevertheless, the above results show that the system indeed exhibits chaotic bubble behavior and both system parameters demonstrate the capability to shift the bifurcation points during the progression route to chaos. The chaotic attractor position is also shifted by using these system parameters (i.e. they meet the basic three criteria for the OGY control scheme). However, practical devices that can change the column pressure or chamber size fast enough (approximately 20 Hz) in response to the bubble dynamics are somewhat difficult to design let alone build. Therefore, it seems to worthwhile to explore a much simpler and more prominent system manipulated variable.

Knowing the bubble dynamics are sensitive to the pressure variation in the gas supply line, then the stone should be moved in that direction. To overcome the obstacle of assembling a fast response system for the pressure variation, an external perturbation system using sound waves is designed and implemented. The perturbing signals of the input variable are expected to vary the system dependent variable of pressure in the gas

(a)



(b)

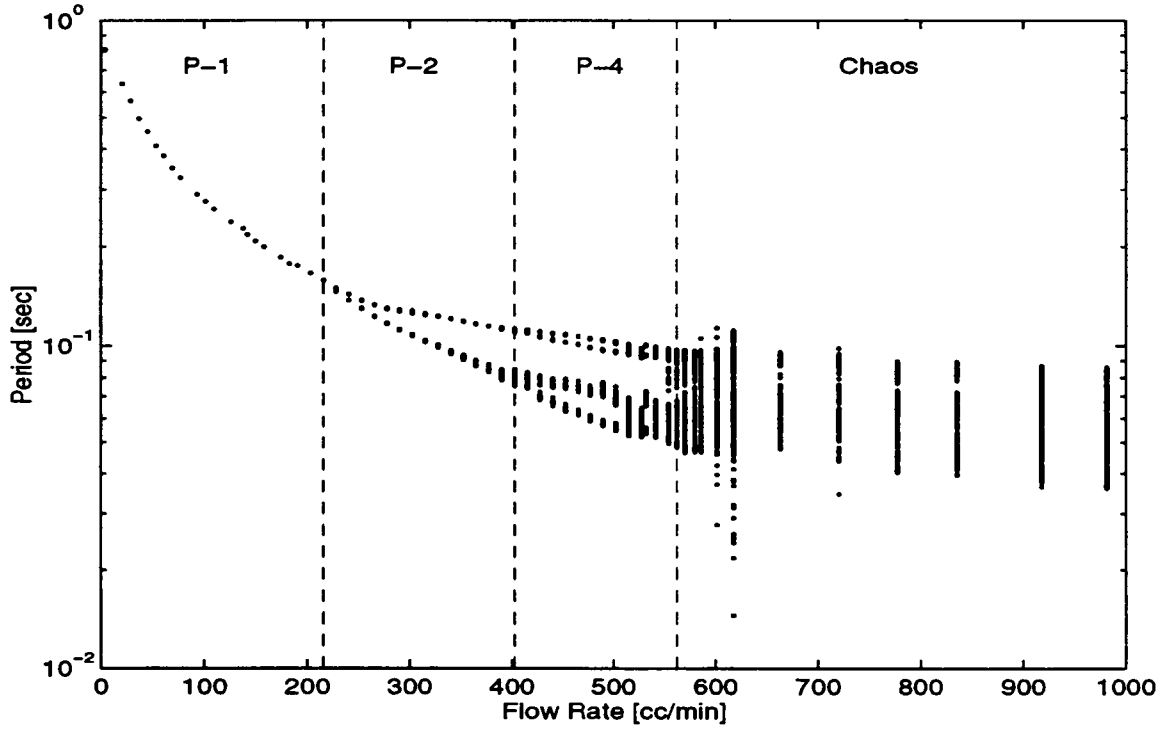


Figure 34. Bifurcation diagram for liquid filled to height of (a) 10 cm and (b) 20 cm

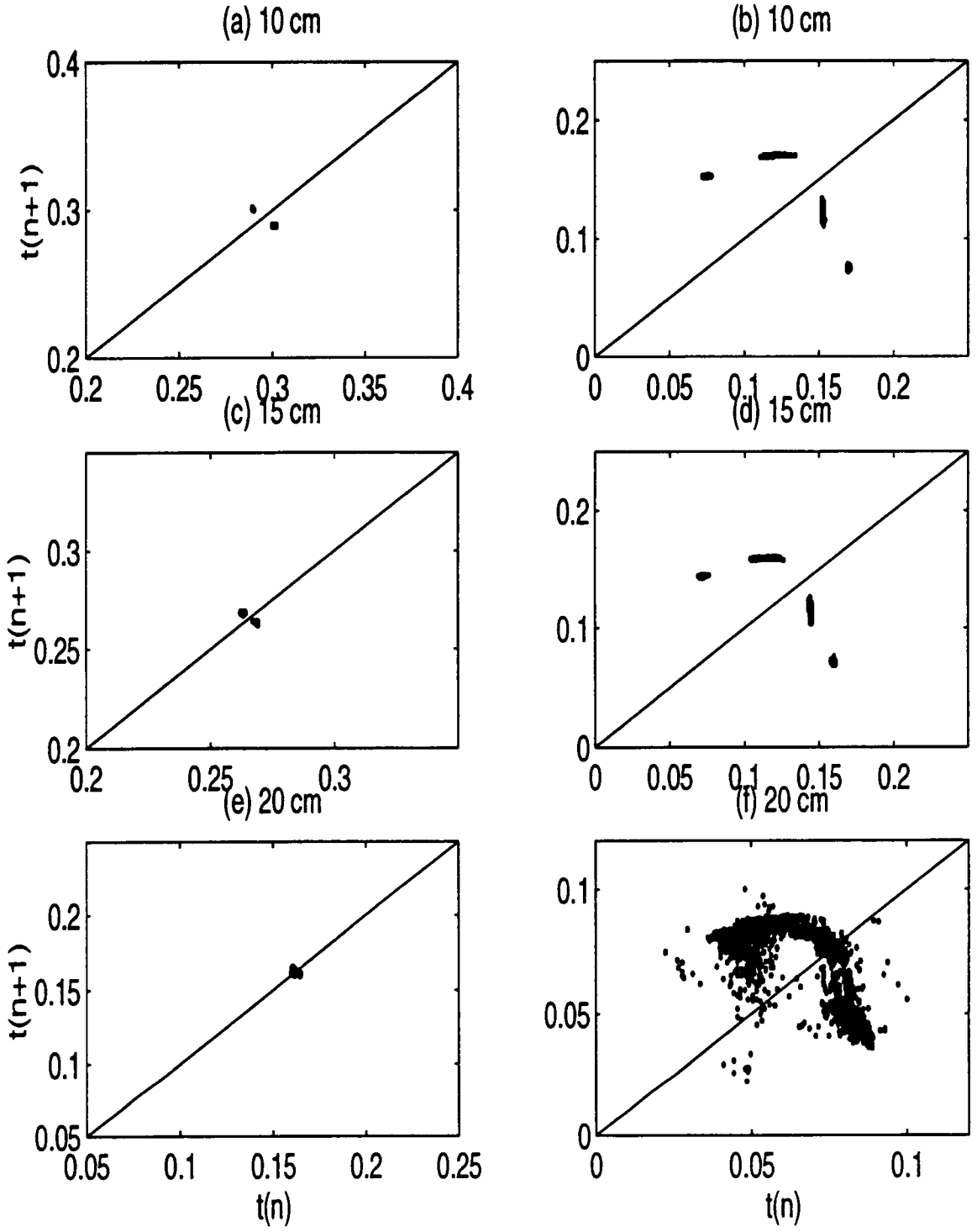


Figure 35. Bubble behavior near the bifurcation point at flow of 190 and 585 cc/min for liquid-filled at 10 cm (a-b), 15 cm (c-d), 20 cm (e-f)

supply line which in turn varies the time for bubble formation and detachment at the nozzle which modifies the movement in the column. This perturbation is attractive as the average flow rate through the column is not changed. It turns out that, the independent variable of sound wave perturbation is incapable of shifting the attractor position. The sound wave perturbation does change the distribution of the system states on the return plot. Such observation indicates that the selected variable fails to meet one of the three criteria for the OGY control method. However, the effects of this perturbation on the bubble dynamics, especially near its bifurcation points, provide important information about the ability of taming chaotic bubble dynamics.

Finally, the response of the bubble dynamics is investigated using discrete gas pulse. It was found that the system dynamics are extremely sensitivity to the pulsing perturbation and depends greatly on the duration and frequency of the pulse. Furthermore, results also showed that it meets all the criteria for the OGY and nonlinear relay control schemes. Therefore, a system input variable to vary the gas flow, was further investigated by using a open-loop signal to an automobile gas injector. The signal to the injector resulted in gas pulse perturbations having constant amplitude, frequency and duration. The details of this investigation are presented in section 5.2.3. Throughout the empirical determination of a system manipulated variable, the study revealed important information about the nature of the bubble dynamics as well as provided a direction for control action.

5.2.2 Effects of Periodic Sound Wave Perturbation on Bubble Behavior

The effects of perturbation on dynamic instabilities of a nonlinear system have attracted considerable interest, specifically, for a system operating near its period-doubling

bifurcation points because these babies of the system are, generally speaking, expected to behave in several universal ways to the effect of perturbation. This study investigates the responses of bubble dynamics due to periodic sound wave perturbation near the bifurcation points. In this type of constant perturbation study, there are three basic parameters:

1. the parameter of bifurcation
2. the amplitude of the perturbation
3. the frequency of the excitation
4. duration of the perturbation

In the following section, the choice of these parameters and the results the perturbation are presented.

5.2.2.1 Perturbation Signals

The frequency generator initiates the perturbation action with the desired period of motion (frequency). The speaker drives the motion of a membrane (oscillator) based on power transfer in the form of traveling sound waves. The corresponding output frequency provides variation of pressure in the inlet gas supply line and then causes the perturbation to the bubble dynamics.

The bubbling response of the system is monitored by the lower laser beam measurement. The perturbation signal response is affected by both amplitude and frequency. As mentioned in chapter 3.2, the amplitude is set to a constant value as it was found changing the amplitude had little effect on the variation measured by the pressure transducer in the gas supply line. The responses of perturbation signals are determined by

a pressure transducer and some of the results are summarized in Appendix A. As shown, the perturbation signals indicate periodic motion when the driving frequency is high (above 5.5. Hz). For low driving frequencies (i.e. 1 - 5 Hz), the perturbation signals show a nonlinear effect such as a discontinuous response. Such nonlinearties are caused by movement of the magnet, speaker cone response, the diaphragm size, and the diaphragm response. Therefore, only those frequencies (i.e. 5.5 Hz and above) that give periodic perturbation signals are used in this experimental study. The details of the experimental apparatus have been outlined in Chapter 3.

5.2.2.2 Suppression and Shift near Bifurcation Points

Based on the constructed bifurcation diagram, all of the air flows for this study are chosen near bifurcation points. Since the perturbing signals vary the time dependent variable of pressure, the perturbing system is considered to be operated by one oscillator (bubbling system) with external forces from the speaker so that the output bubbling action in the column is caused by resonant parametric perturbation. Detailed theory for the perturbing system can be developed in terms of classic mechanics for specific physical models, which is beyond the scope of the present study. However, based on experimental observations and reports from investigations on other similar perturbing systems, there seems little doubt to speculate that the theory of resonance is able to interpret the astonishing phenomenon of suppression of chaos as well as shifts in unstable operating states (bifurcation points).

To illustrate a simple example of the basic perturbation procedure, consider the general equation of the bubbling system as:

$$\frac{dV}{dt} = F(p, u) \tag{21}$$

where : $V(t)$ = rising bubble characteristic in the system

$p(t)$ = pressure in the gas holdup section without perturbation

$u(t)$ = system parameters and variables affecting bubble behavior

The perturbing signals are simply generalized as:

$$F = F_o \cos(2\pi f - \phi) \tag{22}$$

and the instantaneous power transfer to the system is:

$$P = F * u_o = F_o u_o \cos(2\pi f - \phi) \tag{23}$$

where : ϕ = sound wave traveling phase angle

u_o = sound wave travel velocity

f = speaker driving frequency

F_o = driving amplitude

In such a case, the time dependent forcing term varies the pressure in the holdup section as:

$$p'(t) = p(t) + F_o u_o \cos(2\pi f - \phi) \tag{24}$$

Therefore, the perturbing bubble formation and its movement in the column is due to:

$$\frac{dV}{dt} = F(p', u) \tag{25}$$

Considering the system is undergoing a steady periodic motion and is free from external forces, the natural bubble oscillation frequency is assigned as ω. When the perturbation is applied at time $t = t'$, the perturbing force changes the bubble velocity at

that instant by an amount which is written in the following terms: perturbing force, perturbing pressure in the section, damping parameter, and other related system parameters. In the subsequent motion immediately after the impulse, the bubble oscillator is again free from external forces, and the case of oscillatory decay is dependent on the damping parameter of the system. Since a constant periodic forcing function is applied all time, the response of the perturbed system is expected to exhibit constant output variations in the bubbling motion. This variation results from the interference between the steady state bubbling motion with frequency ω of the free motion of the oscillator, and driving motion with the frequency ω' of the speaker. When the interference between the two motions goes from destructive to constructive, the oscillatory frequency ω of the bubbles in the system is considered to have reached the resonance frequency ω_o.

Because of the difference in both the perturbing force and the damping parameter for the perturbed system, the anticipation of several resonance states conveyed from it seems reasonable. Moreover, the assumption that the perturbed system exhibits strong and weak resonant cases seems reasonable. The strong cases carry enough energy to give a forced motion of larger resonant bubbling motion while weak cases yield smaller resonant forces to excite the bubbling process. In fact, the assumptions made so far seem to be consistent with the experimental observations obtained from this bubble dynamics study because larger resonant forces restrain the bubble behavior to its prior and subsequent regimes while small resonant forces can only retain the bubble behavior near a new steady state.

Initially, all the system states are sampled including the transient response of the

system. Figure 36 depicts a time history of bubble behavior at an air flow of 290 cc/min with variation in perturbation frequencies. Since the first period-doubling bifurcation point (i.e. period-1 to period-2) is observed at 240 cc/min based on the bifurcation diagram, the selected flow of 290 cc/min is considered close to that point. The corresponding return maps and power spectra plots for different perturbation signals are summarized in Figure 37 and Figure 38, respectively. For the system without perturbation, the return plot shows two points which reflect the system undergoing a period-2 bubbling motion, and the power spectrum shows the bubbling frequencies of 4.6 and 2.2 Hz. The harmonic frequencies on the plot are considered to be produced by digitizing the analog signal and the algorithm of the power spectrum analysis tool.

As shown in the power spectrum plot of Figure 38b, a perturbing signal oscillating at 6.7 Hz is added when the bubble oscillation is 4.6 Hz at the nozzle. The bubbling pattern seems to change from period-2 to a noisy period-1 as shown in both Figures 36 and Figure 37b. This observation indicates a change in the velocity and volume of the bubble to a new bubbling state due to the forced perturbation. The noisy period-1 bubbling pattern is interpreted as the perturbed system reaching the resonance frequency of a strong case. This resonance frequency is caused by a large resonance force that carries enough oscillatory energy to push the perturbed system to bubbling at a period-1 state.

When a 7.1 Hz perturbing frequency is applied, period-2 bubbling with smaller time intervals is observed in the return plot of Figure 37c. This period-2 bubbling with smaller time intervals indicates that the velocity of the bubbles rising in the column is higher than the period-2 bubbling action without perturbation. This bubbling pattern with

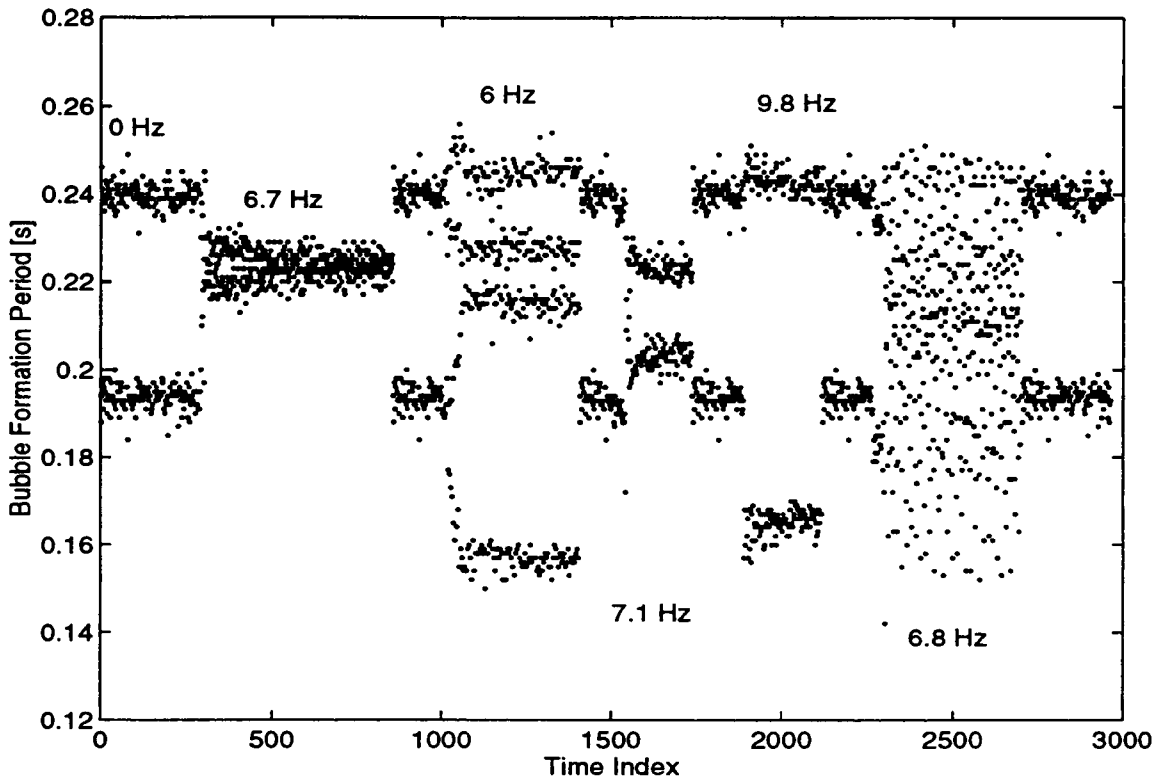


Figure 36. Bubble behavior with different perturbation frequencies at flow of 290 cc/min

smaller time intervals is caused by the perturbing bubble column reaching the resonance of a weak case. Since these resonance forces carry insufficient oscillatory energy, the weak case only excites the perturbed column to make bubbles at the period-2 bubbling action. A similar observation is obtained for the system perturbed at 9.8 Hz, and the corresponding return plot is shown in Figure 37d. This observation indicates a weak resonant force that only manages to bubble the system at period-2 at a relatively lower bubble velocity and with larger spacing between bubbles.

When perturbing signals oscillating at 6.0 Hz are added to the system, a period-4 bubbling action is observed in Figure 36, and the corresponding return plot is depicted in

Figure 37e. This observation indicates that the perturbing system reaches the resonance of a strong case such that the system is stimulated to a higher bubbling frequency. An interesting observation is that the perturbing frequency at 6.7 Hz pushes the system to a period-1 bubbling pattern while an aperiodic bubble behavior is obtained at the 6.8 Hz perturbation, which is depicted in Figure 36. In fact, all the perturbing signals that cannot drive the system to resonance destroy the bubble dynamics and the motions become destructive causing the chaotic phenomenon. The transient times for the perturbing signals which drive the system to resonant bubbling motion are very short. Therefore, for the following trails, all the system states are sampled after the decay of the transients.

An air flow of 464 cc/min was chosen since the flow rate was considered near the second bifurcation point (i.e. period-2 to period-4). Figure 39 illustrates the time history during the bubble formation period, and the corresponding return plots are depicted in Figure 40. As shown, the bubble behavior undergoes a period-4 bubbling pattern with a dominant bubbling frequency at 3.2 Hz along with bubble frequencies at 4.8 Hz, 8.1 Hz, and 9.6 Hz. By adding the perturbation signal at 16.4 Hz, the system appears to reach the resonant frequency of a weak case. Therefore, a similar period-4 bubbling pattern is observed. When the perturbing signals at 8.1 Hz and 11.5 Hz are added, the period-4 bubbling pattern is observed to behave as a noisy period-2. Such observation suggests that the system is bubbling at the larger force resonances of the strong cases. Besides the above perturbing frequencies, aperiodic bubble behavior is observed within the investigated perturbing frequencies (i.e. 5 - 40 Hz). Based on this investigation, the responses of bubble dynamics exhibit different bubbling patterns with the proper perturbations.

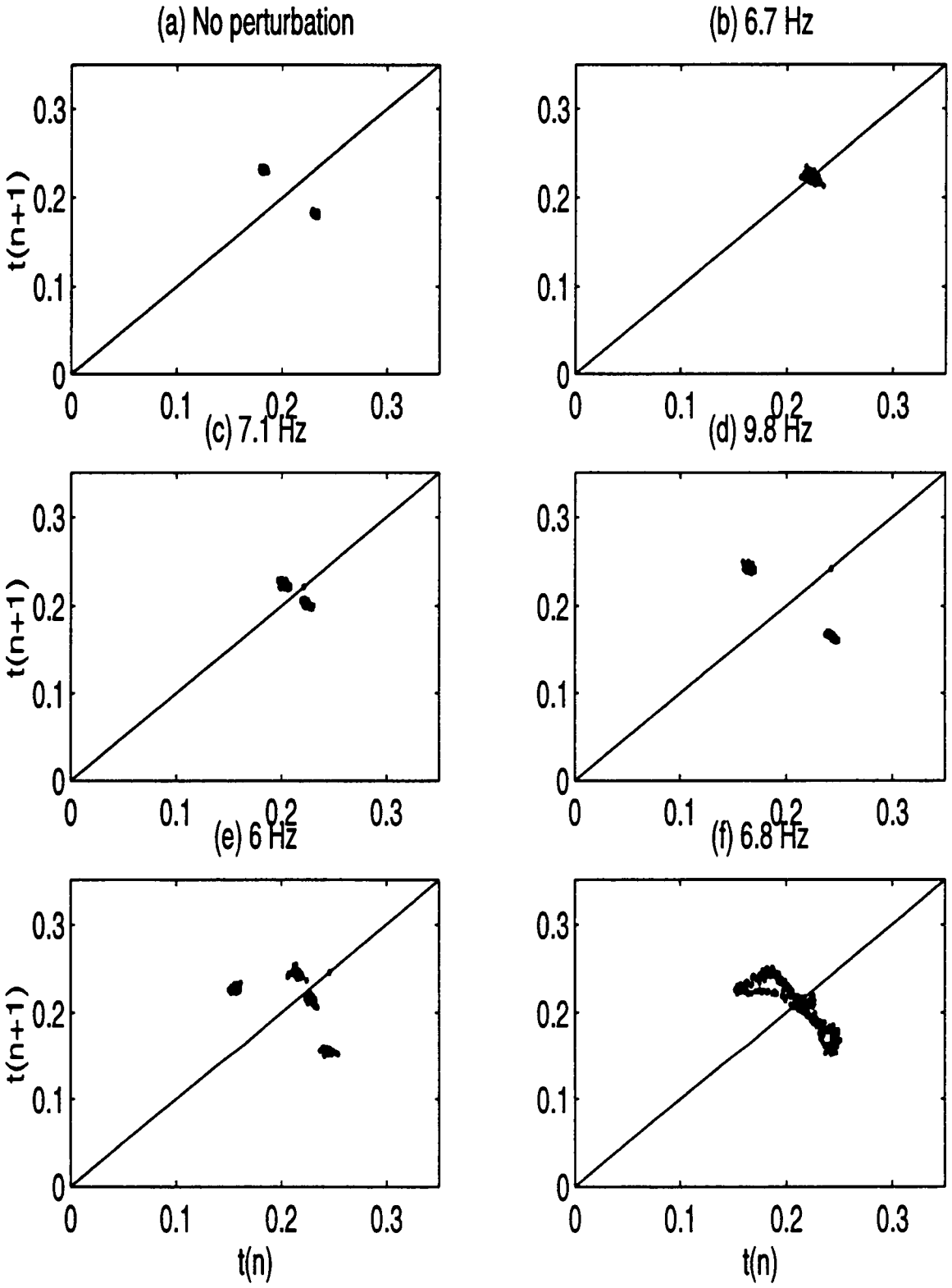


Figure 37. Time return plots for different perturbation frequencies at flow of 290 cc/min

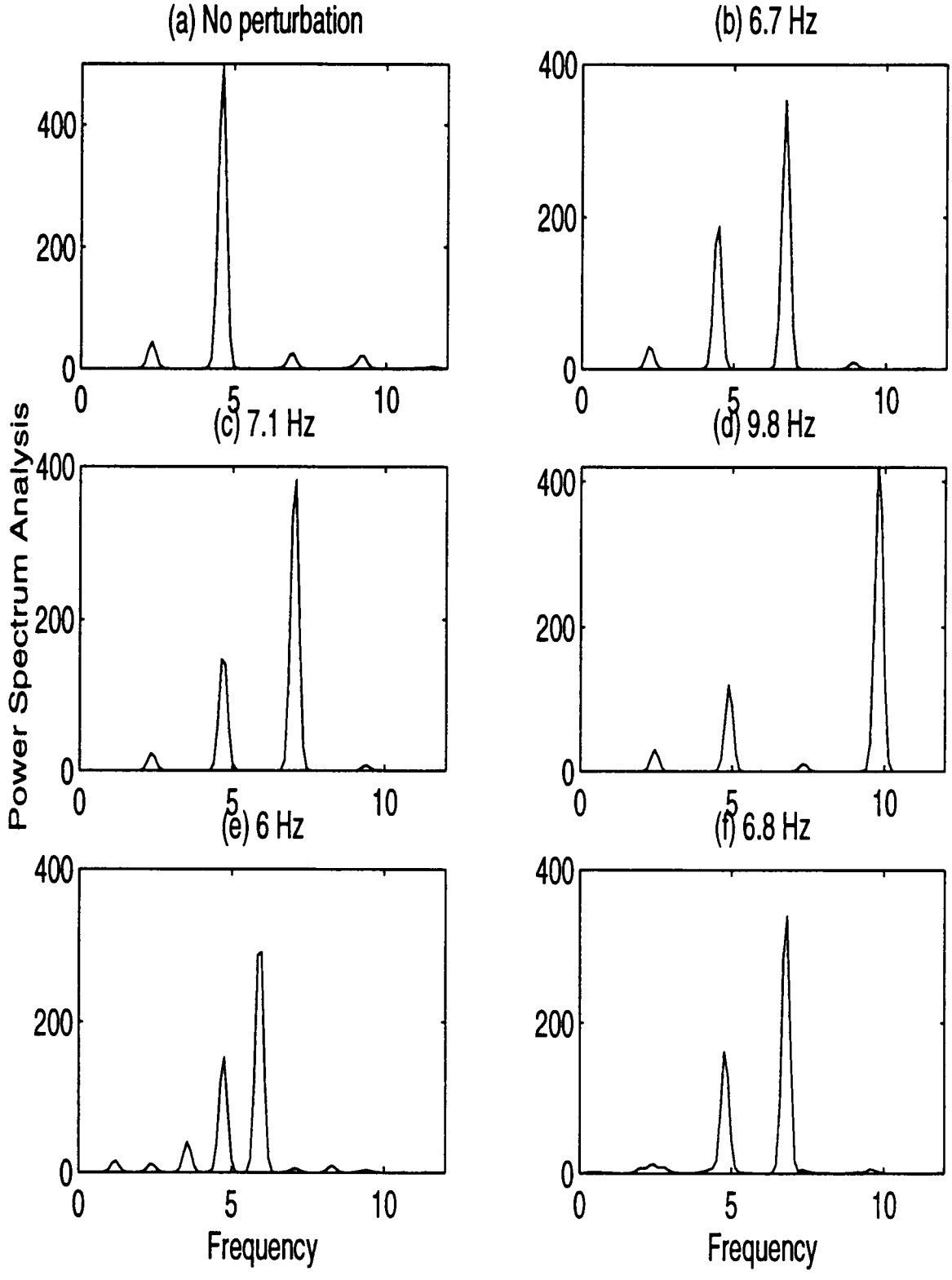


Figure 38. Power spectra for different perturbation frequencies at flow of 290 cc/min

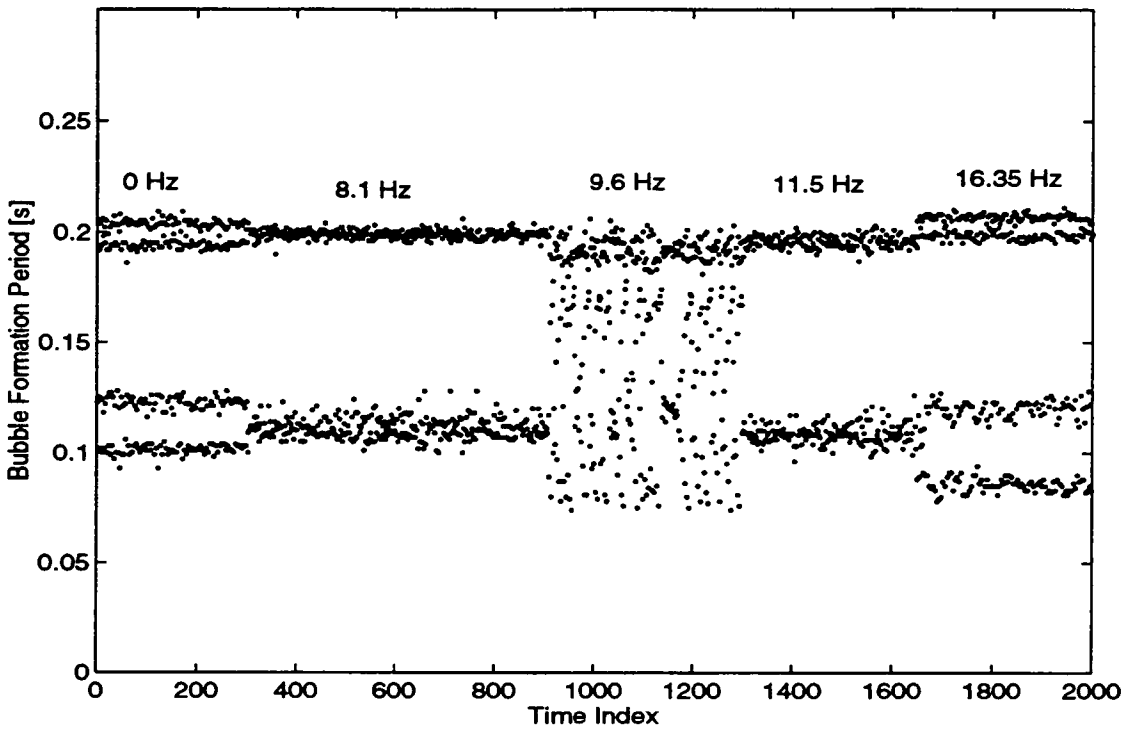


Figure 39. Bubble behaviors with different perturbation frequencies at flow of 464 cc/min

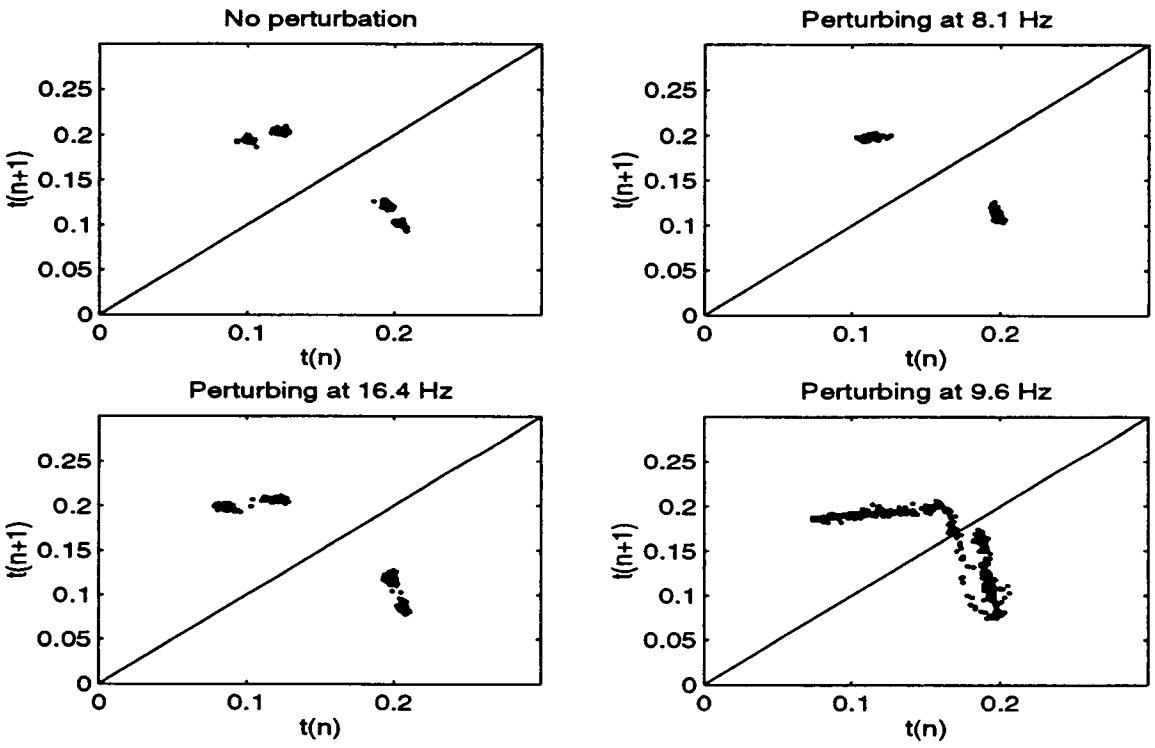


Figure 40. Time return plots for different perturbation frequencies at flow 464 cc/min

All these periodic bubbling patterns near the bifurcation points can be subdued, and the suppression are mainly attributable to resonant parametric perturbation.

The previous studies indicate that bifurcation points in the periodic regimes can be suppressed. Now, what about the bifurcation point for the onset of chaos? Since the onset of chaos occurs around a flow of 561 cc/min, two flows of 601 cc/min and 605 cc/min were investigated. Time return plots are summarized in Figure 41 and Figure 43 for those two flows. For air flow of 601 cc/min without perturbation, the layered appearance of the mapping region represents the attractor of the system. By adding the perturbation signals at 6.0, 7.0, and 14.0 Hz, the distributions of the mapping points changes, and most of the system states seem to stay in the regions of 0.06 and 0.15 on the return plot. The change in mapping point distribution indicates that the perturbing frequencies are at or very close to the resonances so that they can push the system to make bubbles with time intervals around 0.06 and 0.15 per second. The representative return plots are summarized in Figure 41(b,c,d). When an oscillating perturbing signals at 35.0 Hz is applied to the system, a noisy period-4 is observed, and the corresponding return plot is depicted in Figure 41f. This perturbing frequency seems to restrain the system to the larger resonance force of a strong case. This observation suggests that the chaotic bubble behavior is suppressed and the bifurcation point is shifted toward higher flow rate.

When a 12.5 Hz perturbation is applied, a noisy period-2 bubbling pattern is observed, and the mapping points accumulate in the regions of 0.06 and 0.15. The power spectrum plot shows the system is undergoing the motion at a period-2 mode of 8.3 Hz,

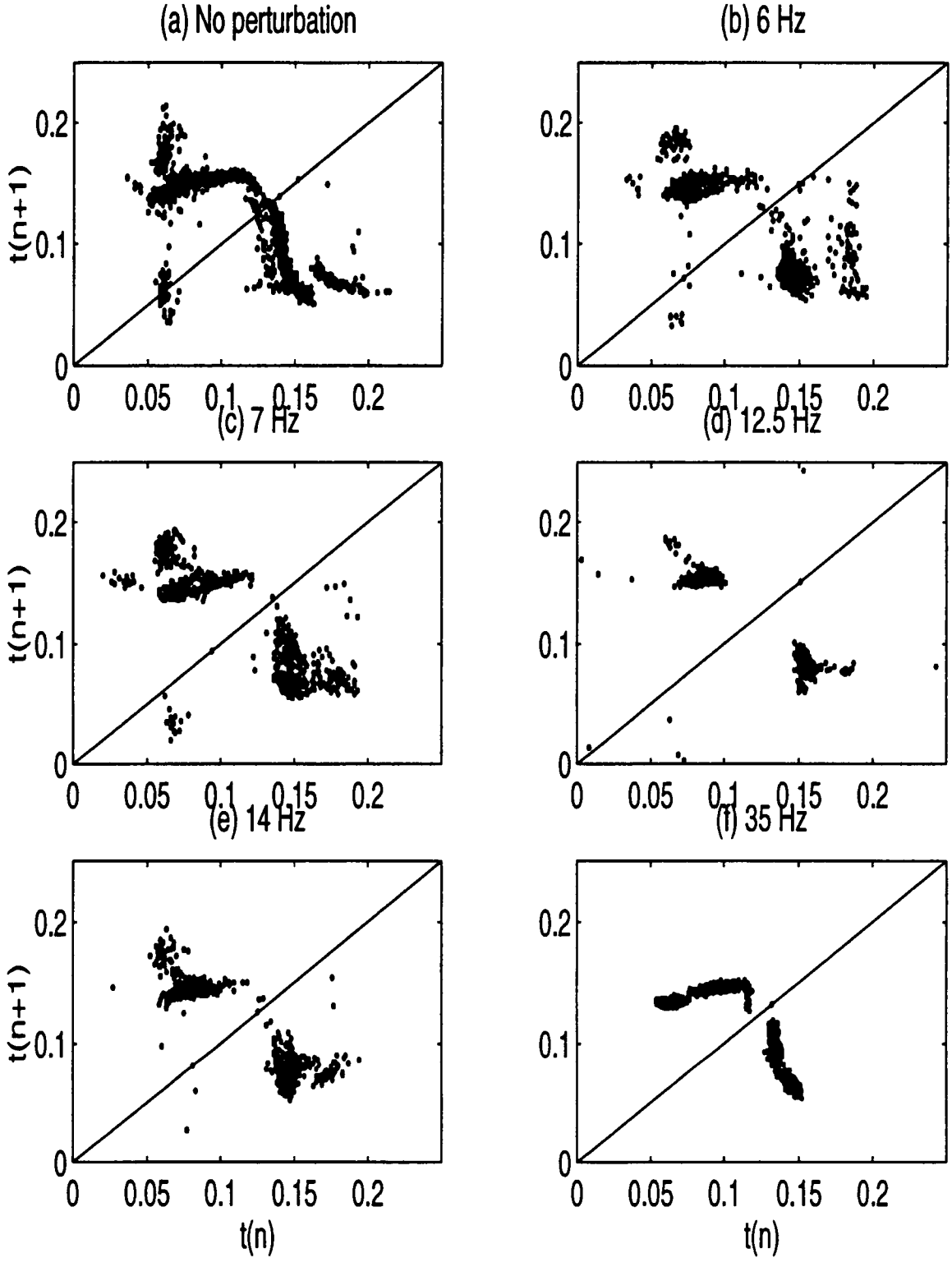


Figure 41. Time return plots for different perturbation frequencies at flow of 601 cc/min

4.1 Hz, and a dominant 12.5 Hz perturbation. This result is illustrated in Figure 42.

This observation indicates the system is indeed bubbling at a periodic motion due to resonant parametric perturbation. Consequently, the establishment of the theory of taming of chaos to its resonant periodic motion is certainly positive. In addition, the above observations also imply the possible existence of two limit cycles in the system.

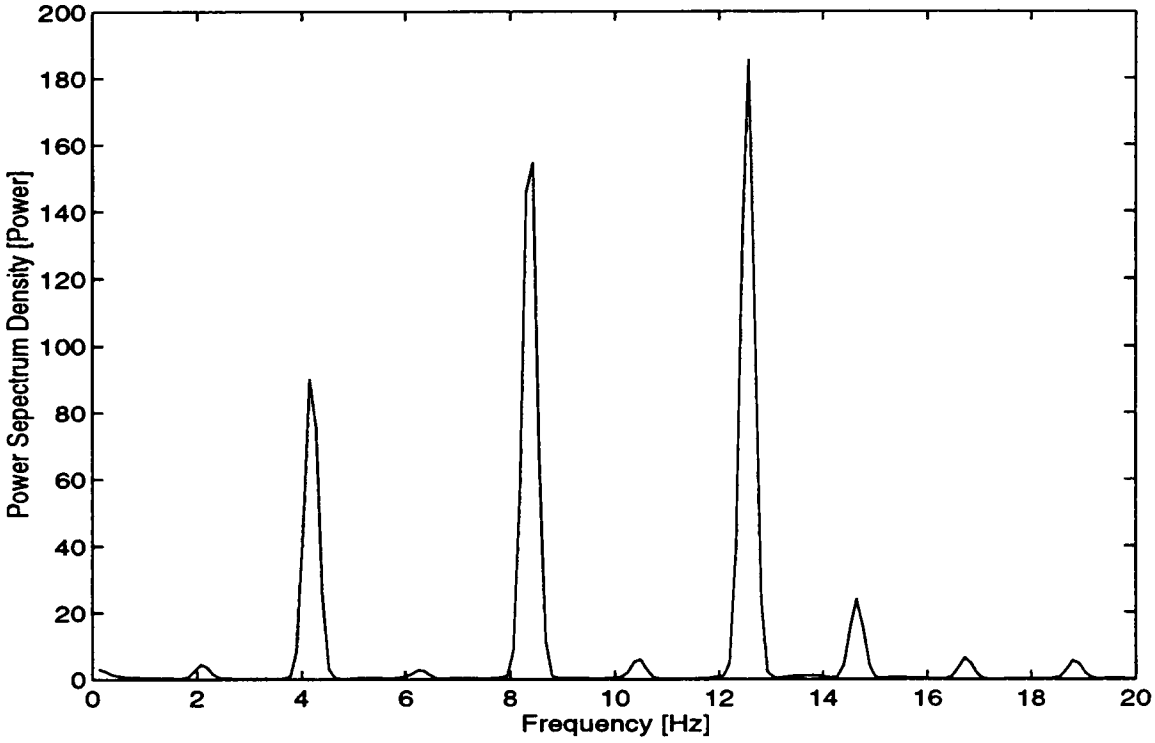


Figure 42. Power spectrum for describing bubble behavior at 12.5 Hz perturbation

The argument of taming chaos and the existence of limit cycles seems to be consistent with the perturbing system state motion produced by using an air flow of 605 cc/min. As shown in Figure 43a, one can observe that the attractor of the system shows the appearance of a 'walking stick' type. By appropriately adding the perturbation signals, the mapping points to describe the bubble behavior accumulate in the regions of 0.06 and

0.13 as shown in Figure 43(c,e,f). A slight change in the accumulation regions is understandable because the appearance of the attractor is calculated based on spacing between the bubbles at different flows. Also, a noisy period-4 pattern is seen in Figure 43b when a 7 Hz oscillating signal was added. By carefully applying the perturbation at 13 Hz (12.5 Hz for flow of 601 cc/min), the noisy resonant period-2 bubble behaviors are observed, and the return plots are depicted in Figure 43d. Such observation further confirms the argument for the existence of limit cycles in the system. In other words, the strange attractor of the chaotic bubble behavior is held by two isolated limit cycles with very small regions of stability. When one of the system states lands inside a cycle region, all the successor system states follow and oscillate on that cycles. Because a unique property of a chaotic system is to be extremely sensitive to perturbations, all perturbation types such as gas flow deviation, temperature and pressure variation, viscosity change, and noise possibly affect the system motion. Therefore, when one of the system states fails to t_o land inside the stable cycle region, the following states wander around in the bounded region so that the layered appearance of the attractor is obtained.

The interpretation of the existence of these limit cycles can be demonstrated by the experimental data as shown in Figure 44. This plot represents the attractor for a flow of 605 cc/min with sound perturbation of 13 Hz. The numbered points in the return map show a walk-out sequence (points 322 to 325) from the limit cycles and walk-in sequence to the limit cycle (points 325 to 330). When the system state for example at point 323 lands outside the region, the whole walking sequence is initiated, and all the consequent states wander around outside the cycles. Such movement is not terminated until the

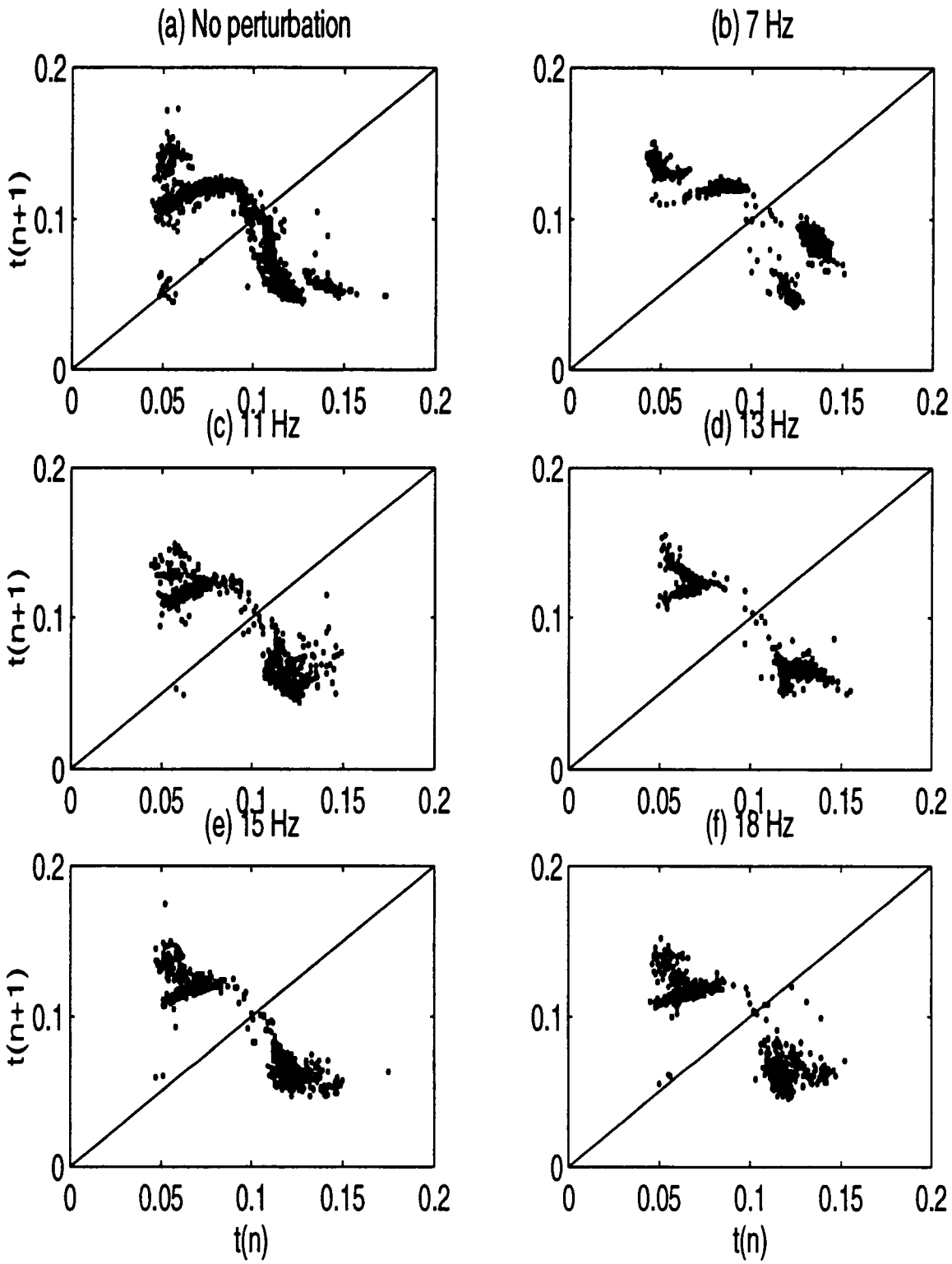


Figure 43. Time return plots for different perturbation frequencies at flow of 605 cc/min

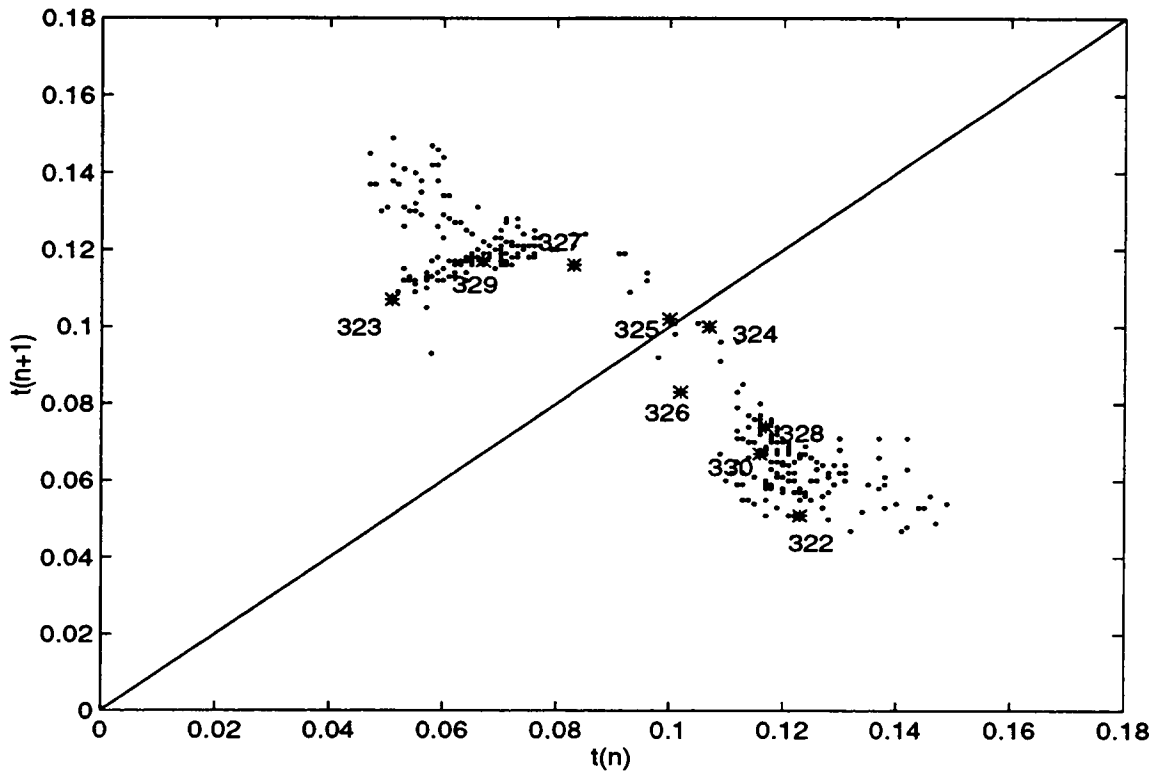


Figure 44. Illustration for the system states motion

system state (329) finally lands inside the stable region and then is locked into the oscillation stable region as shown on the return plot. In fact, the bubbling system exhibits self-sustained oscillations in these two cycles even in the absence of external perturbation. Such oscillations provide information for the investigation of the entrainment of chaos to its periodic cycles by using a discrete air flow pulsing technique, which is presented in section 5.2.3. The walk-out sequence of mapping points toward the diagonal on the return plot, provides the experimental information needed for the OGY period-1 control or Bruns relay control strategies.

The perturbation trials on the system operating in a deep chaotic state does not

seem to have the success from the standpoint of taming of chaos. However, the perturbation does push the system to bubble at favored frequencies as well as changes the distribution of the states on the map. Trails for flows slightly away from the periodic bifurcation points are summarized in the return plots shown in Figure 45 and Figure 46. Based on the investigation of the perturbation effect on dynamic bifurcation points of the bubble column, two major properties about this period-doubling bifurcation system are observed: 1) the instability or bifurcation point can be suppressed and subsequently shifted toward a higher flow rate when a proper open-loop perturbation is applied. 2) this bubbling system is dominated by two limit cycles in high gas flow regime and these cycles attract all the system states if perturbation signals are appropriately applied.

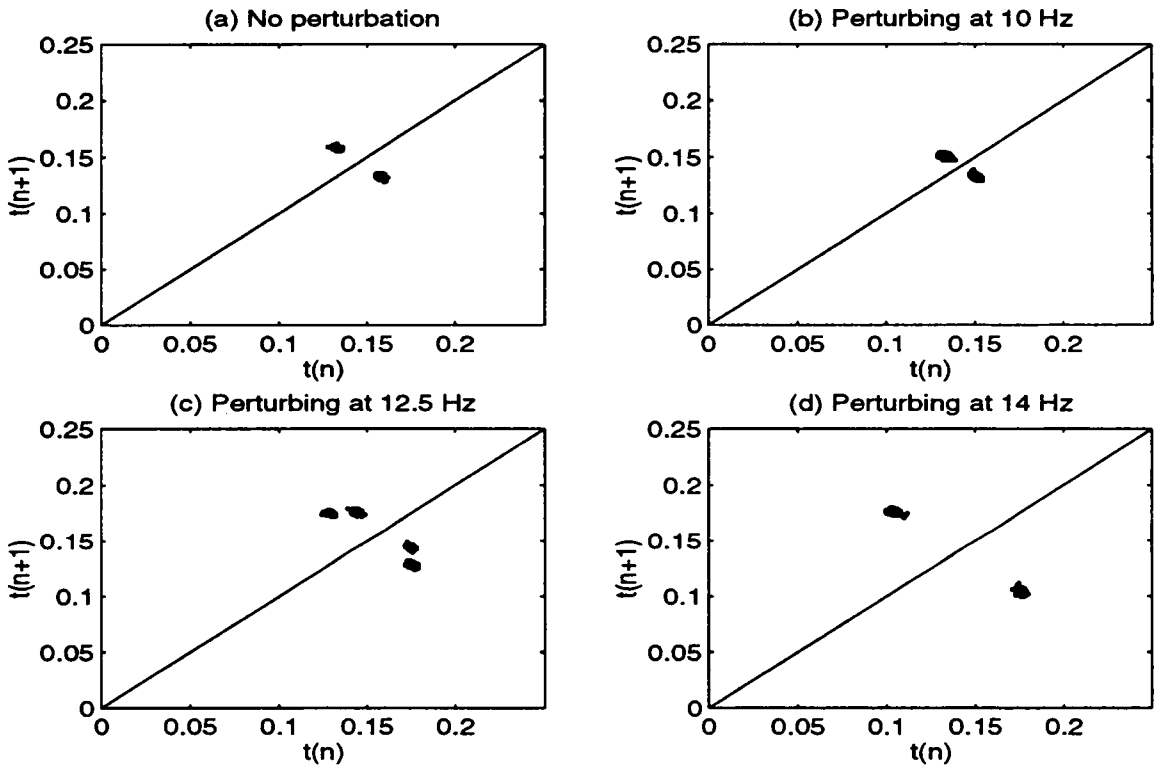


Figure 45. Time return plots for period-2 perturbing system at flow of 327 cc/min

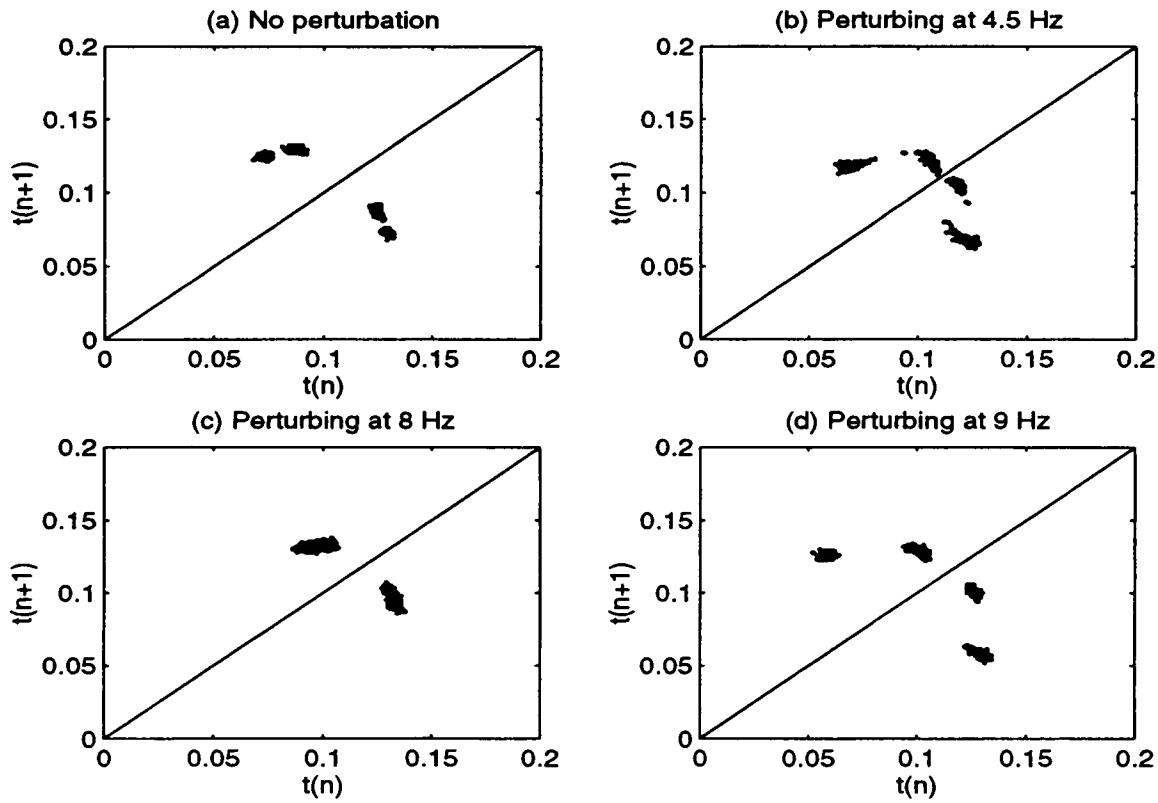


Figure 46. Time return plots for period-4 perturbing system at flow of 506 cc/min

5.2.3 Entrainment of Chaos to Periodic Cycles

The presence of limit cycles identified from previous open-loop external perturbation, leads one to believe that the chaotic bubble behavior can be entrained to its periodic orbits. The proposed occasional proportional feedback (OPF) control method as discussed in Chapter 2, has demonstrated the ability to control both the low-dimensional and high-dimensional unstable steady states by using the discrete pulse of an available system variable. The OPF method of using discrete pulses to control steady states and periodic orbits in experiments, requires careful tuning of the control scheme parameters of time trigger, duration, and amplitude.

The external perturbation evaluated in this section is an air pulse produced by the

saturation type pulse injector. The experimental procedures have been described in Chapter 3, and the configuration of the experimental apparatus has been illustrated in Figure 8. Depending on the nature of bubble behavior and pulse action, it was found that the chaotic system can be entrained to periodic cycles based on the following open-loop perturbation variables: system operating condition of gas flow, pulsing amplitude, and pulsing duration. Based on the results obtained from the effects of sound wave perturbation, the bubble system appears to behave several ways if the system is operating near the bifurcation point, at least the suppression of chaos should be duplicated by using different external perturbation variables. Therefore, an air flow of 585 cc/min is chosen for the aperiodic bubbling motion. As recalled from Figure 8 for the configuration of the pulsing system in Chapter 3, the perturbation action is initiated and controlled by an intel 80486-based microcomputer with a 12 bit resolution data acquisition board. The computer sends the desired pulsing duration signals with 300 mA and 3 V to a solid state relay (DC to DC), the power supply device and the relay convert to a 3 A and 14 V signal in order to open the injector valve for the desired perturbation action. The measured bubble signals, once bandpass filtered, are sent to both the oscilloscope and data acquisition computer. The oscilloscope samples the signals to obtain a digitized time series for further statistical analysis while the computer converts them into the form of a return map plot for the purpose of monitoring the bubble behavior. Both data acquisition devices collect the data at a sampling rate of 1000 points per second. Without losing generality of the system dynamics, the graphing rate is set at 100 points per second to reduce the use of memory during the monitoring process (computer system has 8 MB ram). Since the perturbation is

an open-loop type constant gas pulsing action, all the pulsing variables used such as the pulse amplitude, pulse timing, and pulse duration, for this study are fixed referring to Table 1 in Chapter 3. The opening and closing times for the injector valve according to the manufacture specifications, are 1 ms and 2 ms, respectively.

The bubbling motions with different pulsing perturbations are depicted in Figure 47. The return plots to describe the motion of system states are depicted in Figure 48a-d. The curved appearance of the attractor shows that the system is undergoing an aperiodic bubbling motion. The corresponding mutual information plot shown in Figure 48(b,d), further confirms the argument of aperiodic bubbling. The mapping points intensely accumulate in the regions around 0.06 and 0.14, which indicates the existence of limit cycles in the dynamics. Owing to the unique character of the sensitivity of chaotic systems to small perturbations, a small amount of gas pulsing (system control parameter of pulse amplitude) is expected to yield a radical change in bubble behavior. In fact, the pulsing gas is about 2.6 % of that supplied for aperiodic bubbling; refer to Table 1 in Chapter 3.

When gas pulsing is added, a very short period of transient time shows that the pulsing gas momentarily disrupts the no perturbation aperiodic bubbling motion and behaves irregularly based on the return plot observation. After the transient decays, the forced bubbling system seems to lock into a noisy period-2 mode of bubbling motion, and all the system states are observed to oscillate in these two limit cycles. Figure 48c shows a better visual observation of the system motion, and the periodic behavior is confirmed by the mutual information plot (Figure 48d). This periodic state bubbling observation and its argument for existence of limit cycles is consistent with the results obtained from the

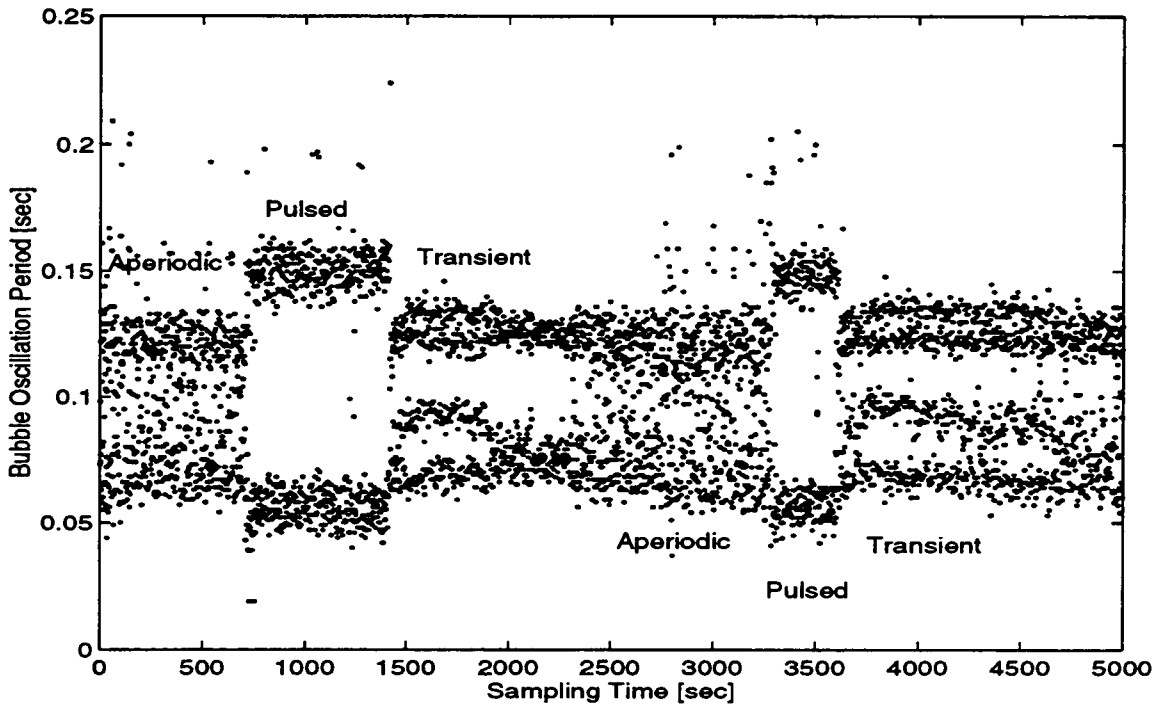


Figure 47. Overview of bubble behavior at flow of 585 cc/min

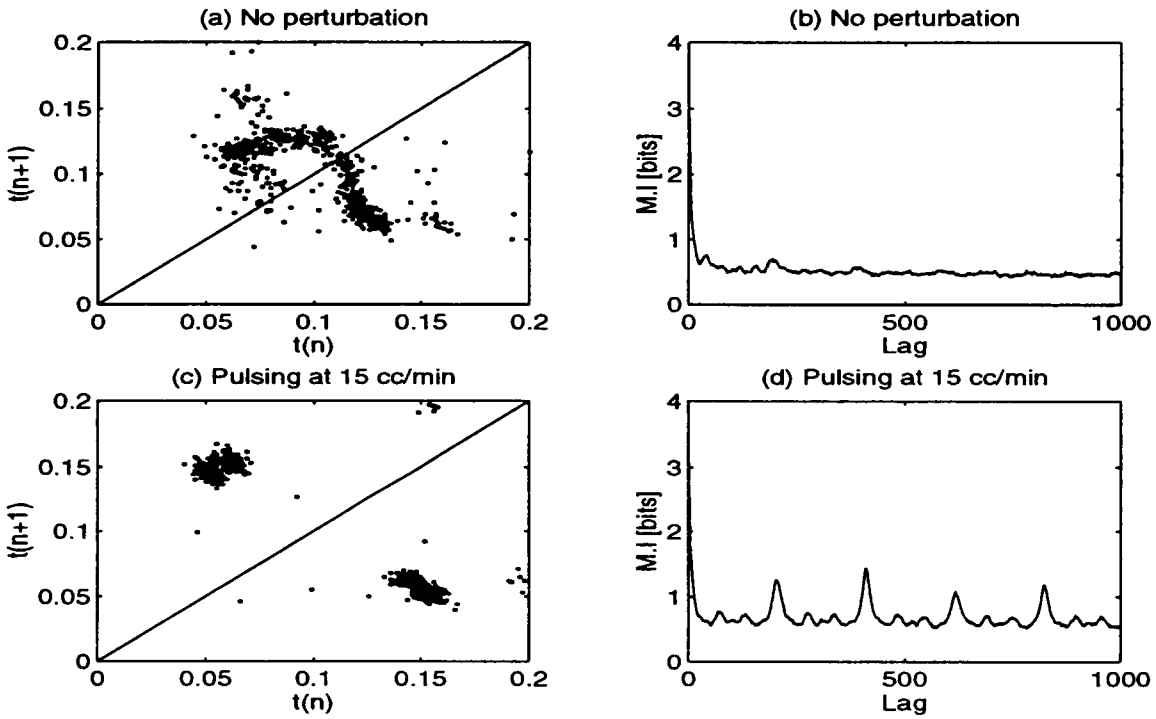


Figure 48. Bubble behavior due to entrainment at flow of 585 cc/min

forced periodic sound wave perturbation. However, the limit cycle regions are not observed at the same locations when compared with the results obtained from sound wave perturbation. Such observation is reasonably explained by the difference in the perturbation types. The forced sound wave perturbation vary pressure without changing the average net gas flow to the nozzle while the pulsing perturbation changes the average net flow compared to the no pulsing average flow. Obviously, the pulsing action might appear to be just pushing the system to the subspace of the periodic window; however, the occurrence of periodic windows after the onset of chaos seems to be attributable to the existence of limit cycles in the system. Therefore, the observation strongly suggests that this bubbling system has two limit cycles in the chaotic regime.

Some of the mapping points which occasional fail to land inside the cycles are possibly interpreted as the noise effect from the surroundings or the lack of tight perturbation to the system. When the collected data are mounted on the computer, a very short time interval of millisecond is required to save the data temporarily on the hard-drive due to the small memory size. This time interval stops all perturbation action and causes an unsmooth injection operation. When perturbation is not applied to the system, the system states escape from the cycles and wander around the bounded region. Once perturbation is applied again, the system motion finally settles and reaches perturbing steady state. Despite these walk-out system states, the bubble behavior is expected to be stabilized in the desired region when the perturbation is applied at all times.

Near the bifurcation point of dynamic bubble system, the application of external gas pulsing is shown to amplify the periodic signal and shifts of the bifurcation point, thus

stabilizing the periodic state at its limit cycles. Also, a very short transient time is required for the system to lock into the limit cycles. Now, what about the response of the system after the perturbation is removed? Will the states wander around in the bounded region? It turns out that here as well as the constant pulsing perturbation can have a drastic influence on the bubble system. Referring to Figure 47, which depicts the overall bubble behavior after switching off the perturbation, it shows that the system wanders around in the bounded region without settling and forms a unique bubbling state. This phenomenon can be described as the system is excited to a new bubbling state, and the system states cannot find their fixed point after leaving the close orbits of limit cycles. Suddenly, the system states settle at a period-4 bubbling motion since the no perturbation aperiodic state is suppressed and shifted by the pulsing perturbation. The system seems to find "permanent" steady states at this period-4 bubbling pattern for a substantial period during the transient decay process. When the transient is further decayed, the system states continuously change their bubbling motion under the form of a noisy period-2 oscillation for another lengthy period. Finally, with the complete decay of the transient, all the system states realize their no perturbation states of aperiodic bubble behavior and start to fill the entire bounded region of the return plot with an aperiodic bubbling motion. An overview of the transient bubble behavior is summarized in Figure 49 for a clear visual observation.

The ability to tame chaotic behavior by external pulse perturbation and its lengthy periodic transient time, is somewhat surprising and provides important entrainment information as if the periodic motion is highly desired. Obviously, the most desirable situation is the complete control of the dynamic behavior of the system so that the system

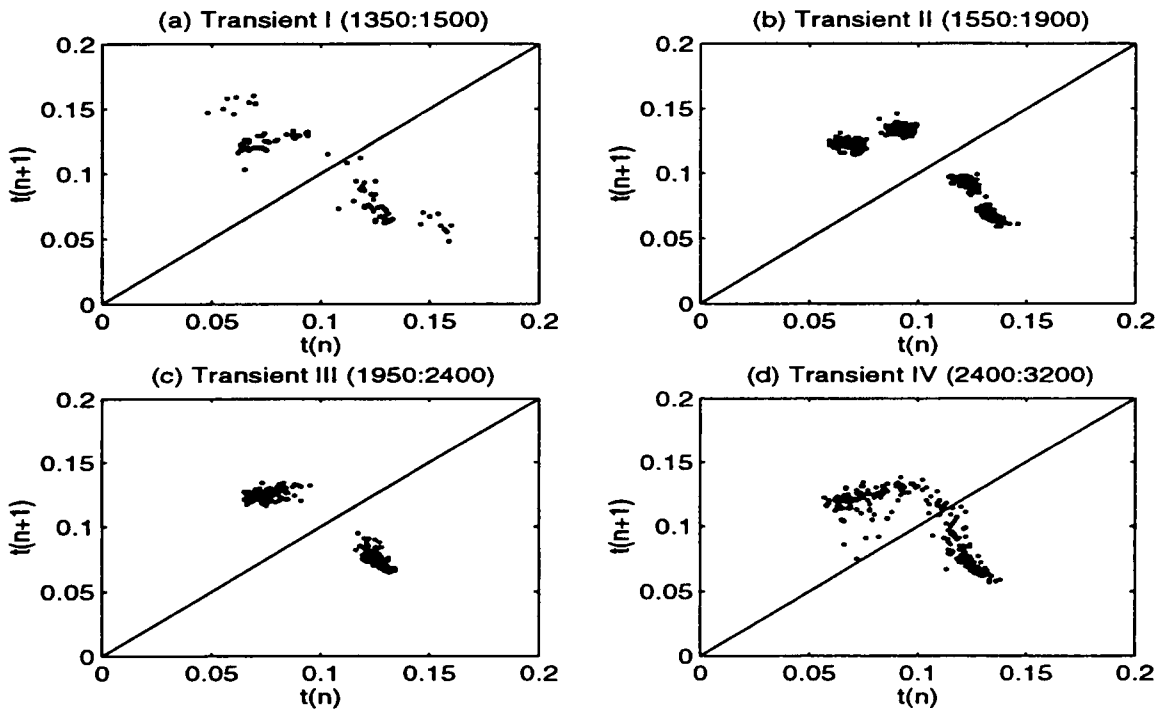


Figure 49. Transient bubble behavior after entrainment at flow rate of 585 cc/min

could be operated optimally. However, from engineering needs, entraining the system to evolve to prespecified dynamic behavior might be acceptable. In this case, a small percentage of the gas flow is pulsed compared to the operating gas flow in order to modify the complex chaotic bubble behavior to its periodic motion. This entrainment method relies on the unique property of chaos system sensitivity to external perturbation of and the existence of limit cycles in the deep chaotic regime.

Figure 50 demonstrates a stabilization to periodic states in the bubble column using a continuous external pulsing perturbation. Again, the unique feature of a long transient behavior through periodic states is exit. In the plot, the aperiodic bubble behavior is continuously stabilized by adding the proper pulsing perturbation. With perturbation,

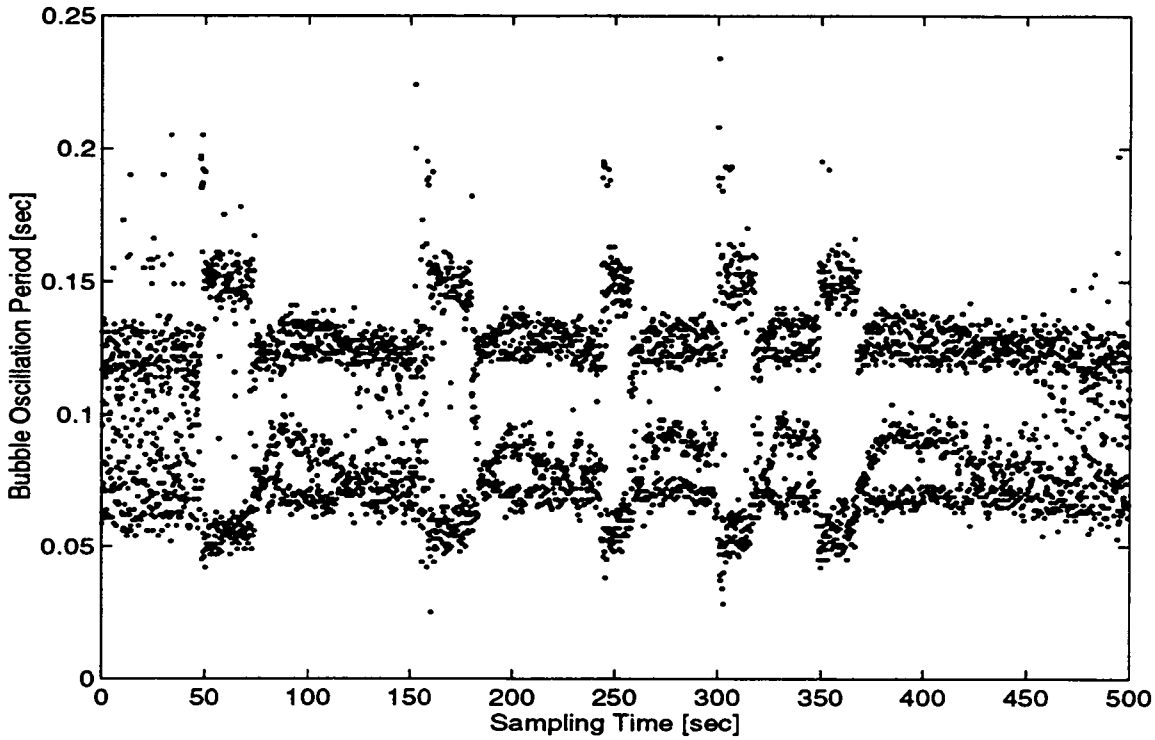


Figure 50. Bubble behavior with continuous entrainment at flow rate of 585 cc/min

the system is forced to operate at noisy period-2 limit cycles. When perturbing is switched off, the bubbles first oscillate in a period-4 behavior then the system states lock into a period-2 bubbling motion for a relatively long time before becoming chaotic. When the transient is almost decayed, perturbation is turned on, and the system is pushed into periodic motion again. Such continuous periodic bubble behavior makes one believe that the control of chaotic bubble behavior can be achieved by using the modified feedback control model of the pulsing perturbation (i.e. the OPF control method).

The entrainment of chaos to its periodic cycles has been demonstrated for a system operating near the bifurcation point. To further test the entrainment approach, a similar pulsing perturbation at a higher operating air flow of 617 cc/min is used in the

pulsing perturbation at a higher operating air flow of 617 cc/min is used in the investigation. The results show that the suppression of chaos can also be obtained with external perturbation. Figure 51 depicts the time return plot for a system with and without perturbation. The system states without perturbation fill a layered region on the return plot along with two regions intensely visited by the system states. These regions seem to attract most of the system states when the pulsing perturbation is applied. Although the corresponding return plot shows a "fuzzy" period-2 bubble behavior, the mutual information plot clearly indicates periodic bubble behavior in the column. Also, the entrained cycles of 0.05 and 0.15 are consistent with the one stabilized using an air flow of 585 cc/min.

Results from both the sound wave and gas pulsing external perturbation methods show that near the bifurcation points of the dynamic bubbling system, the application of external perturbations causes a suppression of chaos and a shift in the bifurcation point to a higher flow, thus stabilizing the periodic states. Also, results from both methods indicate the existence of limit cycles in the bubble dynamics of the investigated column. A derivation of physical model for the dynamical system is not required for either method. However, careful tuning of system perturbation variables is required. In addition, results obtained from the open-loop gas pulsing perturbation make one believe that the control of periodic state in a deep chaotic regime is practical. By carefully tuning the control parameters (pulsing amplitude, duration, timing), the present bubbling system is conjectured to entrain to periodic cycles even without a control model. Furthermore, it is believed that the system is controllable by using the modified OPF method similar to the

control model used by Vasu et al. [28].

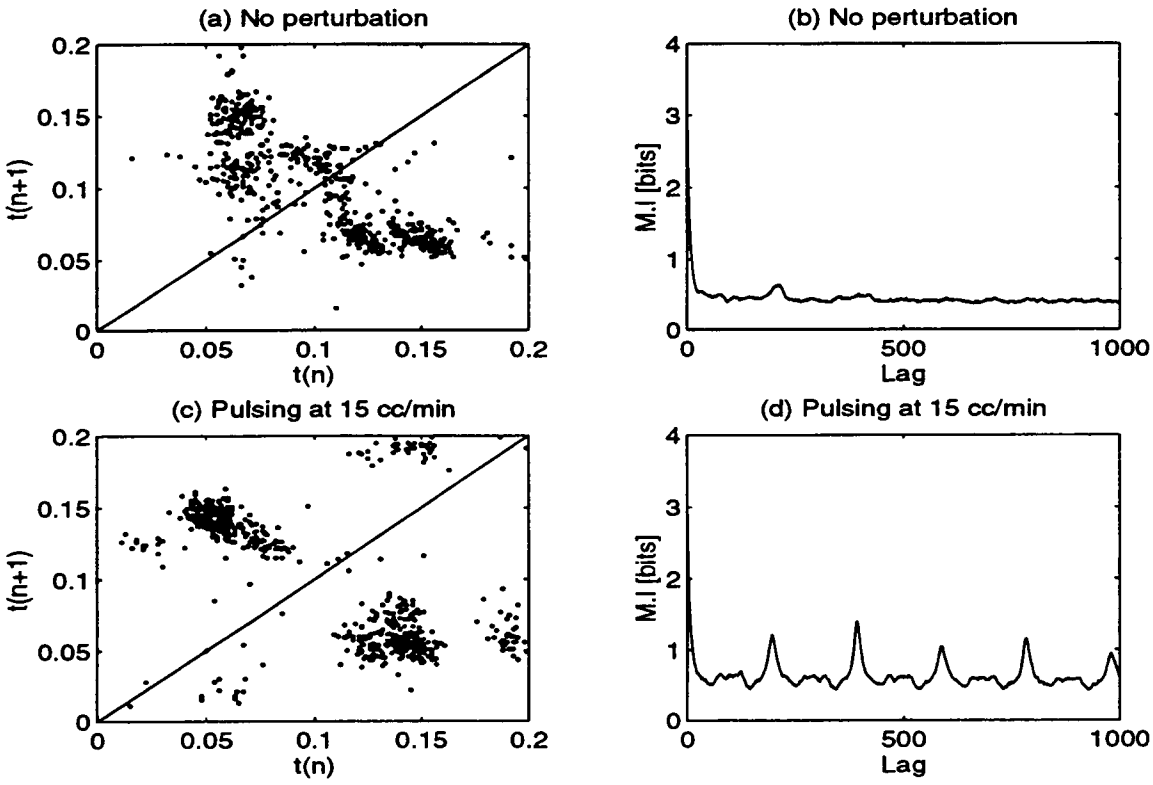


Figure 51. Bubble behavior due to entrainment at flow of 617 cc/min

The key differences for sound wave and pulsing perturbation methods are 1) the pulsing perturbation only entrains the system to its limit cycles while forced periodic sound wave perturbations yield different periodic orbits. 2) the perturbation by sound wave varies the pressure in the gas supply line with no change in the average gas to the nozzle while pulsing slightly (~2%) increase the average gas flow to the column. Note the change in average flow can be adjusted by slightly closing the main supply needle valves. The average gas flow could be manipulated with a standard control system.

5.3 EVALUATION OF THE FEEDBACK CONTROL METHODS

Results from constant perturbations make one believe that implementation of the OGY or Bruns control method is practical for the investigated bubbling system. Therefore, the remaining portion of this study is to evaluate the possible implementation of these control methods for the bubbling system. The main purpose of this section is to demonstrate the method for calculating the manipulate variables for control. Both of these control strategies use a linearized unstable second order model for their controller design. The OGY method calculates and implements a manipulated variable change for every system state on the return map. The Bruns nonlinear relay control strategy only uses two valves for the manipulated variable depending on the system states. Otherwise, these two control strategies are very similar. In order to simplify the presentation of the controller design, only the OGY method is presented.

5.3.1 The OGY Design Calculations

The OGY control method uses the inherent irregularity of a chaotic system and its strong sensitivity to perturbations, to control the behavior of a physical system to a fixed point. The study on gas pulsing perturbation shows that the bubble dynamics are extremely sensitive to such perturbation. Thus, the control variable of gas flow is used as the manipulated variable for the OGY control implementation. In addition, this input variable also meets the three basic criteria for the OGY control method. The experimental techniques should be similar to the gas pulsing perturbation studies (refer to section 5.4 of this chapter).

Since the OGY control method is based on an approximate unstable linear second order model about a fixed point, the local dynamics around the desired fixed point needs to be addressed. A simple outline of the OGY linear model is described in Chapter 2. Typical experimental data for chaotic bubble behavior are illustrated in Figure 52. In addition, a walk-in and walk-out sequence of the system states is shown on the plot. The fixed point and its linearized region needs to be chosen properly, in order to minimize the noise effect on the Jacobian matrix construction and also to retain the validity of linearization. Basically, mapping points from walk-in sequence toward the diagonal provides the empirical data for the model's stable eigenvector while walk-out sequences provide data for the unstable eigenvector.

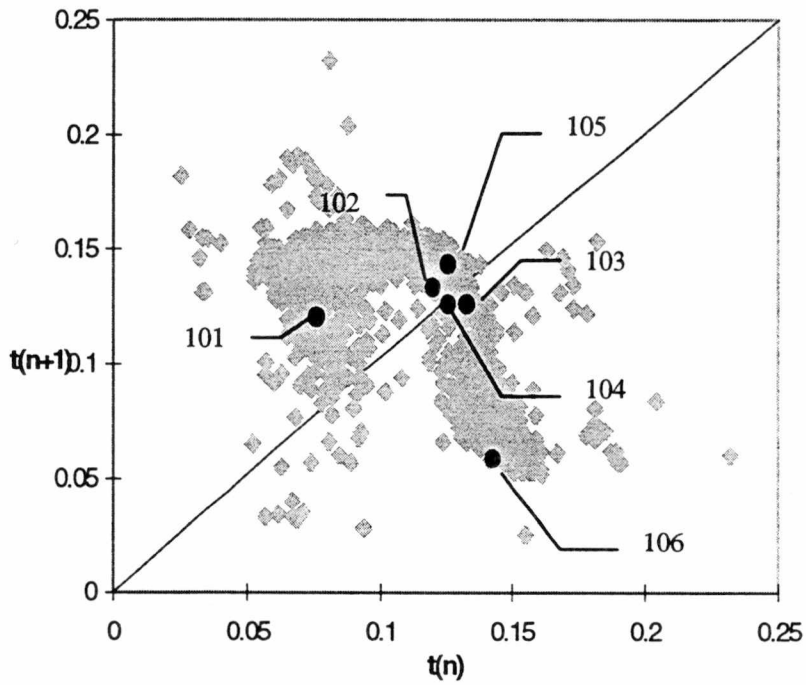


Figure 52. System states motion around an unstable fixed point from a chaotic attractor at flow of 585.8 cc/min

The linearized model that represents system states starts from a two-dimensional map:

$$\begin{pmatrix} \Delta t_n \\ \Delta t_{n+1} \end{pmatrix} = \begin{pmatrix} a_3 & a_4 \\ a_1 & a_2 \end{pmatrix} \begin{pmatrix} \Delta t_{n-1} \\ \Delta t_n \end{pmatrix} \tag{26}$$

Since a two-dimensional map is constructed by arranging the system mapping points as:

$$t_n = \begin{pmatrix} t_1 & t_2 & t_3 & . & . & t_{n-1} \\ t_2 & t_3 & t_4 & . & . & t_n \end{pmatrix} \tag{27}$$

One can further simply the entries of the M matrix as:

$$M = \begin{pmatrix} 0 & 1 \\ a_1 & a_2 \end{pmatrix} \tag{28}$$

Using this M, Eq. (26) is simplified as:

$$\begin{matrix} \uparrow \\ (t_{n+1} - x_F) \\ \downarrow \end{matrix} = \begin{pmatrix} a_1 \\ a_2 \end{pmatrix} \begin{pmatrix} \uparrow & \uparrow \\ t_{n-1} - x_F & t_n - x_F \\ \downarrow & \downarrow \end{pmatrix} \tag{29}$$

A simplified multiple regression model is written as :

$$t_{n+1} = a_1 t_{n+1} + a_2 t_n + (1 - a_1 - a_2) x_F \tag{30a}$$

which is:

$$t_{n+1} = a_1 t_{n-1} + a_2 t_n + c \tag{30b}$$

where : $c = (1 - a_1 - a_2)\, x_F$

All the sequential experimental data in the finite linear region are placed in the pattern:

$$\begin{pmatrix} \uparrow \\ t_{n+1} \\ \downarrow \end{pmatrix} = \begin{pmatrix} a_1 & a_2 & c \end{pmatrix} \begin{pmatrix} \uparrow & \uparrow & \uparrow \\ t_{n-1} & t_n & 1 \\ \downarrow & \downarrow & \downarrow \end{pmatrix} \tag{31}$$

Now, which data are qualified to be put into the matrices for the OGY quantities computation? To answer this question, a fixed-point along with its finite region needs to be pre-chosen for this period-1 control scheme. The pre-chosen fixed point ought to be located on the diagonal of the map where data points are intense. Also, the chosen sequence of time return points must maintain the linearization theory and must overcome the noise effect on the system state mapping points. In fact, the need for linear behavior (small region) and to overcome nose (large region) becomes a "jeopardy" for the proper calculation of the OGY quantities. A crucial software package provided by Dr. Daw helps to select both the appropriate data points and the finite region for control. The program also computes the theoretical fixed point to compare with the calculated fixed point based on the OGY method. The idea of this data selection method, called a cluster analysis technique, is to determine the walking sequences of all the data toward the control region with a cut-off range (i.e. the number of points for each data sequence that can be used in the region). Moreover, the algorithm also approximates the geometric structures of stable and unstable manifolds.

Once properly chosen, the data points can be put into Eq. (31) for computation. The least square solution of constant c provides the theoretical fixed point value. Using this value and recalling Eq. (29), the least square solution of constants a_i for Jacobian matrix construction can be computed:

$$\Delta t_{n+1} = (a_1 \quad a_2)\Delta t_n$$

then

$$(a_1 \quad a_2) = \frac{\Delta t_n{}^T \Delta t_{n+1}}{\Delta t_n{}^T \Delta t_n} \tag{32}$$

To verify the constructed Jacobian is faithful, the following mapping technique is used:

$$x_F = Mx_F \tag{33}$$

If the output of this mapping point appears reliable, then the local stable and unstable eigenvalues and eigenvectors can be calculated using the straightforward method described in chapter 2 of Eq.(11a-b)

$$Me_u = \lambda e_u \tag{11a}$$

$$Me_s = \lambda e_s \tag{11b}$$

where the subscripts u and s represent the unstable and stable directions. Because of the sensitivity of chaotic systems to small perturbations such as noise, the calculated results based on the above procedures seem to be unfaithful with large errors in the system's stable and unstable manifolds. Therefore, the development of another method for calculating control variables seems worthwhile.

Results from cluster analysis provide important and conclusive information about the system states motion, specifically, the identification of stable and unstable eigenvectors based on the states motion on the map. It was found that the walk-in sequence is always initiated by the system state, which falls a short distance from one side of the attractor edge. The very next point of the sequence is observed to "jump" into the control region. Also, the escape states constantly land on the other side of the edge. These observations obtained from the cluster analysis provide important information about the calculation of the stable and unstable manifolds. By using the states who initiates the walk-in sequence,

the stable manifold is computed with respect to the fixed point in a least square sense. The simple regression model is shown as:

$$\begin{pmatrix} \uparrow & \uparrow \\ x_F & x_F \\ \downarrow & \downarrow \end{pmatrix} = \beta_1 \begin{pmatrix} \uparrow & \uparrow \\ t_n & t_{n+1} \\ \downarrow & \downarrow \end{pmatrix} + \beta_2 \tag{34}$$

Similarly, the least square direction for an unstable manifold can be constructed. The return plots are depicted with constructed manifolds for three flows in Figure 53-55.

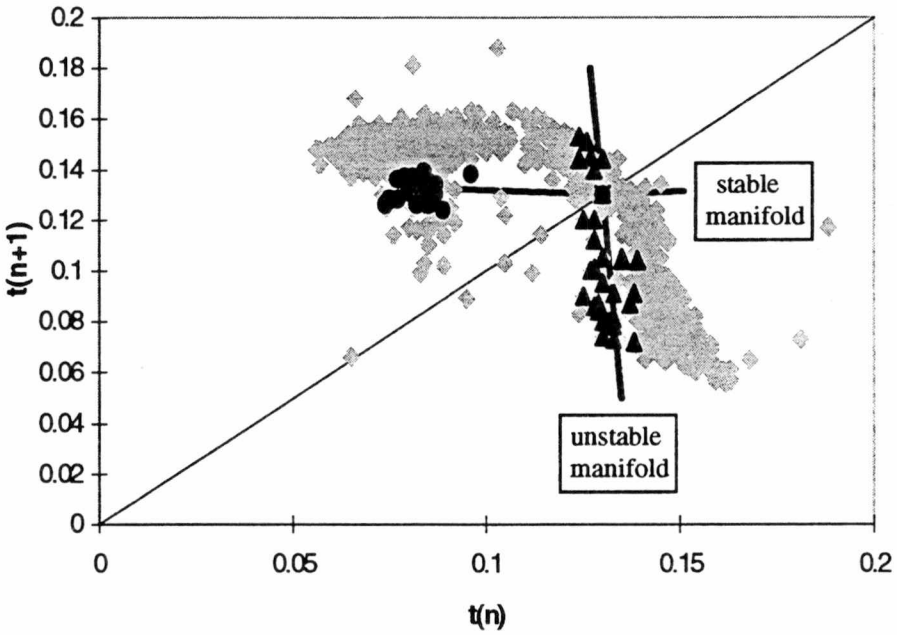


Figure 53. Illustration for stable and unstable manifolds at flow of 569.8 cc/min

Note : circle represents walk-in states; triangle represents walk-out states

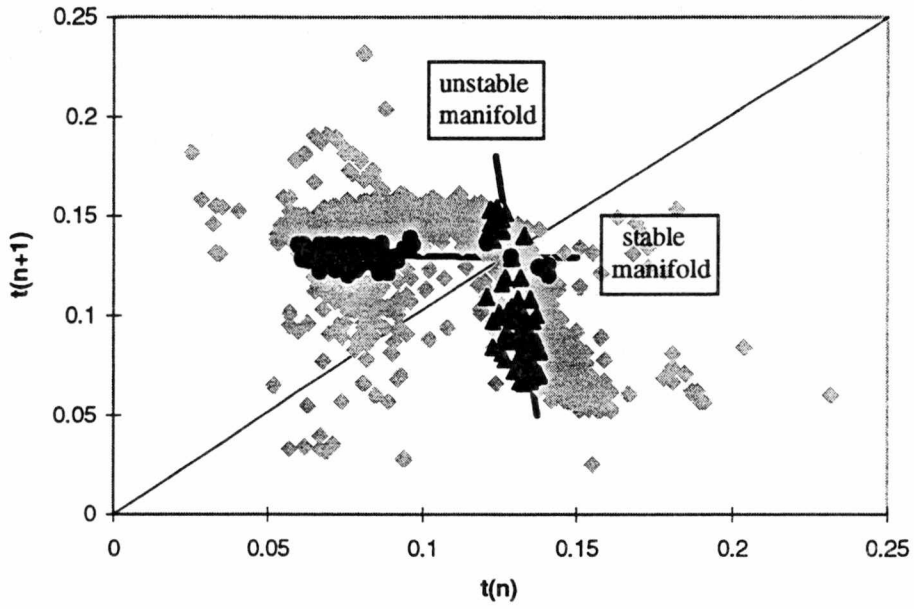


Figure 54. Illustration for stable and unstable manifolds at flow of 585.8 cc/min

Note : circle represents walk-in states; triangle represents walk-out states

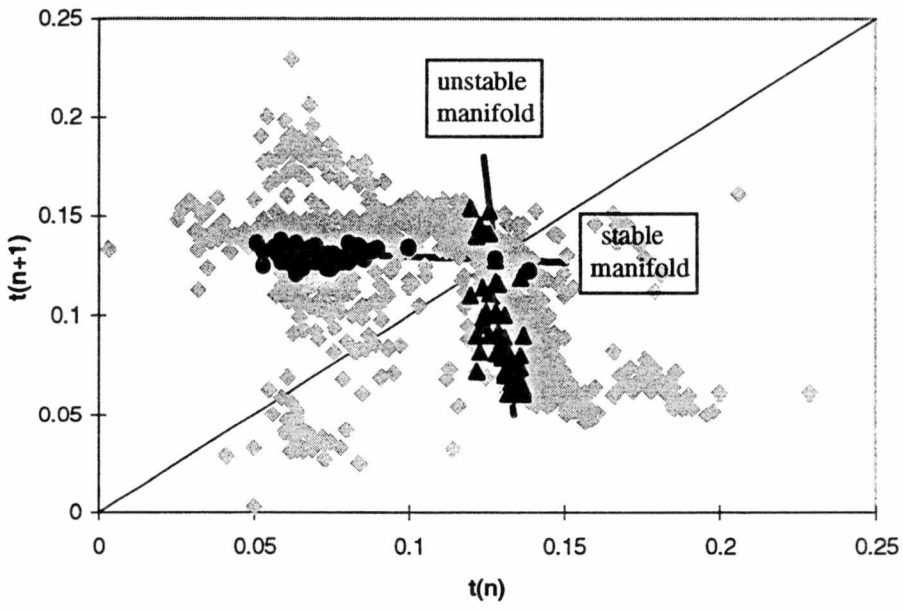


Figure 55. Illustration for stable and unstable manifolds at flow of 601.7 cc/min

Note : circle represents walk-in states; triangle represents walk-out states

By knowing these eigenvectors, one can calculate the corresponding eigenvalues based on the following procedure. Considering two mapping points perturbed from fixed point:

$$p_1 = (t_n, t_{n+1})$$
$$p_2 = (t_{n+1}, t_{n+2})$$

The slope between these two points is:

$$m = \frac{t_{n+2} - t_{n+1}}{t_{n+1} - t_n} \tag{35}$$

Since they are located on the same eigenvector, the generalized solution for the mapping points can be written like $t_{n+k} = \lambda^k t_n$. Therefore, Eq. (35) can be further simplified as:

$$m = \frac{\lambda^2 t_n - \lambda t_n}{\lambda t_n - t_n} = \frac{\lambda(\lambda - 1)}{(\lambda - 1)} \tag{36}$$

It turns out that, the eigenvalues around the fixed point is equal to the slopes of the eigenvectors as shown:

$$m = \begin{cases} \lambda & \lambda \neq 1 \\ \lambda & \lambda = 1 (L'HopitalRule) \end{cases}$$

Since the relationship between the perpendicular basis vectors $\{f_u, f_s\}$ and the old basis vectors $\{e_u, e_s\}$ is held as $f_s^T e_s = 1 = f_u^T e_u$: the basis vectors are just an inverse of eigenvectors.

$$\begin{bmatrix} f_s^T \\ f_u^T \end{bmatrix} = \begin{bmatrix} e_s & e_u \end{bmatrix}^{-1} \tag{12}$$

The shift vector s due to the perturbation is calculated based on two related fixed points:

$$s = \frac{t_F(p_{n+1}) - t_F(p_n)}{p_{n+1} - p_n} \tag{13}$$

where : p_n, p_{n+1} = operating conditions

$t_F(p_n), t_F(p_{n+1})$ = the corresponding fixed points

Table 3 summarizes the desired manipulated variables for the OGY control scheme based on the cluster analysis technique.

Table 3. The OGY quantities calculations

Air Flow	569.8 (cc/min)	585.8* (cc/min)	601.7 (cc/min)
Fixed Point	0.131	0.129	0.128
Stable Eigenvalues	-6.405e-16	6.458e-16	-0.0522
Unstable Eigenvalues	-16.333	-9.667	-13.200
Stable Eigenvectors	$\begin{pmatrix}0.150\\0.130\end{pmatrix}$	$\begin{pmatrix}0.150\\0.129\end{pmatrix}$	$\begin{pmatrix}0.150\\0.127\end{pmatrix}$
Unstable Eigenvectors	$\begin{pmatrix}0.127\\0.180\end{pmatrix}$	$\begin{pmatrix}0.126\\0.180\end{pmatrix}$	$\begin{pmatrix}0.124\\0.180\end{pmatrix}$
Basis Vectors $(f_s \quad f_u)^T$	$\begin{pmatrix}17.138 & -12.082\\-12.377 & 14.282\end{pmatrix}$	$\begin{pmatrix}16.300 & -11.682\\-11.202 & 13.584\end{pmatrix}$	$\begin{pmatrix}15.998 & -11.278\\-11.029 & 13.331\end{pmatrix}$
Shift Vector (w/r *)	$\frac{-1}{16}\begin{pmatrix}.002\\.002\end{pmatrix}$	0 *	$\frac{-1}{16}\begin{pmatrix}.001\\.001\end{pmatrix}$

*Note : the controlling state is based on flow rate of 585.8 cc/min

With the previous values, the perturbation required for control action at each iteration is calculated by:

$$\Delta p = \frac{\lambda_u}{\lambda_u - 1} \frac{f_u{}^T \delta x_n}{f_u{}^T s} = C f_u{}^T \delta x_n \tag{14}$$

The linear model of the OGY control method for period-2 is similar to period-1 except for using a three-dimensional map and controlling two fixed points.

The OGY method states that the control action needs to be applied every period of the map only if the calculated quantities are reliable. However, it is reasonable to apply control twice for the period-2 control based on the viewpoint of tight control. Similarity, a period-4 control scheme can be performed by controlling four fixed points on the diagonal of the 5-dimensional return map. The tight controlling action requires the application of the algorithm four times per period.

5.3.2 Experimental Concerns for the Bubbling System

Because of the sensitivity of chaotic systems to small perturbation, the effect of noise on the dynamical system needs to be handled carefully. Noise can cause the control procedure to lose control and the system state escape to the chaotic attractor. Possible sources of noise for this bubble column are conjectured to come from surroundings, small foam bubbles in the column, or high dimensional measuring device such as a laser beam. The second caution for the implementation of both the OGY and Bruns control methods is the problem introduced by system drifting phenomenon. Possible sources of drift for this bubble column are conjectured to come from temperature variations and viscosity variation due to the absorption of moisture by the liquids. Consequently, the experimental

adjustments previously mentioned, need to be made for successful OGY control implement. Nevertheless, this portion of study for evaluating the potential implementation of the OGY control method, seems to provide conclusive information about the investigated bubbling system. Moreover, all the endeavors of this study are intended to serve as a progress report for revealing the bubble dynamics as well as the control of chaotic bubble behavior.

CHAPTER 6

CONCLUSIONS AND RECOMMENDATIONS

Concepts based on chaos theory have been used to describe the complex bubble dynamics for moving bubbles in liquid. There is no doubt that this theory will continue to aid in understanding bubble systems. Chaos can also be used to interpret various aspects of order-disorder transitions that arise in bubbling systems as well as unstable behavior. The characterization portion of this thesis is aimed at increasing fundamental knowledge about bubble dynamics from a standpoint of deterministic chaos. The results from the investigated bubble column illustrate the progression of period-doubling bifurcation route to chaos as well as its character of low dimension. The existence of periodic cycles is experimentally verified, and the results provide useful information for further endeavors such as entrainment and the OGY or Bruns control methods. In addition, the spatial and temporal character for the bubble column is also experimentally quantified. Consequently, the knowledge from the characterization portion of the study, provides clues for rationalizing ongoing research, process development, and forms a foundation for empirical designs.

The suppression of chaos for the investigated system near period-doubling bifurcation points is experimentally verified using a sound wave periodic perturbation. The period-doubling bifurcation points are shifted as well. The bifurcation route to chaos is found to be extremely sensitive to the pressure variation in the gas holdup section.

The experimental investigation on the subject of entrainment of chaotic bubble behavior to its periodic states is also successful. Results from both perturbation methods

suggest the bubble column is dominated by two limit cycles in the chaotic bubbling regime. Although the results of system entrainment are impressive, a feedback control scheme is highly desired to take complete control of the complex bubble behavior so that the system can be operated at its optimum condition. Therefore, a feedback controller is designed based on the OGY or Bruns control schemes to control the chaotic bubble behavior.

Evaluation of the potential OGY control method is performed by designing the control algorithm to change the manipulate variable as well as by determining the optimal fixed points for control. The results indicate the implementation of these models on the current bubbling system is practical. However, because of the sensitivity of a chaotic system to the effects of perturbation can be highly amplified leading loss of control at a high noise level. The problems introduced by system drift also present challenges for current controller design as well. Also, because the control schemes localize the chaotic motion about an unstable periodic orbit that lies on the attractor, and the control perturbation is continuously dependent on system errors, the re-evaluation of the manipulate variables calculation during the experiment is highly recommended.

Nevertheless, the ability to control the bubble column is anticipated and highly recommended for future study. The implication from the entrainment study that relate to OPF control scheme is also recommended for further investigation. Also, a system with multiple-nozzles is recommended for investigation from the viewpoint of industrial needs. The effort of this thesis, in fact, is likely to provide fundamental and conclusive information for the future chaos control implementation. Successful control implementation can bridge the gap between the science of chaos and its technological

applications in terms of finding both practical motivation and new needs in engineering arts.

REFERENCES

REFERENCES

1. Braiman, Y, Goldhirsh, I. (1991). "Taming chaos dynamics with weak periodic perturbation", Phys. Rev. Lett. **66**, 2545-2548

2. Bruns, D.D. and Bailey, J.E. (1975). "Process operation near an unstable steady state using nonlinear feedback control", Chemical Engineering Science, **30**, 755-762

3. Bruns, D.D. and Bailey, J.E. (1977). "Nonlinear feedback control for operating a nonisothermal CSTR near an unstable steady state", Chemical Engineering Science, **32**, 257-264

4. Carr, T.W. and Schwartz,I.B. (1995). "Controling high-dimensional unstalble steady states using delay, duration and feedback", Special Project in Nonlinear Science, Code 6700.S

5. Chacon, R. (1995). "Suppression of chaos by selective resonant parametric perturbations", American Phy. Society **51**, 761-764

6. Chakka, Pitchaiah. (1994) . "An experimental study of chaotic behavior of bubbles in liquid columns", Master Thesis

7. Clift, R.Grace,Jr and Weber, M.E. (1978). "Bubble, Drops, and Particles", Academic Press, New York

8. Davidson, J.K. and Schuler, B.O.G.(1960). "Bubble formation at an orifice in a viscous liquid" Transactions Institution of Chemcial Engineers, 38

9. Daw, C.S. and Halow, J.S.(1990). "Modeling determinstic chaos in gas-fluidized Beds", AICHE symposium syries **88**:289,61-69

10. Devanathan, N and Dudukovic. M.P.(1995). "Chaotic flow in bubble column reactors", Chemcial Engineering Science **50**:16, 26661-2667

11. Ditto, W.L., Lindner, J.F, Spano, M.L. (1995) . "Techniques for the control of chaos", Physica D, **86**, 198-211

12. Dreyer, K. and Hickey, F.R. (1991). "The route to chaos in dripping water faucet", American Journal of Physics, **59**:7, July

13. Garfinkel, A., Spano, M.L., Ditto, W.L., and Weiss, J.N. (1992). Science **257**, 1230

14. Helsby. F.W. and Tuson. K.R.(1955). "Behavior of air bubbles in aqueous solutions" Research 8

15. Mittoni, L.J, Schwarz. M.P., and La Nauze. R.D.(1995). "Deterministic chaos in the gas inlet pressure of gas-liquid bubbling systems", American Institute of Physics, Phys. Fluid **7**:4, April

16. Moon, C.Francis. (1992). "Chaotic and Fractal Dynamics", John Wiley & Sons,Inc.,

17. Nguyen, K, Bruns, D.D, Daw, C.S, Chakka, P, Cheng, M, Finney, C.E.A, (1996). "Spatio-temporal dynamcis in a train of rising bubbles", Draft for Publication in Chemical Engineering Journal

18. Ott, E., Gregobi, C. and Yorke, J,A.(1990). "Controlling Chaos" Phys.Rev. Letters **64**,1196-1199

19. Rollins R.W, Parmananda P, and Sherard P. (1993). "Controlling chaos in highly dissipative systmes: A simple recursive algorithm", Physical Review E **47**:2, February

20. Schouten, J.C., Takens, F, and Van der Bleek, C.M. (1994). "Maximum-likelihood estimation of the entropy of an attractor", Physical Review E, **49**:1, 126-129

21. Schouten, J.C.,T akens, F, and Van der Bleek, C.M. 1994). "Estimation of the dimension of a noisy attractor", Physical Review E **50**:3

22. Schouten, J.C., Van der Stappen, M.L.M,Takens, F, and Van den Bleek C.M.(1995). "Dimension, entropy and correlation integral of fluidized beds as spatio-temporal systems", Draft of Manuscript for Publication in Physical Reviw E, April

23. Shannon, C.E and Weaver, W. (1949). "The mathematicla theory of communications" University of Illinois Press, Urbana

24. Shaw, R. "The dripping faucet as a model chaotic system", Aerial Press, Box 1360, Santa Cruz, CA 95061

25. Spano, M.L. and Ditto, W.L. (1993). "Controlling chaos", Naval Research Review XLV

26. Strogatz, S.H. (1994). "Nonlinear Dynamics and Chaos", Addison-Wesley Publishing Co.

27. Tritton, D.J. and Egdell. C. (1993). "Chaotic bubbling", American Institute of Physics, Phys. Fluids **5**:2,February

28. Vasudevan, M., Finney, C.E.A., Nguyen. K., Van Goor. N.A., Bruns. D.D., and Daw. C.S. (1995). "Stabilization and destabilization of slugging behavior in a laboratory fluidized bed", ASME **2**, 1001-1014

29. Wu, Xiaomao and Schelly, Z.A. (1989). "The effect of surface tension and temperature on the nonlinear dynamics of the dripping faucet", Physica D, 40

30. Wu, Xiaomao, Tekle, E, and Schelly, Z.A. (1989) "Dripping faucet apparatus with temperature and high-solution timing and flow rate controls", Rev. Sci. Instrum., **60**:19

APPENDICES

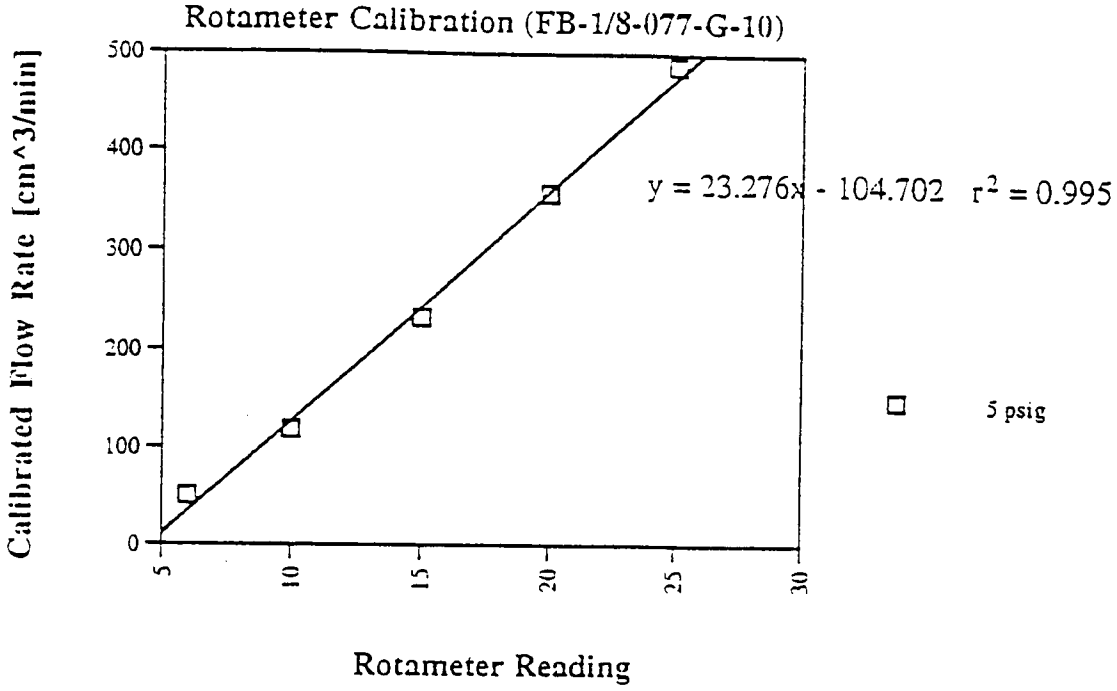
APPENDIX A

Table A1. Calibration for rotameter (FB-1/8-077-G-10)

Pressure	2 psig		7 psig			10 psig			12 psig		
Rot. Reading	Flow [cm^3/min]	Flow Diff [cm^3/min]	Rot. Reading	Flow [cm^3/min]	Flow Diff [cm^3/min]	Rot. Reading	Flow [cm^3/min]	Flow Diff [cm^3/min]	Rot. Reading	Flow [cm^3/min]	Flow Diff [cm^3/min]
3.50	4.19		10.00	140.96		20.00	426.01		20.00	458.39	
4.00	12.30	8.11	10.50	153.42	12.46	20.50	441.94	15.93	20.50	474.31	15.92
4.50	20.40	8.11	11.00	165.88	12.46	21.00	457.87	15.93	21.00	490.24	15.92
5.00	28.51	8.11	11.50	178.33	12.46	21.50	473.80	15.93	21.50	506.16	15.92
5.50	36.62	8.11	12.00	190.79	12.46	22.00	489.73	15.93	22.00	522.08	15.92
6.00	44.72	8.11	12.50	203.24	12.46	22.50	505.66	15.93	22.50	538.01	15.92
6.50	52.83	8.11	13.00	215.70	12.46	23.00	521.59	15.93	23.00	553.93	15.92
7.00	60.93	8.11	13.50	228.16	12.46	23.50	537.52	15.93	23.50	569.85	15.92
7.50	69.04	8.11	14.00	240.61	12.46	24.00	553.45	15.93	24.00	585.78	15.92
8.00	77.14	8.11	14.50	253.07	12.46	24.50	569.38	15.93	24.50	601.70	15.92
8.50	85.25	8.11	15.00	265.53	12.46	25.00	585.31	15.93	25.00	617.62	15.92
9.00	93.35	8.11	15.50	277.98	12.46						
9.50	101.46	8.11	16.00	290.44	12.46						
10.00	109.57	8.11	16.50	302.90	12.46						
10.50	117.67	8.11	17.00	315.35	12.46						
11.00	125.78	8.11	17.50	327.81	12.46						
11.50	133.88	8.11	18.00	340.27	12.46						
12.00	141.99	8.11	18.50	352.72	12.46						
12.50	150.09	8.11	19.00	365.18	12.46						
13.00	158.20	8.11	19.50	377.64	12.46						
13.50	166.30	8.11	20.00	390.09	12.46						
14.00	174.41	8.11	20.50	402.55	12.46						
14.50	182.51	8.11	21.00	415.01	12.46						
15.00	190.62	8.11	21.50	427.46	12.46						
			22.00	439.92	12.46						
			22.50	452.37	12.46						
			23.00	464.83	12.46						
			23.50	477.29	12.46						
			24.00	489.74	12.46						
			24.50	502.20	12.46						
			25.00	514.66	12.46						

Table A2. Calibration for Rotameter (R-2-15-D,stainless)

8 psig			13 psig		
Rot. Reading	Flow [cm^3/min]	Flow Diff [cm^3/min]	Rot. Reading	Flow [cm^3/min]	Flow Diff [cm^3/min]
55.00	605.67		60.00	791.56	
60.00	663.10	57.44	65.00	854.84	63.28
65.00	720.54	57.43	70.00	918.12	63.28
70.00	777.97	57.44	75.00	981.40	63.28
75.00	835.41	57.43	80.00	1044.68	63.28
80.00	892.84	57.44	85.00	1107.96	63.28
			90.00	1171.24	63.28
			95.00	1234.52	63.28
			100.00	1297.80	63.28



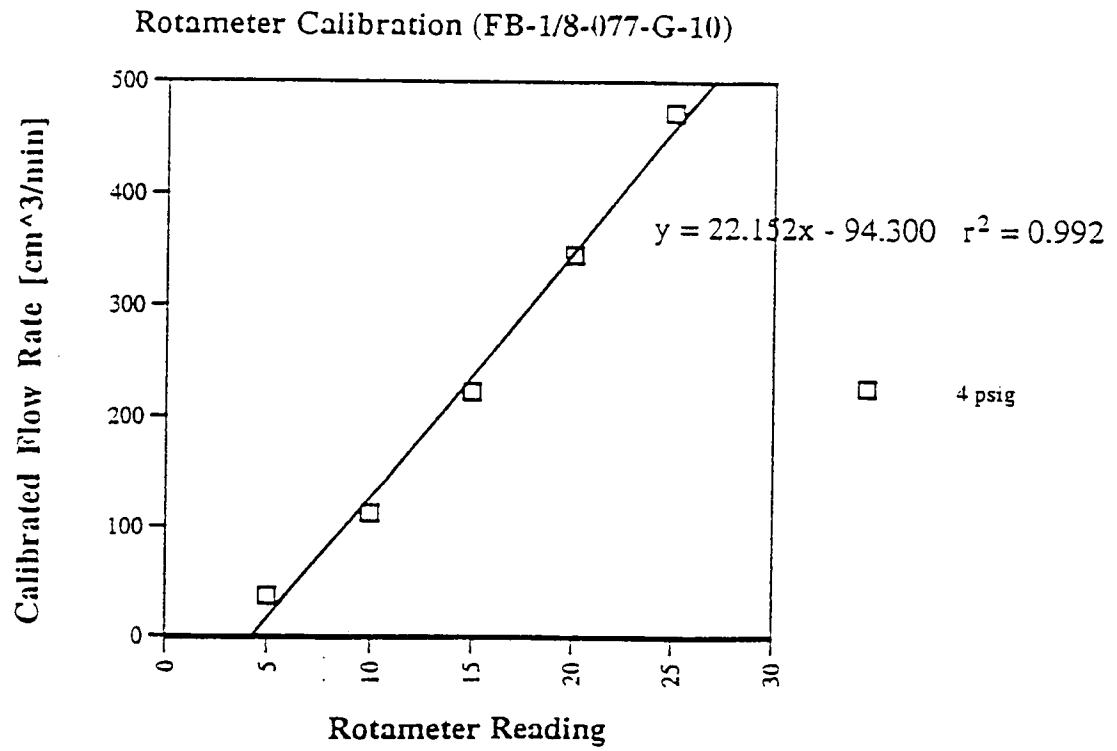


Figure A1. Rotameter (FB-1/8-077-G-10, stainless) calibration at inlet pressures of 4 and 5 psig

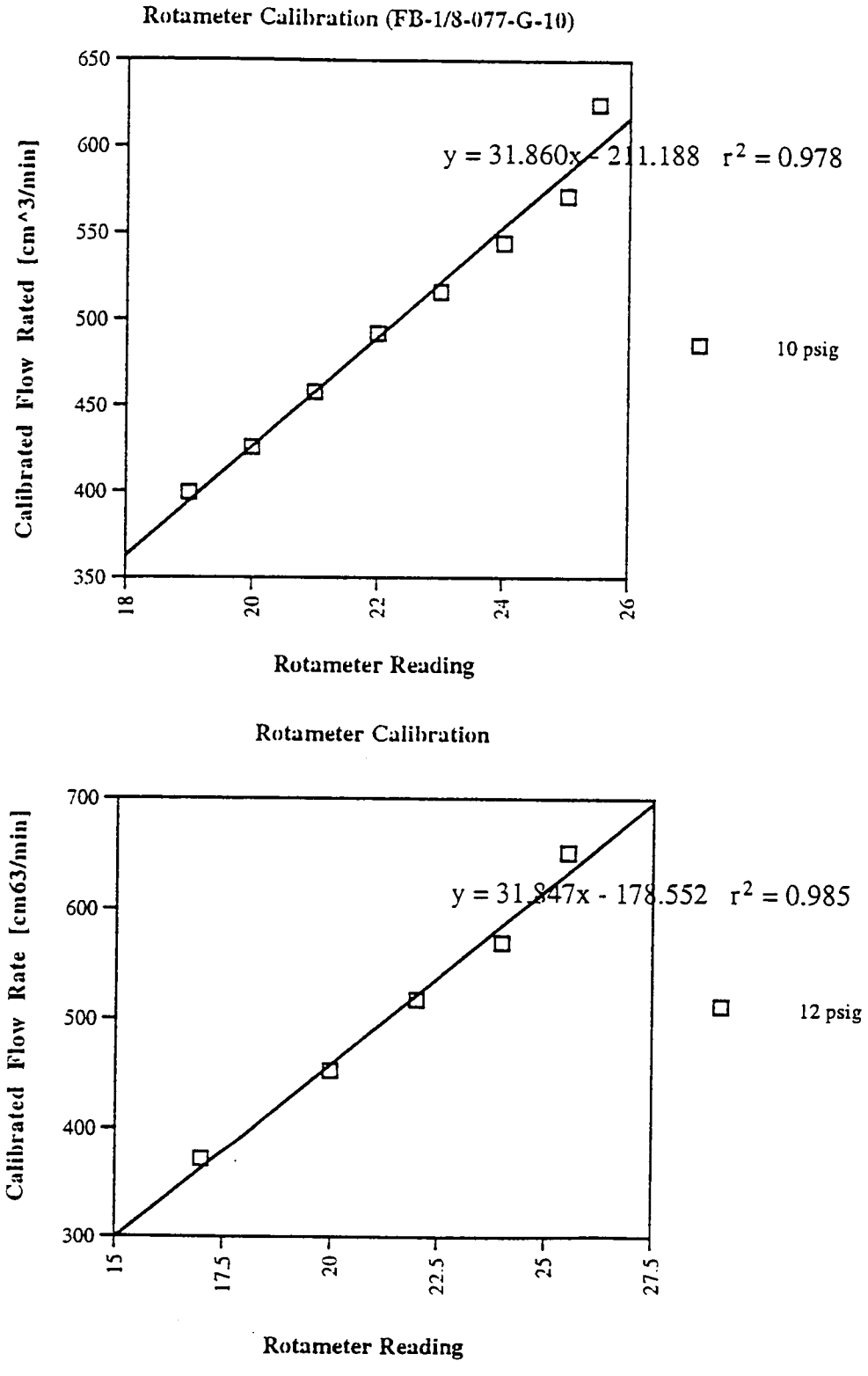


Figure A2. Rotameter (FB-1/8-077-G-10, stainless) calibration at inlet pressures of 10 and 12 psig

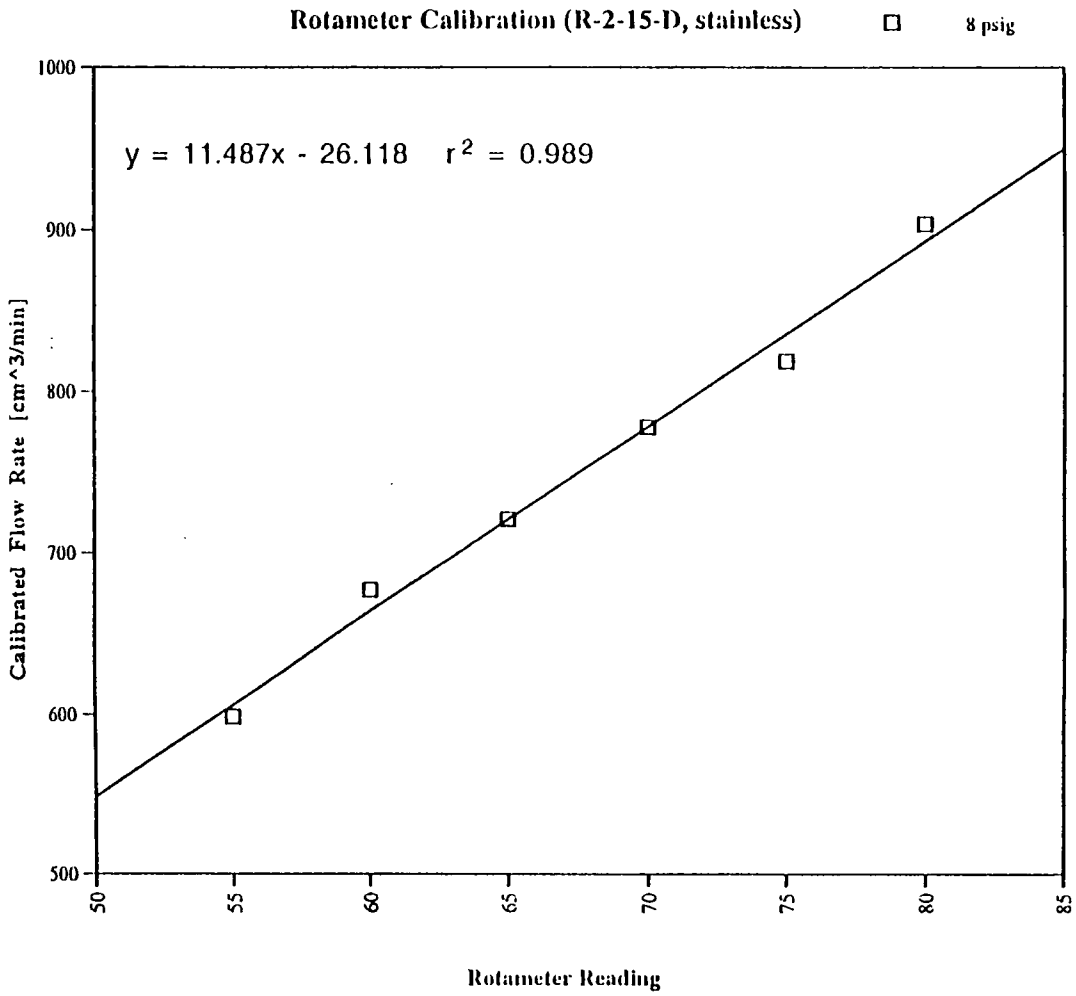


Figure A3. Rotameter (R-2-15-D, stainless) calibration at inlet pressure of 8 psig

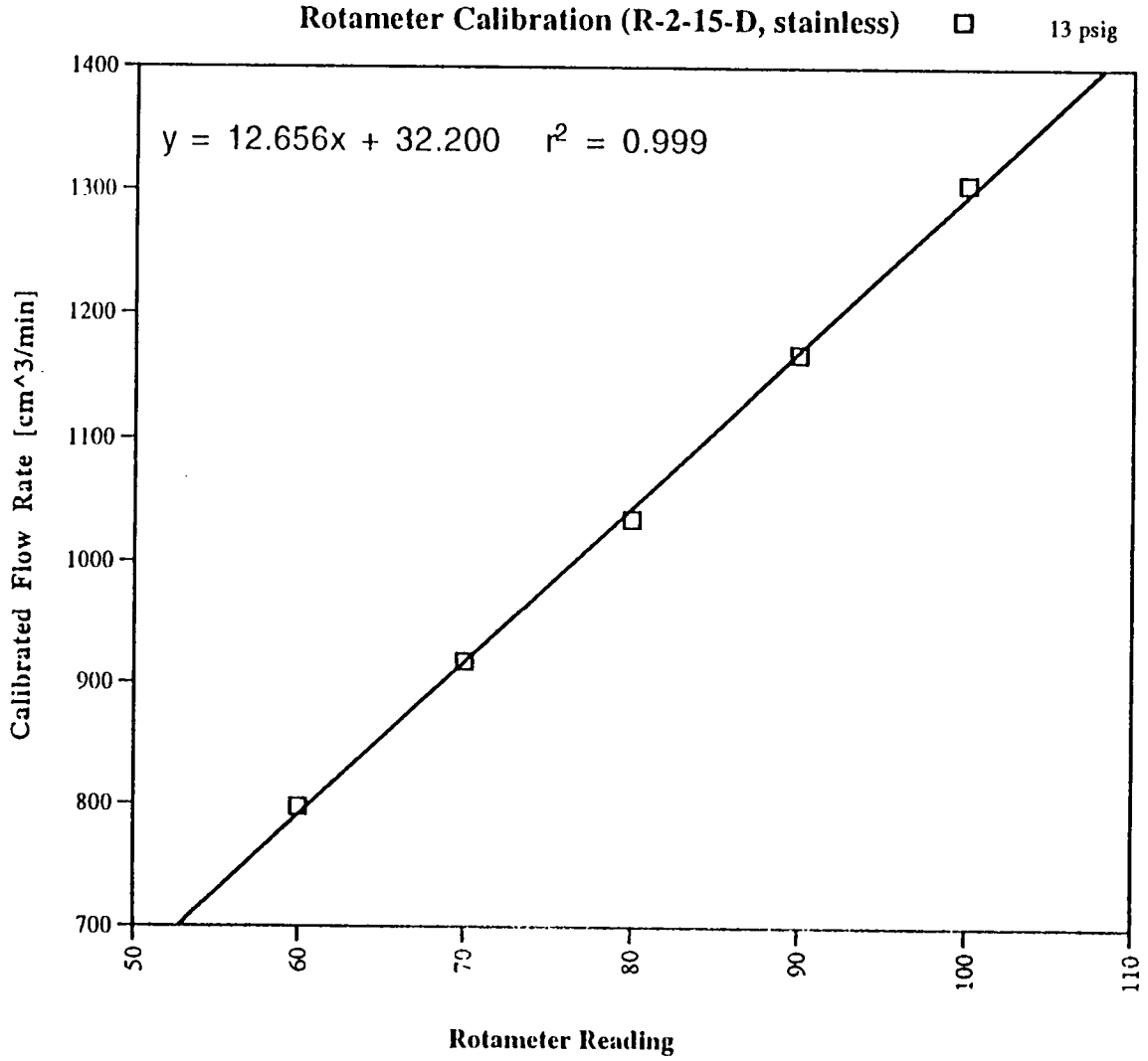


Figure A4. Rotameter (R-2-15-D, stainless) calibration at inlet pressure of 13 psig

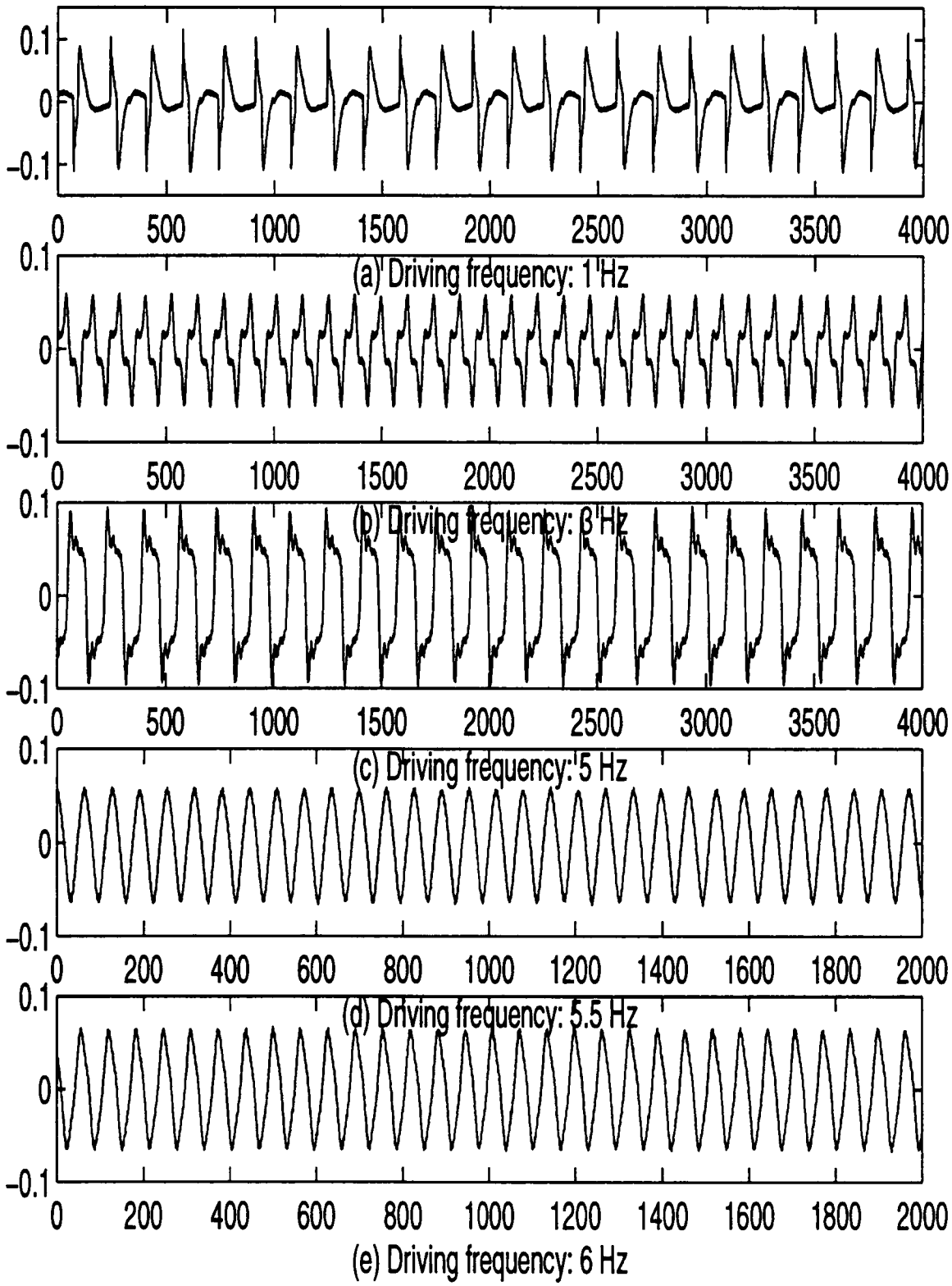


Figure A5. Time series for testing speaker

APPENDIX B

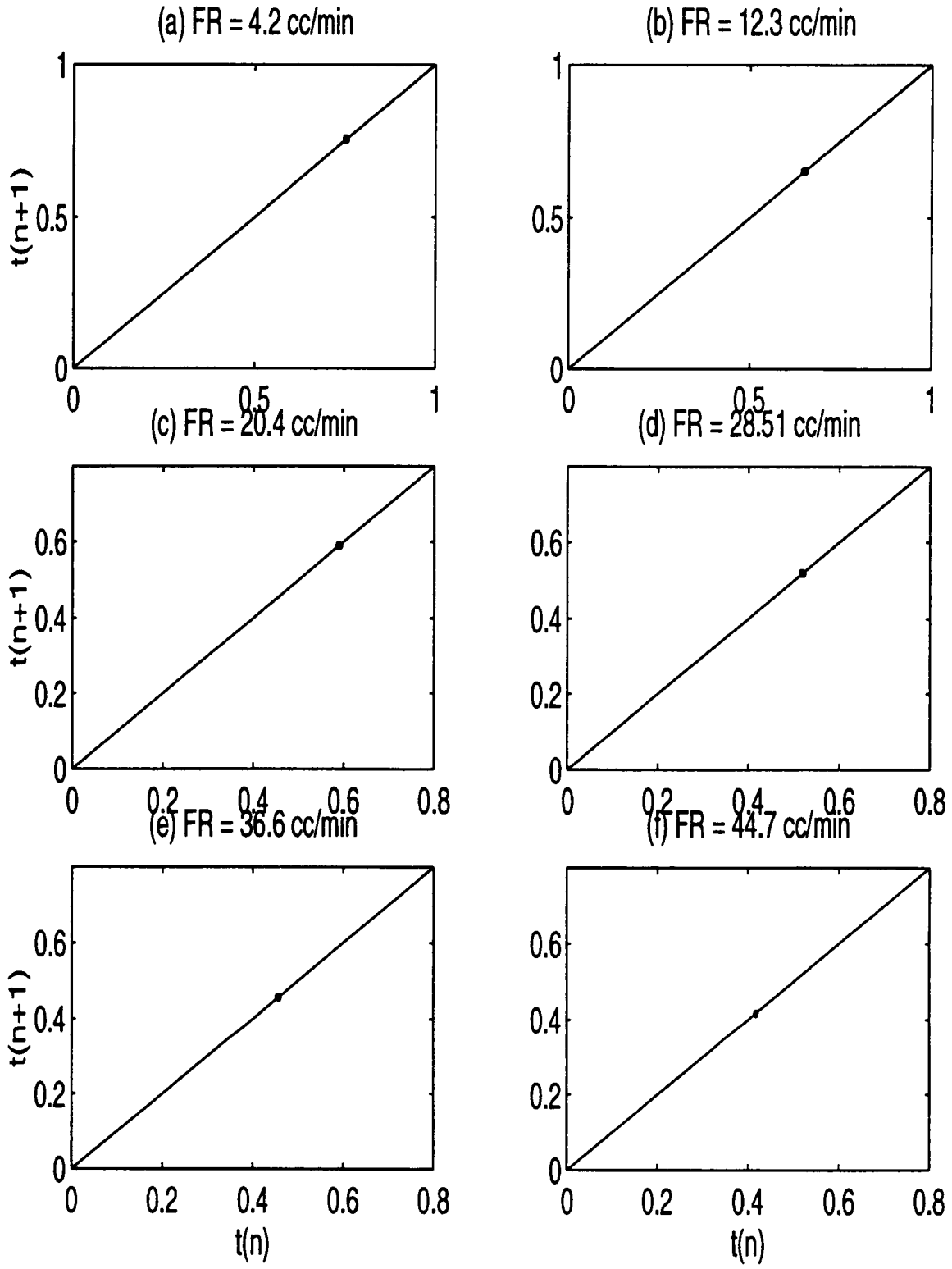


Figure B1. Time return maps of pressure measurements for air flows between 4.2 and 44.7 cc/min

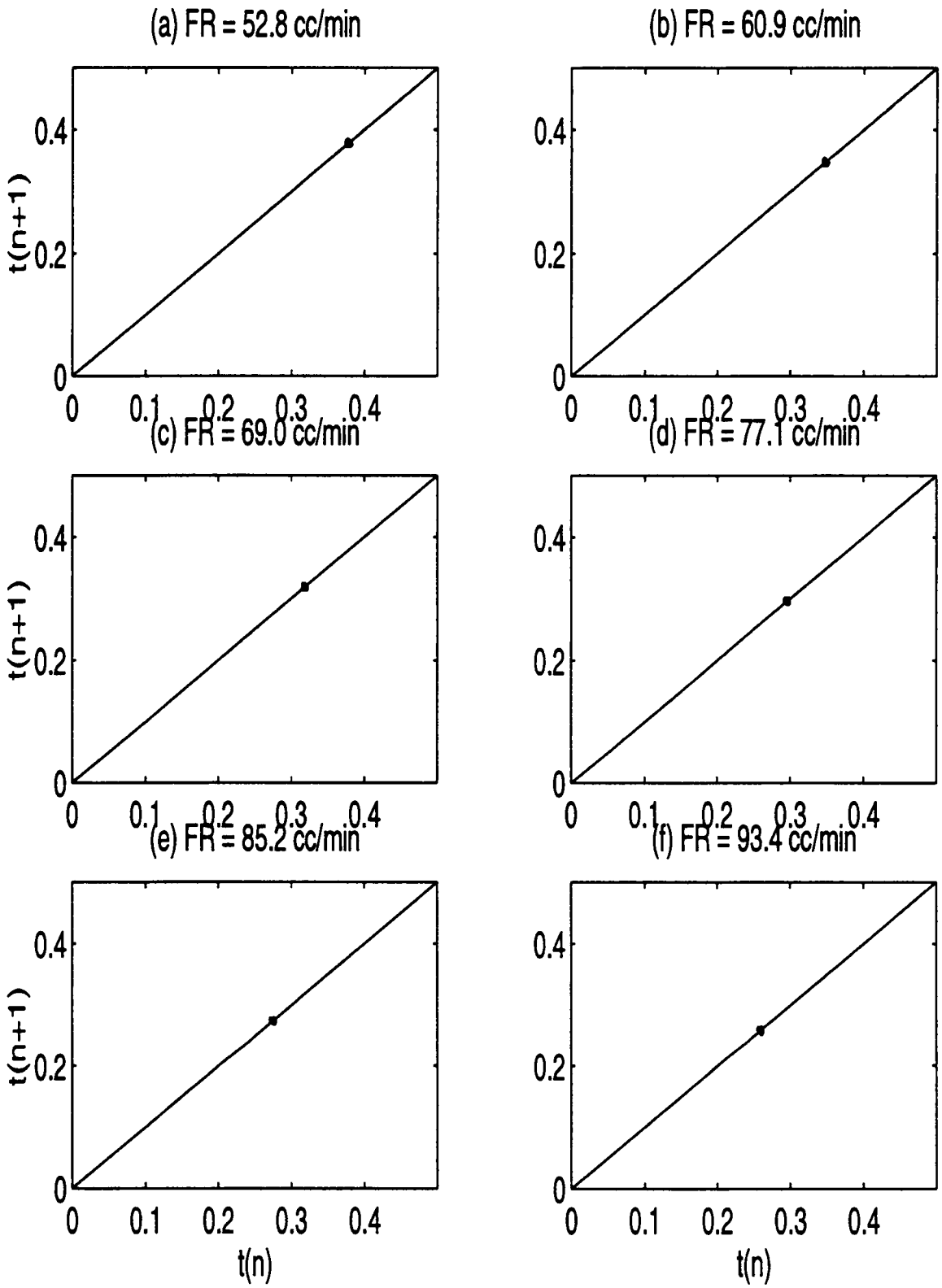


Figure B2. Time return maps of pressure measurements for air flows between 52.8 and 93.4 cc/min

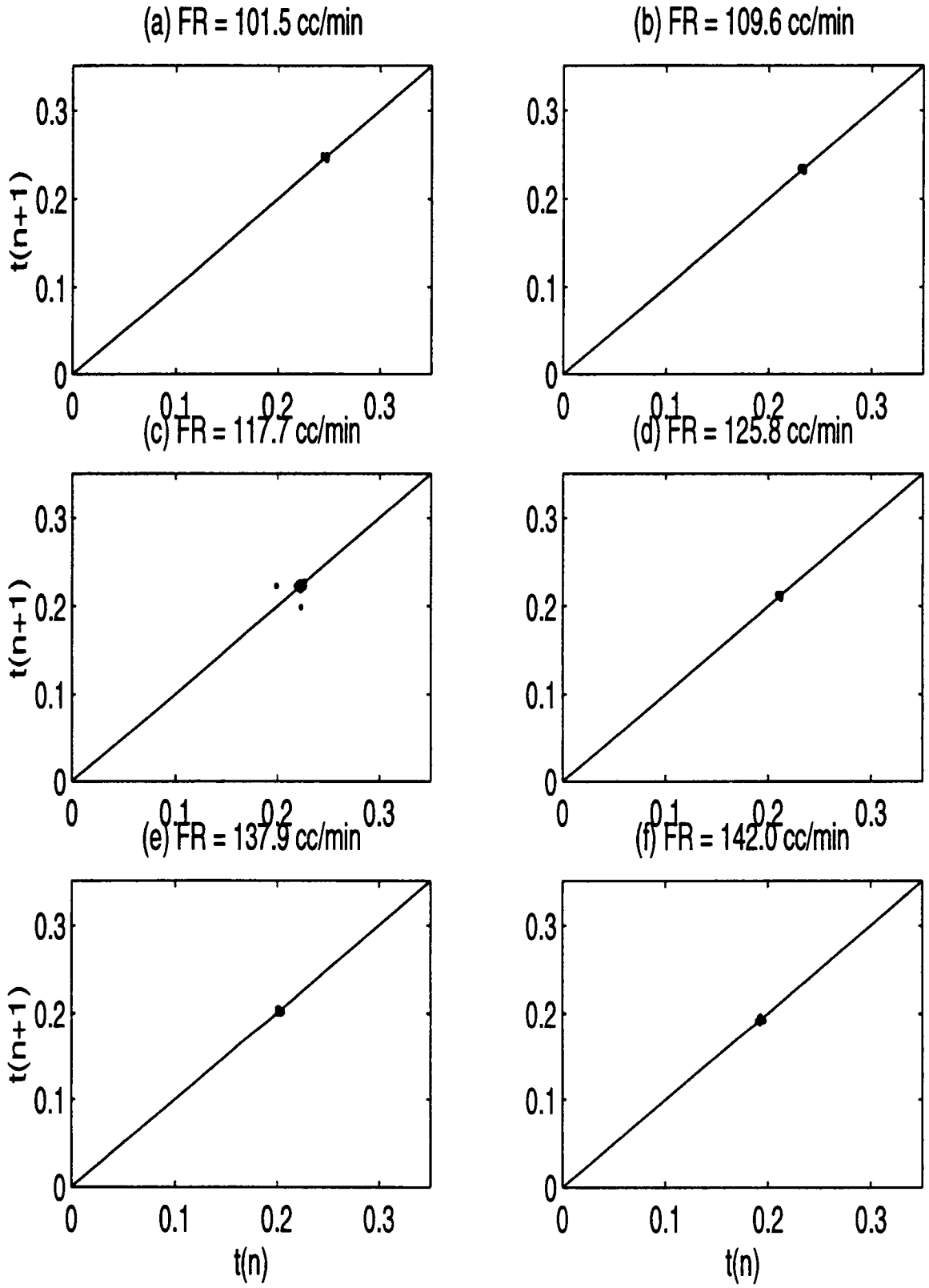


Figure B3. Time return maps of pressure measurements for air flows between 101.5 and 142.0 cc/min

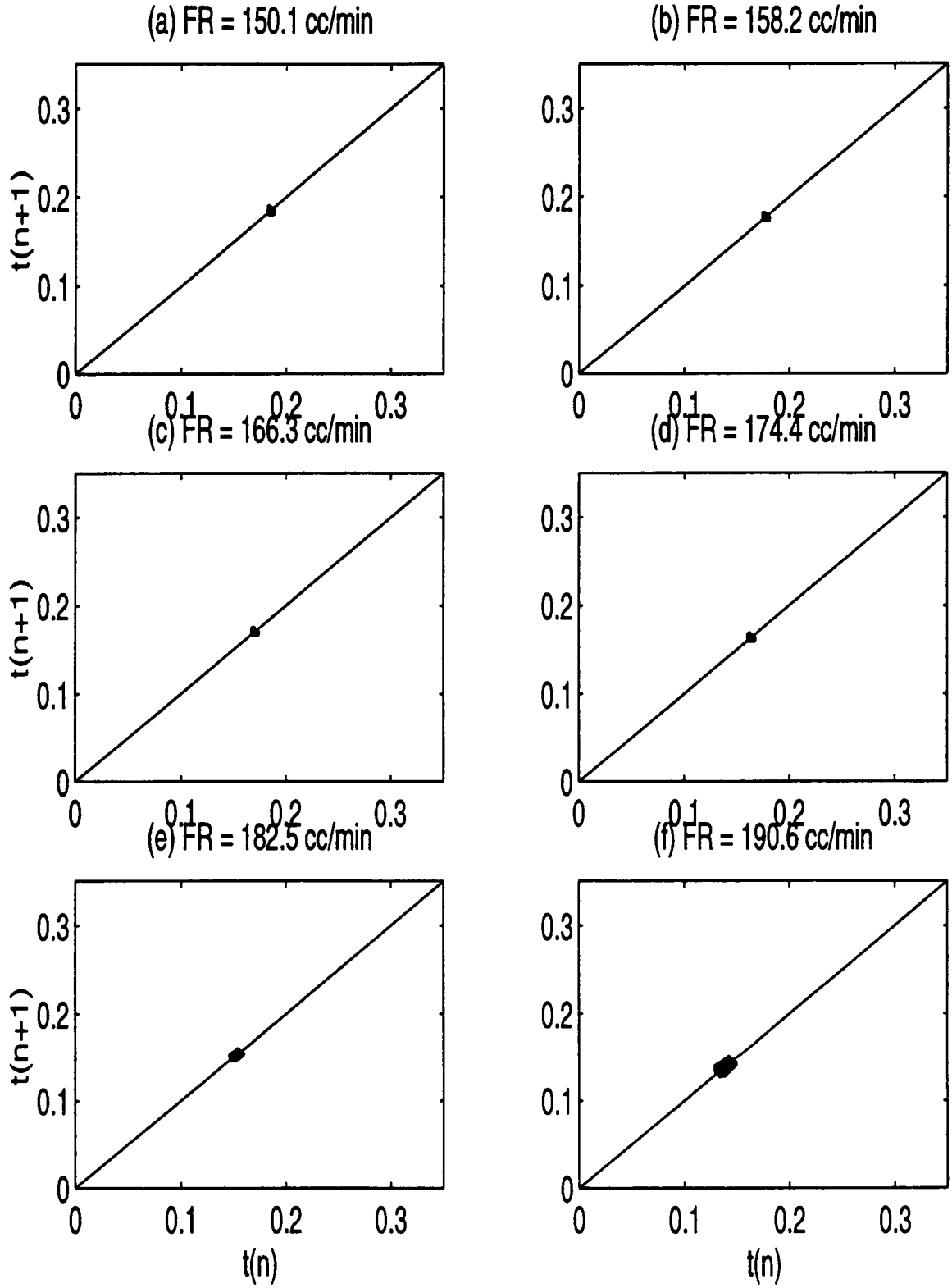


Figure B4. Time return maps of pressure measurements for air flows between 150.1 and 190.6 cc/min

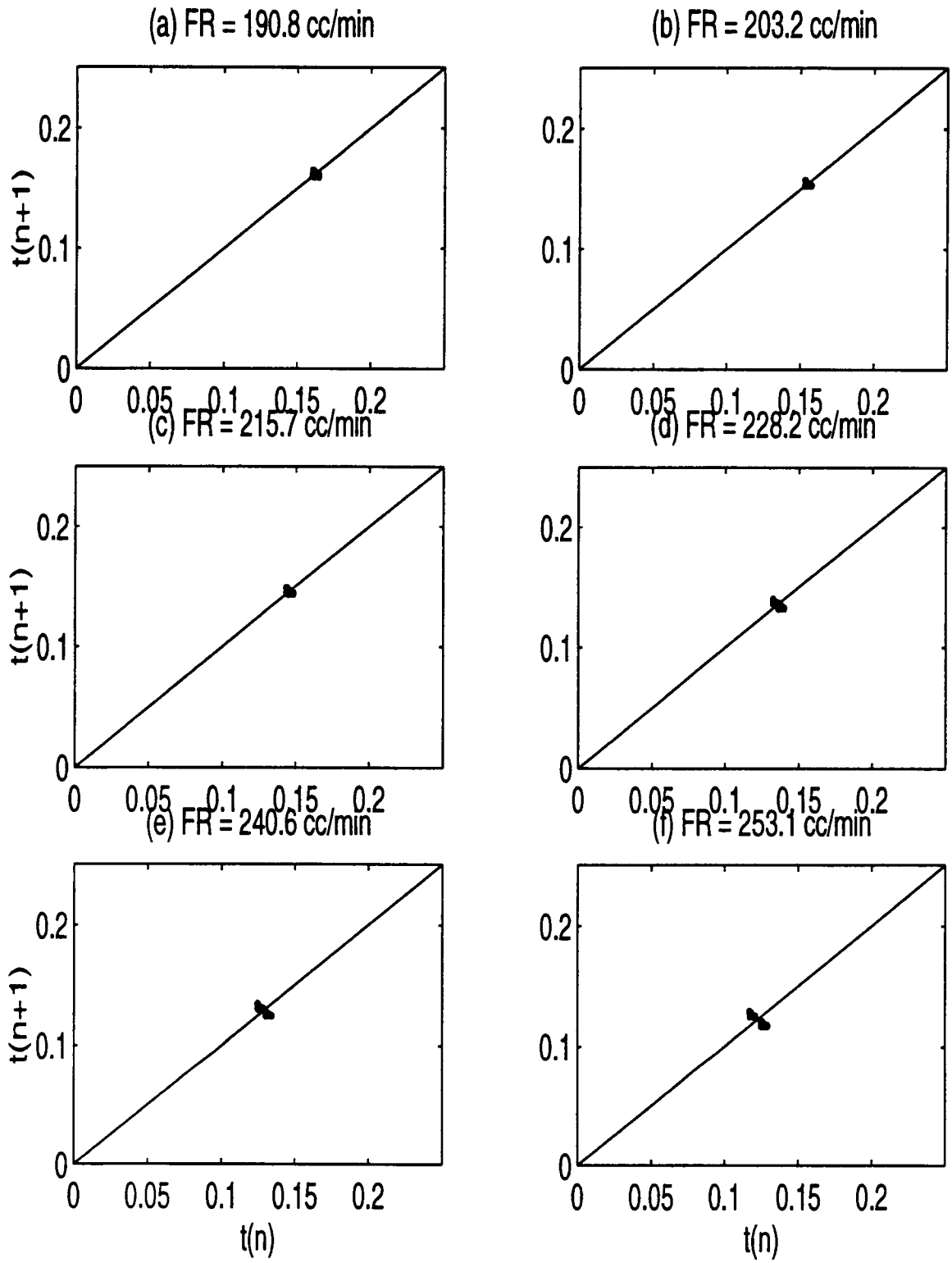


Figure B5. Time return maps of pressure measurements for air flows between 190.8 and 253.1 cc/min

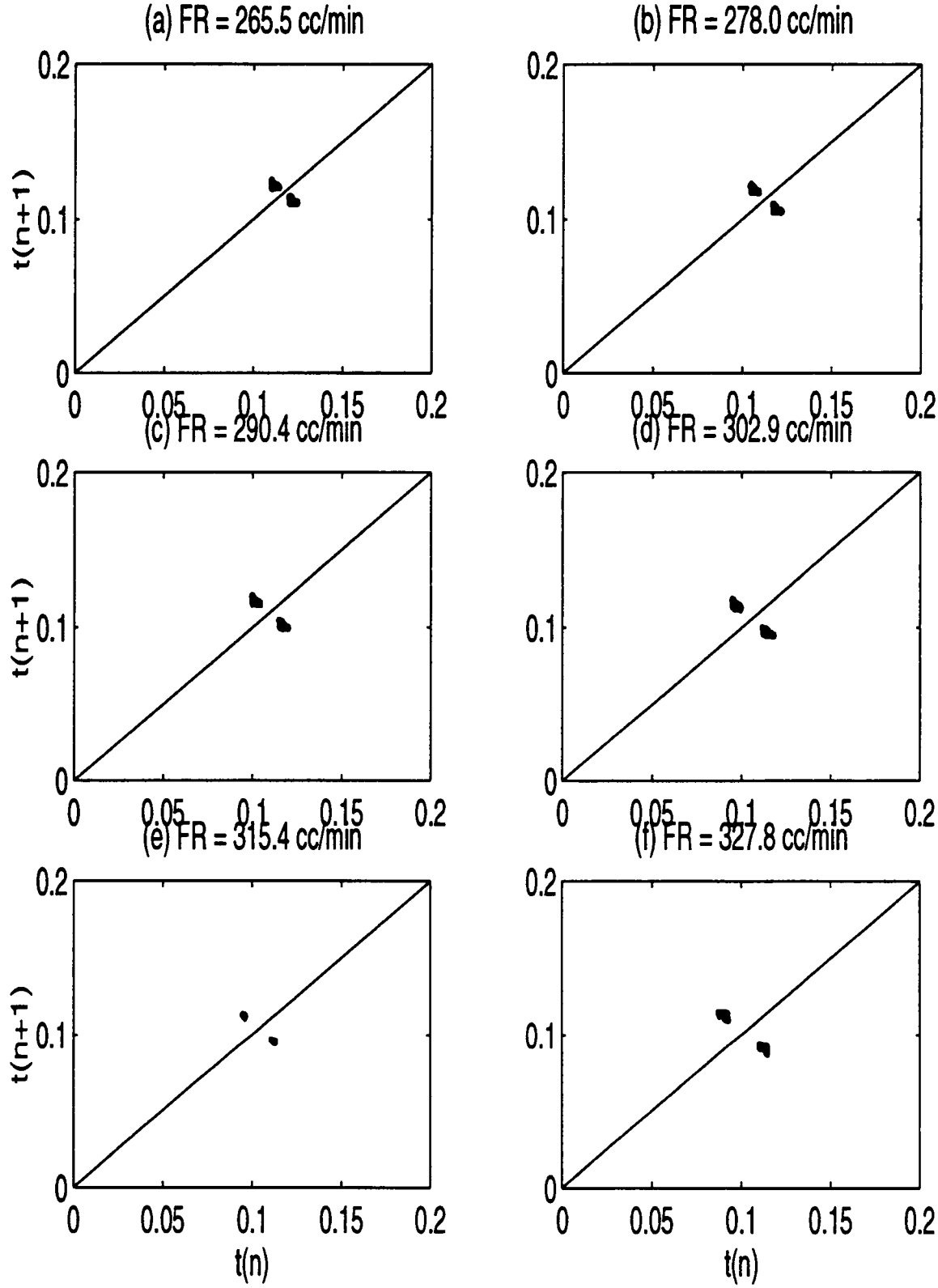


Figure B6. Time return maps of pressure measurements for air flows between 265.5 and 327.8 cc/min

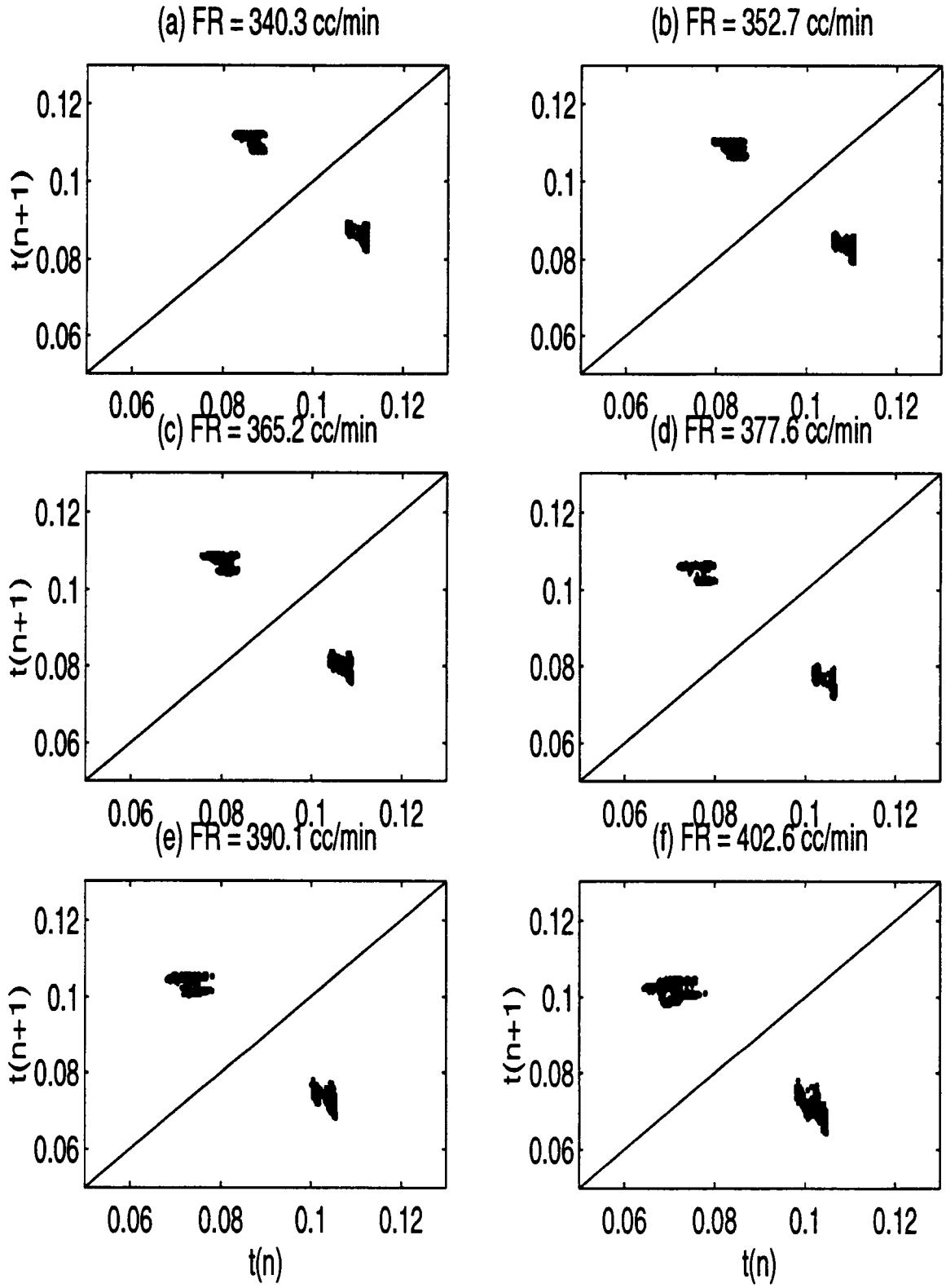


Figure B7. Time return maps of pressure measurements for air flows between 340.3 and 402.6 cc/min

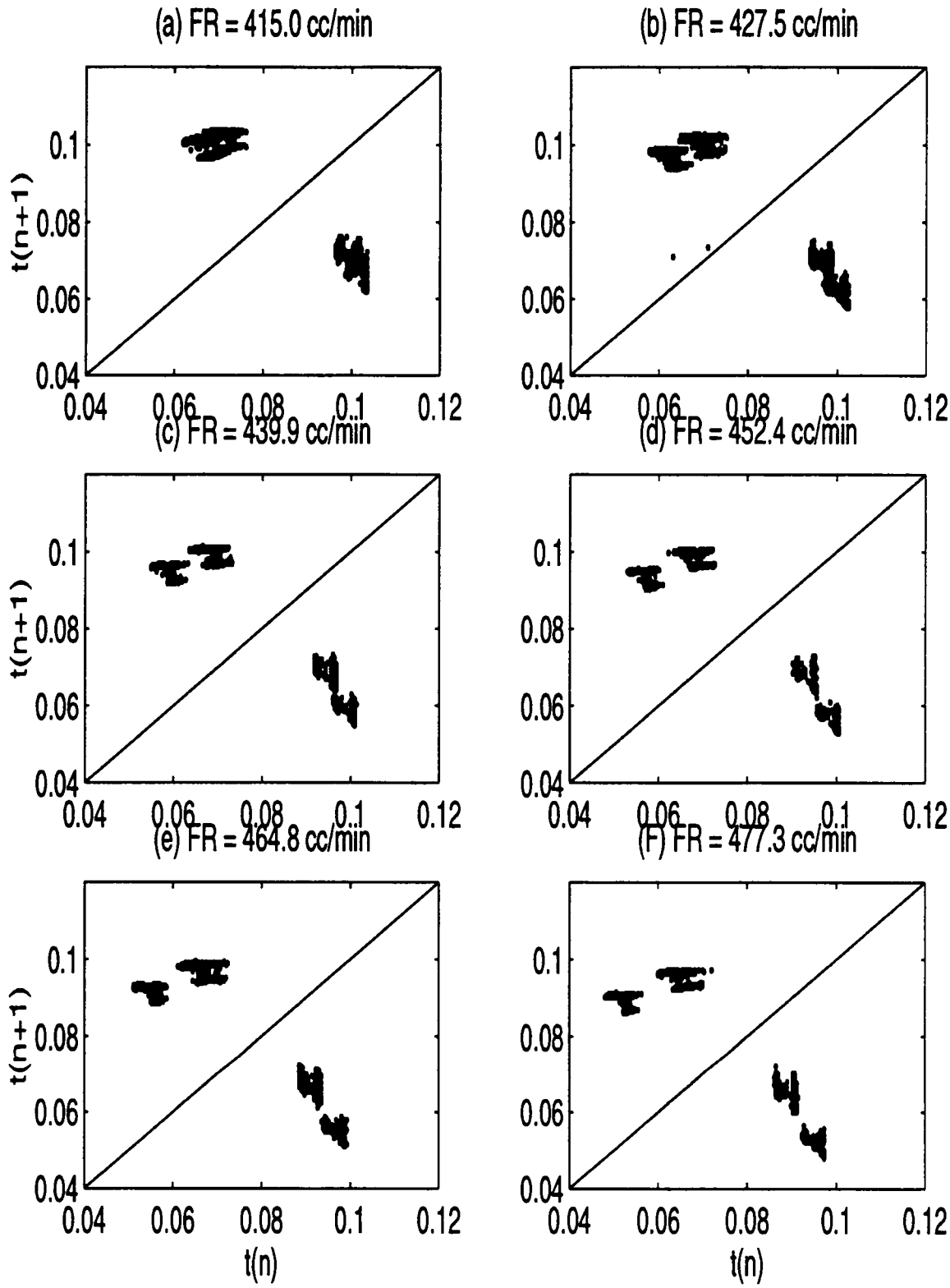


Figure B8. Time return maps of pressure measurements for air flows between 415.0 and 477.3 cc/min

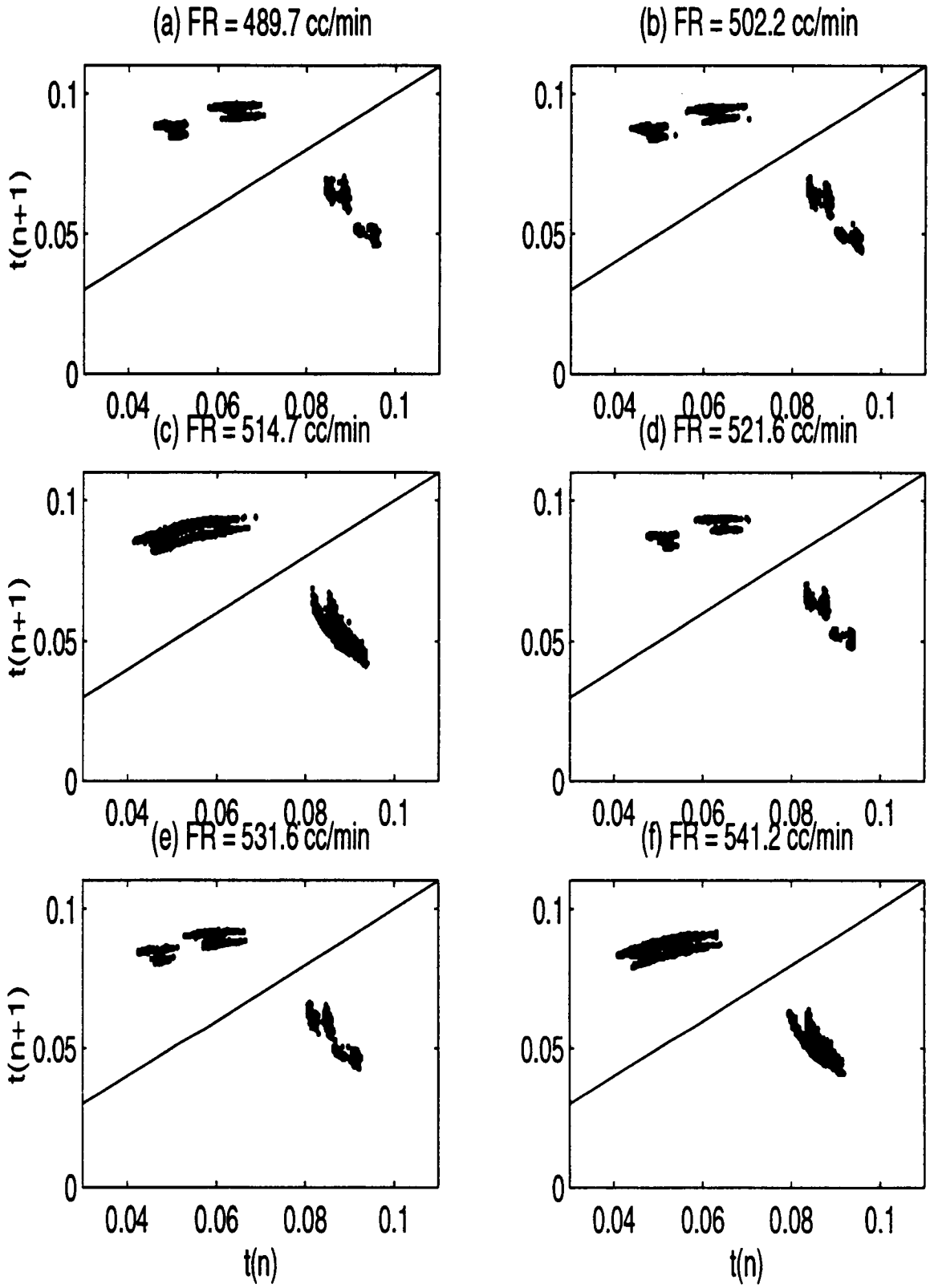


Figure B9. Time return maps of pressure measurements for air flows between 489.7 and 541.2 cc/min

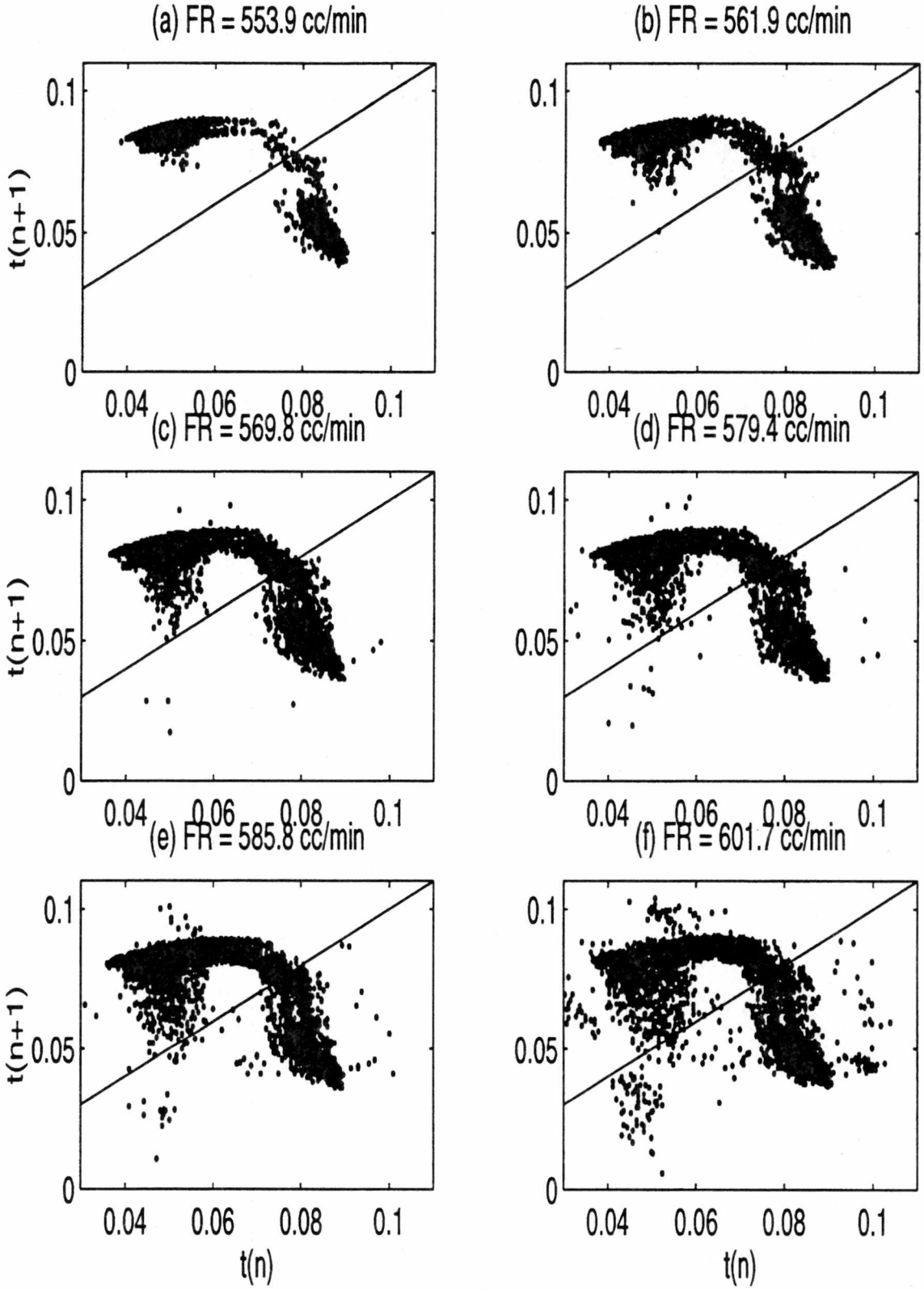


Figure B10. Time return maps of pressure measurements for air flows between 553.9 and 601.7 cc/min

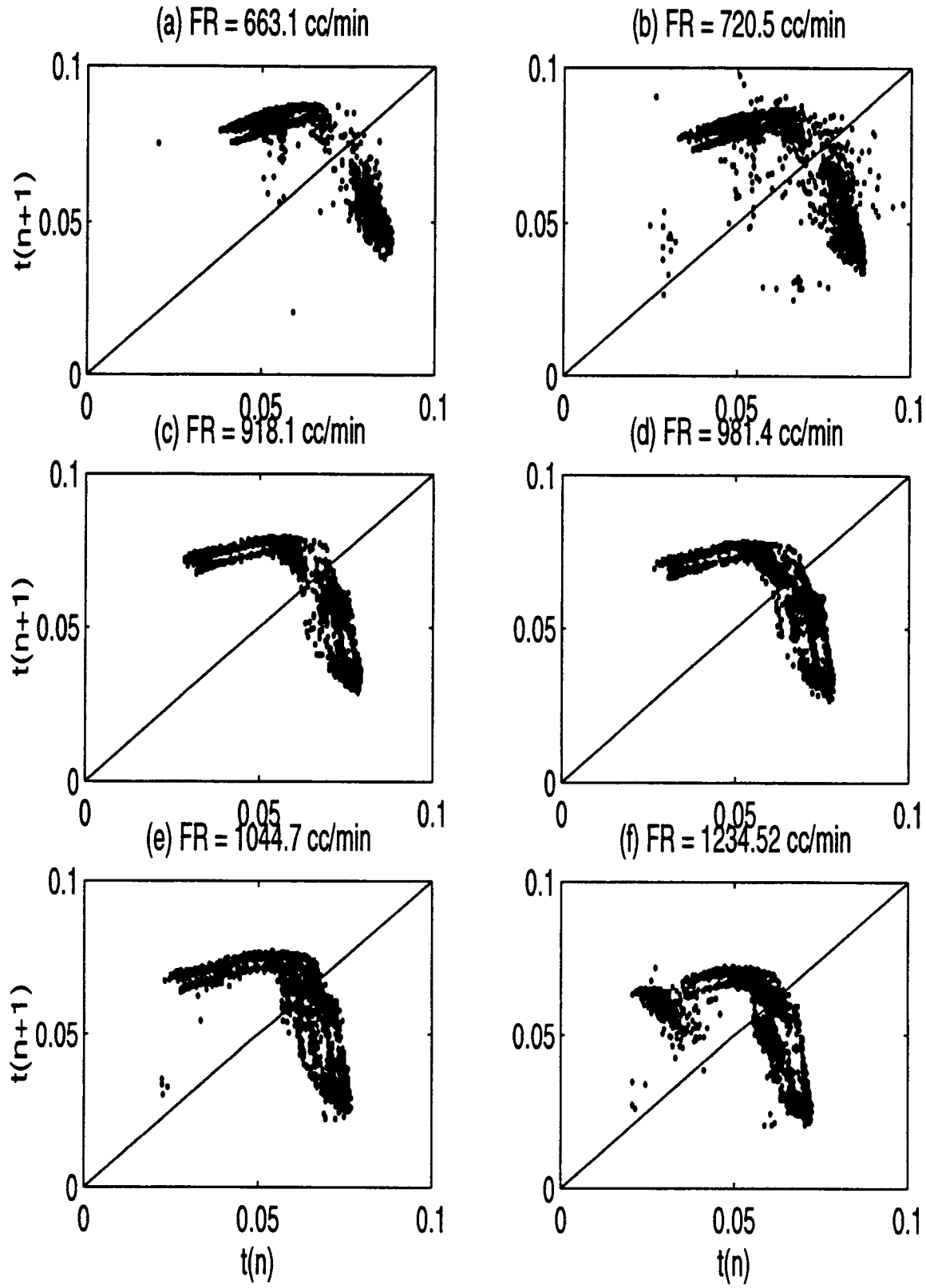


Figure B11. Time return maps of pressure measurements for air flows between 663.1 and 1234.5 cc/min

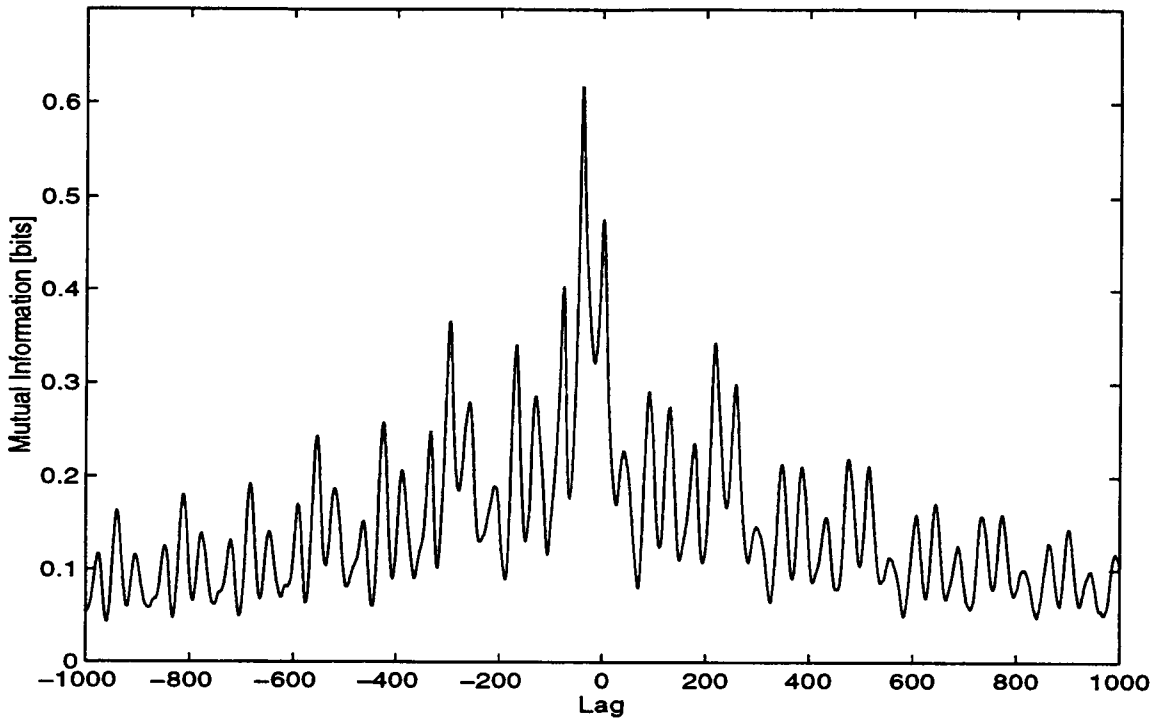


Figure B12. Mutual information for laser signals at 2 cm above nozzle tip with respect to pressure singals at flow of 918 cc/min

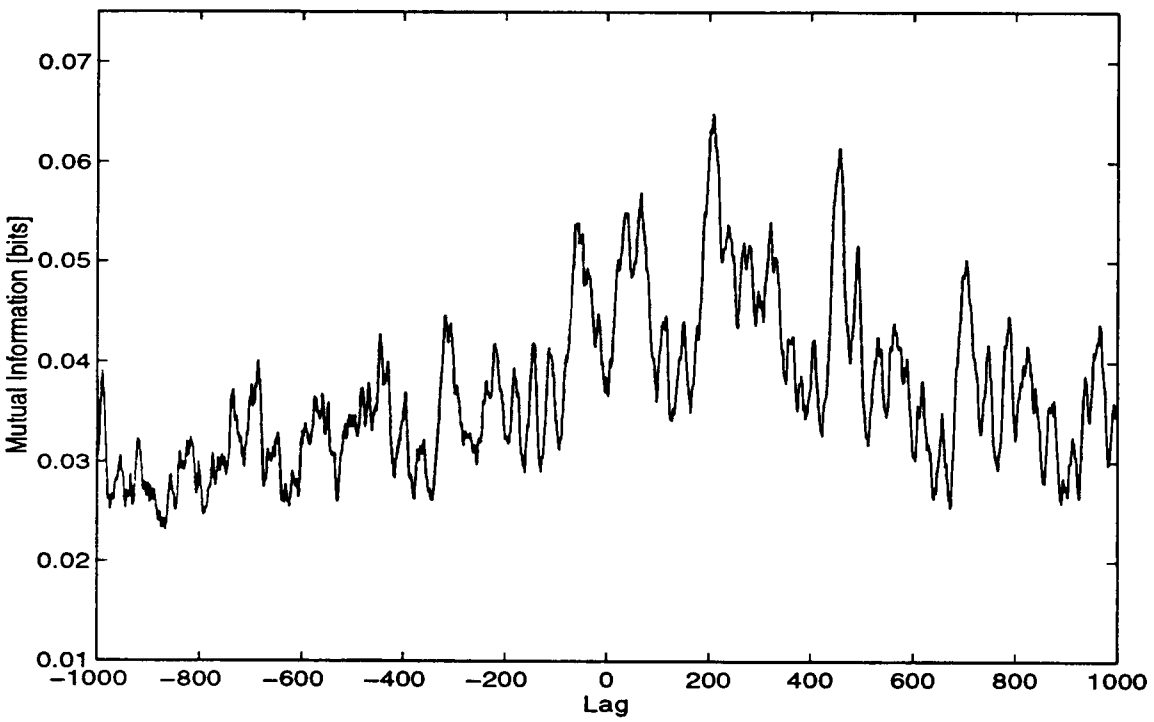


Figure B13. Mutual information for laser signals at 8 cm above nozzle tip with respect to pressure singals at flow of 918 cc/min

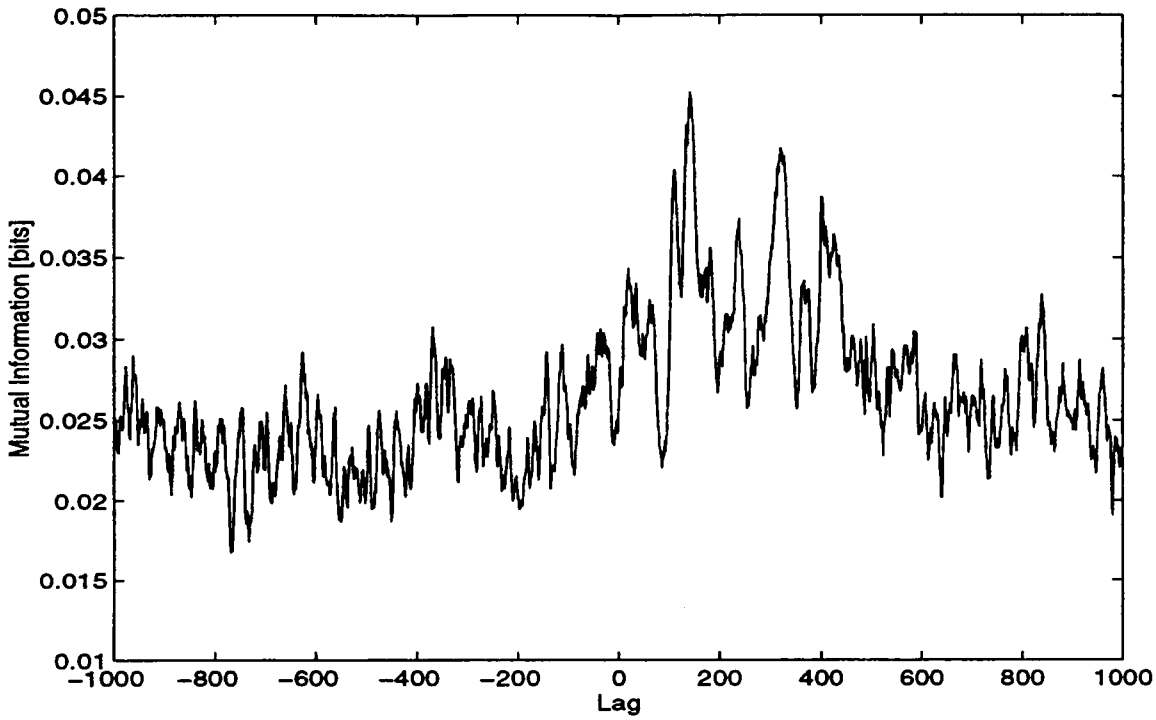


Figure B14. Mutual information for laser signals at 10 cm above nozzle tip with respect to pressure singals at flow of 918 cc/min

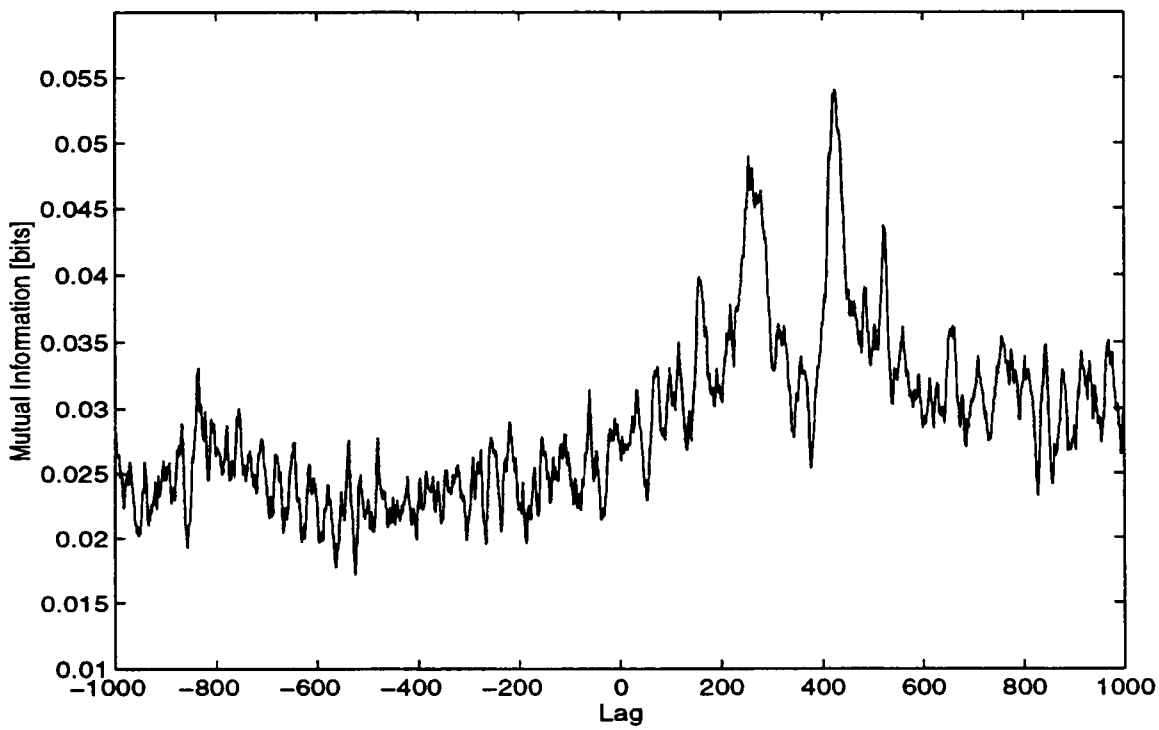


Figure B15. Mutual information for laser signals at 12 cm above nozzle tip with respect to pressure singals at flow of 918 cc/min

VITA

Yuen Cheng was born in Shanghai, China on April 12, 1970. He majored in Chemical Engineering at the University of Tennessee, Knoxville, and graduated in May, 1994. After receiving his Bachelor of Science degree, he began graduate study at the University of Tennessee, Knoxville in August, 1994, where he was awarded the Master of Science in December, 1996.